University of Stavanger

FACULTY OF SCIENCE AND TECHNOLOGY

MASTER'S THESIS

Study programme/specialisation: Petroleum Technology/Reservoir Engineering	Spring semester, 2020 Open

Author:	Dennis Troy Ginn

Supervisor: Ingebret Fjelde

External Supervisor: Bergit Brattekås

Title of master's thesis:

Effects of Potential Determining Ions and pH on the
Wettability of Intermediate Wet Outcrop Limestone

Credits:
          30

Keywords: Carbonate Outcrop limestone Crude oil Smart water Surface determining ions Wettability alteration Surface complexation modeling Bond product sum pH Fracture	Number of pages: ………………… + supplemental material/other: ………… Stavanger, 13 July 2020 date/year

Acknowledgement page

I would like to express my gratitude to Dr. Ingebret Fjelde for his guidance and perseverance. I am thankful for Professor Fjelde's continued support. I have learned a great deal under his mentorship.

I am also thankful for the support I was given by the staff at the University of Bergen. To my external advisor, Dr. Bergit Brattekås. Her guidance in the laboratory, locating research papers and organizing the flow of this report was instrumental in completing this project. A special thank you to Professor Martin Fernø for allowing me to use the laboratories and facilities. And to the Senior Engineer Marianne Steinsbø for her instruction and assistance. She guided me through laboratory procedures, safety and how to plan and assembly the experimental equipment. It has been an interesting and rewarding journey.

Thank you to PhD Samuel Erzuah for his instruction and clarification on PHREEQC and surface complexation modeling.

I am grateful for the support given by my family. This venture has been a challenge for us all with many long hours, neglect and extra responsibilities. You gave more than anyone should be asked to. Thank you!

Prefix

Dennis Ginn thesis amendment

This thesis was submitted in partial fulfillment of the UiS Petroleum Engineering – MSc Programme on July 13th 2020.

The thesis was planned to be mostly experimental, where laboratory facilities at the Department of Physics and Technology, University of Bergen (UiB) would be used. Due to the global outbreak of Covid-19 the laboratory facilities at UiB were, however, closed down for six weeks. This strongly affected the progress of the master thesis, which was heavily dependent on laboratory work.

This study focused on wettability alterations of limestone core material using brines with concentrations of positive determining ions (PDI) higher than those found in sea water. The experiments were conducted at normal and elevated temperatures, and normal and elevated pH levels. The student designed and assembled the experimental setup himself. The experimental setup was nearly completed when the university closed on March 13th. He was allowed to return to his experiments on April 28th, and modified his experimental plan to include shorter test times for aged cores (10 days rather than 20 days). The student lost valuable time during the Covid-19 lock-out from laboratory facilities, but resumed and completed all his planned laboratory work.

Sincerely,

Bergit Brattekås
Co-supervisor (UiB)

Abstract

The intent of this study is to determine if the wettability of slightly oil wet limestone can be shifted toward water wet using "Smart Water". The theory of "Smart Water" in carbonates proposes that increasing the composition of potential determining ions (PDI) such as Mg^{2+}, Ca^{2+} and SO_4^{2-} above those found in seawater can improve oil production. The mechanism for improved recovery is a shift in wettability of the carbonate surface that is in contact with the polar components of crude oil from slightly oil wet to water wet. Calcite $(CaCO_3)$ is the main mineral in carbonates and its surface is predominately positive due to a layer of Ca^{2+} ions. The negatively charged carboxylate groups $(RCOO^-)$ in the crude oil bind to the positively charged calcite surface at points called exchange sites. When a multi-valent cation such as Ca^{2+} or Mg^{2+} approaches an exchange site occupied by a carboxylate group it reduces the strength of the bond between the surface and the carboxylate. This allows the SO_4^{2-} to exchange place with the carboxylate group at the exchange site. Due to strong hydration of the Mg^{2+} ion it is more effective when temperatures exceed 100°C. At temperatures below 100°C the Ca^{2+}ion is more effective. Smart Water is a relatively inexpensive and environmentally friendly means of enhancing oil recovery: no hazardous chemicals are used, and it can be injected using the same equipment as seawater.

The experimental study was conducted using cylindrical outcrop Edwards limestone cores with similar properties. Four limestone cores were used in the initial strongly water-wet condition, while three were dynamically aged to slightly oil wet conditions. The Amott-Harvey displacement index was measured for each of the cores, performing full cycle spontaneous and forced imbibition of each fluid, and production data and end point relative permeability compared. To facilitate elevated pressure and temperature spontaneous and forced imbibition, an experimental setup was built that applied a Hassler core holder as a modified spontaneous imbibition cell. The cores were tested using one of three brines for both spontaneous and forced displacements: a synthetic formation water (FW); a brine with concentrations of PDI 1.5 times higher than that found in seawater; or PDI brine with elevated pH (PDI pH~9).

The experimental results revealed that the use of PDI brine had no effect on water wet cores. This was expected because the cores were drained using non-polar decane as the oil phase. The Amott-Harvey index measured with PDI pH~9 brine was low, at IAH = 0.45 (50% lower than PDI and FW), indicating a shift in spontaneous water imbibition and Amott water index caused by the elevated pH. In aged cores oil production was recorded for the first 24 hours when the core was exposed to FW but was attributed to thermal expansion of oil and not to spontaneous imbibition of water. The cores exposed to PDI brine began to produce oil after eight days and the PDI pH~9 brine began to produce oil after day three. Oil production started shortly after a rise in effluent pH was measured and continued throughout the 10-day test for both cores. Oil production was attributed to spontaneous imbibition of water and can be an indication of activity at the exchange sites as freed species begin to associate with hydronium.

A surface complexation model (SCM) using the program PHREEQC was used to determine mineral precipitation and to estimate the final wettability by calculating a bond product sum. The compositions of the three brines and a synthetic seawater were tested in open and closed conditions, at 25°C and 90°C, and standalone brine and brine in contact with the carbonate and crude oil surfaces. Modelling indicated that there was no danger of precipitation in the standalone brines but there is a risk of anhydrite precipitation at 90°C. Bond product sums (BPS) indicated that the carbonate/crude oil system was oil wet for all contacting brines at 90°C (calculated to 1.01 for all brines at open conditions, where 0 is completely water wet 1 is considered oil wet. For the same conditions in a closed system the BPS were FW (1.03), PDI (0.94) and PDI pH~9 (1.02)). The calculations gave an approximation of the actual results, although the measured Amott-Harvey index of the PDI pH~9 core was slightly less oil-wet than the PDI core after water exposure.

Nomenclature/Abbreviations/Symbols

Terms and Abbreviations

$[P_i]$	Activity of Gas i
$[X_{min,j}]$	Molar Fractions of Species i on the Mineral Surface
$[X_{oil,i}]$	Molar Fractions of Species i on the Oil Surface
$[i]$	Concentration or Activities of Species i

A	Area or Cross-sectional Area
A, B	Constants or Solute Species
$A, B, C, D \ldots$	Reactants and products of a chemical reaction
$a, b, c, d \ldots$	Stochiometric coefficients of a chemical reaction
A_i	Area of Surface i
a_i and b_i	Ion Specific Parameters
AN	Acid Number
As	Asphaltenes
atm	Atmosphere

B	Base
BJH	Barrett-Joyner-Halenda pore structure analysis
BET	Brunauer–Emmett–Teller surface area
BN	Base Number
BPR	Back Pressure Regulator
BPS	Bond Product Sum

C	Concentration or Constant
CEC	Cation Exchange Capacity
CGS	Centimeter-Gram-Second System of Units
C_i	Concentration or activity of species i given in molarity
C_{inj}	Injected Concentration
C_0	Initial Concentration in the Medium
$COBR$	Crude Oil Brine Rock
$COOH$	Carboxyl Group
cP	Centipoise

D	Darcy, Diffusion or Dispersion
d	Differential, diameter
DI	Deionized Water

D_L	Longitudinal Dispersion
dq	Rate of Sorption
d_s	Distance of the slipping plane from the OHP
D_T	Transverse Dispersion
EDL	Eelectrical Double Layer
EN	Electronegativity
EOR	Enhanced Oil Recovery
F	Flux or Faraday constant
FI	Forced Imbibition
FID	Flame Ionization Detection
FW	Formation Water
g	gram or Gravity Constant
H_3O^+	Hydronium ion
$HPLC$	High-Pressure Liquid Chromatographic
I	Ionic Strength
IAH	Amott-Harvey Displacement Index
IAP_{min}	Ion Activity Product of the Mineral
IFT	Interfacial Tension
IW	Intermediate Wet
J	Joule
K	Equilibrium Constant, Acidity Constant or Kelvin
k	Permeability
K_1	Stability Constant for ion-association equations
K_2	Dissociation Constant for ion-dissociation equations
K_{A-B}	Equilibrium Constant or Selectivity Exchange Coefficient between ions A and B
k_a	Absolute Permeability
K_d	Distribution Coefficient Constant for linear sorption
k_e	Effective Permeability
K_F	Freundlich isotherm constants for non-linear sorption processes
k_o	Effective Permeability of Oil
$k_{r,o}$	Relative Permeability of Oil
$k_{r,w}$	Relative Permeability of Water
K_{SP}	Solubility Product

$K_{SP,min}$	Solubility Product of a specific mineral
K_w	Acidity Constant of Water
k_w	Effective Permeability of Water
L	Liter
l	Length
l_{A_i}	Distance from Imbibition Face i to the No-Flow Boundary
l_C	Characteristic Length
LMA	Law of Mass Action
$l_{o,seg}$	Oil Segment Length
LSW	Low Salinity Water
l_{tubing}	Tubing Length
M	Molar or Molarity
m	Mass or Meter
MAE	Mass Action Equation
MBE	Mass Balance Equations
meq	milliequvalent
m_i	Concentration or activity of species i given in molality
m_o	Sandard State Molality
$mod\ SI$	Modified Spontaneous Imbibition
N	Newton
n	Integer 1, 2, 3…, number of nomponents, phases, units, etc.
n_i^0	Bulk Concentration
n_{ij}	Complex
NWF	Non-Wetting Fluid
OH	Hydroxyl Group
OH^-	Hydroxide ion
OHP	Outer Helmholtz Plane
P	Point on a Surface or Graph, Poise or Pressure
p	Potential of something given in negative common logarithm or Pressure
Pa	Pascal
P_b	Bubble Point Pressure
P_{BPR}	Backpressure from Backpressure Regulator
P_c	Capillary Pressure
P_{conf}	Confinement Pressure

PDI	Potential Determining Ions
pH	Potential of Hydrogen
$PHREEQC$	pH-REdox-EQuilibrium Version C
P_i	Partial Pressure of Gas i
P_{inj}	Injection Pressure
pOH	Potential of Hydroxide
P_{res}	Reservoir Pressure
PV	Pore Volume
q	Flow Rate or Sorption
R	Carbon Group, Gas Constant, Radius or Recovery
r	Radius
R_C	Retardation of the Concentration
$RCOOH$	Carboxylic Acid
$RCOO^-$	Carboxylate Group
R_{max}	Total Recovery
s	Second
$SARA$	Saturate, Aromatic, Resin and Asphaltene
SCM	Surface Complexation Model
SDI	Surface Determining Ions
SEM	Scanning Electron Microscope
SI	Saturation Index, Spontaneous Imbibition or International System of Units
S_i	Saturation of component i
S_{or}	Residual Oil Saturation
STO	Standard Tank Oil
SSW	Synthetic Sea Water
S_w	Water Saturation
S_{wi}	Initial Water Saturation
S_{wir}	Irreducible Water Saturation
T	Temperature
t	Time
TAN	Total Acidic Number
t_D	Dimensionless Time
TEC	Total Exchangeable Cations
TIC	Total Inorganic Carbon
TLC	Thin-Layer Chromatography

V	Volume
v	Velocity
V_b	Bulk Volume
V_{brine}	Volume of Brine
V_{BPR}	Volume Inside the Back Pressure Regulator
V_{cum}	Cumulative Volume
V_{dead}	Dead Volume
V_{EF}	Volume Inside the Core Holder Outlet End Fitting
V_{frac}	Volume of the Fracture
V_i	Volume of component i
v_C	Speed of the Concentration
V_o	Volume of Oil
V_{ofi}	Volume of Oil Forcibly Imbibed
V_{oi}	Initial Volume of Oil
$V_{o,seg}$	Volume of Oil Segment
V_{osi}	Volume of Oil Spontaneously Imbibed
V_p	Interconnected Pore Volume
V_{p_a}	Total Void Volume
$V_{tubing,i}$	Volume Inside Section i of Tubing
v_w	Speed of the Water
V_{wfi}	Volume of Water Forcibly Imbibed
V_{wsi}	Volume of Water Spontaneously Imbibed
v_x	Fluid Flow Velocity in the x-direction
W	Weight
W_{after}	Weight After
W_{before}	Weight Before
W_{decr}	Weight Decrease
W_{dry}	Dry Weight
WF	Wetting Fluid
W_{sat}	Saturated Weight
WW	Water Wet
X	Adsorption Site
x	Distance
z	Height along the z-axis, Surface Potential or Valance or Charge of an Ion
z_d	Potential at the Outer Helmholtz Plane
z_i	Ionic Valency

$å_i$	Effective Diameter of Hydrated Ion i
α	Conversion Factor or Oil Production Decline Constant
β_I	Activity at the Exchange Site (Gaines-Thomas convention)
β_I^m	Activity at the Exchange Site (Vanselow convention)
γ_i	Activity Coefficient
Δ	Algebraic Differential
ΔGr	Gibbs Free Energy
ΔG_r^o	Standard Gibbs Free Energy
ΔH_f^o	Formation Enthalpies
ΔH_r	Reaction Enthalpy
ΔH_r^o	Standard State Reaction Enthalpy
ΔP	Pressure Differential
δ^-	Partial Negative Dipole
δ^+	Partial Positive Dipole
δ_o	Amott-Harvey Displacement-by-Oil Ratio
δ_w	Amott-Harvey Displacement-by-Water Ratio
∂	Partial Differential
ε	Relative Permittivity of Water
ε_0	Vacuum Permittivity
ζ	Zeta Potential
θ	Angle
κ	Debye length
μ	As a Prefix Micro (10^{-6}) or Viscosity
μ_{CO}	Viscosity of the Crude Oil
μ_{brine}	Viscosity of the Brine
μ_{dec}	Viscosity of the Decane
ρ	Density
ρ_{CO}	Density of the Crude Oil
ρ_{brine}	Density of the Brine

ρ_{dec}	Density of the Decane
σ	Interfacial Tension or Surface Tension
τ	Sear Stress Tensor
$\emptyset$	Porosity
$\emptyset_a$	Absolute Porosity
$\emptyset_{eff}$	Effective Porosity
ψ	Surface potential
ψ_0	Potential at the Shear Plane

Superscripts

$-$	Negative Charge
$+$	Positive Charge
$^{\circ}$	Degrees
0	Bulk
a, b	Valance or Charge
o	Standard State

Subscripts

0	Initial
$1, 2, \ldots$	Number One, Number Two,… in a series
A_i	Area of Surface i
C	Concentration
CO	Crude Oil
D	Dimensionless
L	Longitudinal
SP	Solubility Product
T	Transverse
a	Absolute or Acidity
adv	Advancing
b	Bubble Point or Bulk
BPR	Back Pressure Regulator
C	Characteristic
c	Capillary or Contact
$conf$	Confinment
dec	n-Decane
$decr$	Decrease

EF	Core Holder Outlet End Fitting
eff	Effective
f	Formation
fi	Forcibly Imbibed
$frac$	Fractured
i	Component i
inj	Inject
ir	Irreducible
min	Mineral
max	Maximum or Total
nwf	Non-Wetting Fluid
o	Oil or Standard State
oi	Initial Oil
or	Residual Oil
p	Pore
r	Reaction, Relative or Rock
rec	Receding
res	Reservoir
s	Slipping Plane, Solid or Sphere
seg	Segment
si	Spontaneously Imbibed
t	Tube
w	Water
wf	Wetting Fluid
x	x-Direction
y	y-Direction
z	z-Direction

Table of Contents

List of Figures

List of Tables

Chapters:

1) Introduction
A. Background

Oil recovery operations were historically subdivided into three stages, which were based on the order of operations: primary, secondary and tertiary. Since it is not always desirable to produce a reservoir in this order the term enhanced oil recovery (EOR) has become a more accepted term over "tertiary recovery". The primary stage uses the naturally existing energy of the reservoir to displace the oil. Secondary recovery results from the augmentation of natural energy through injection of water or immiscible gas to provide pressure maintenance or to displace oil toward the producing wells. Tertiary processes, or more correctly EOR uses miscible gases, chemicals, and/or thermal energy to displace the oil. (Green 1998)

The basis of "Smart Water" as an enhanced oil recovery (EOR) process is to adjust the composition of the injection water in order to change the wetting properties of the crude oil, brine rock (COBR) system. Alteration of rock wettability from slightly oil wet to water wet has a positive effect on the capillary pressure and relative permeability of oil and water regarding oil recovery (Austad 2013). In relation to traditional methods of EOR, this method is inexpensive and environmentally friendly as no expensive chemicals are added. In addition, there are no injection problems. For best results the smartest water should be used from the start of the water flooding process. (Austad 2013)

A significant number of studies have shown that injecting Smart Water into chalk cores can alter wettability from oil wet to slightly water wet, thereby increasing oil recovery (Zhang and Austad 2006, Strand, Høgnesen et al. 2006a, Zhang, Tweheyo et al. 2007, Fathi, Austad et al. 2010). Additional studies have also confirmed the effectiveness of Smart Water in reservoir limestone cores (Austad, Strand et al. 2008, Ravari 2011, Shariatpanahi, Strand et al. 2012).

Ravari presented a PhD thesis in 2011 comparing the use of Smarty Water in reservoir and outcrop limestone cores. In the thesis Ravari concluded that Smart Water was able to positively alter wettability in the reservoir limestone, but it had little or no effect on the outcrop limestone

cores taken from the Edwards formation in Texas nor a sample provided from France by TOTAL (Ravari 2011). Unlike water-wet reservoir limestone, the outcrop cores tested oil-wet in chromatographic wettability tests even though they had not been exposed to oil. Spontaneous imbibition (SI) tests using a model oil showed the outcrop cores were water-wet, but the surface was non-reactive to the potentially determining ions (PDI) such as SO_4^{2-}, Ca^{2+} and Mg^2. Additionally, Mg^{2+} was not able to substitute Ca^{2+} in a 1:1 reaction. Acidic oils (AN=0.5 and 1.84 mg KOH/g) made the outcrop limestone preferentially oil-wet, and negligible oil was produced in a spontaneous imbibition process using formation water (FW). In contrast to reservoir limestone, no extra oil was recovered from outcrop limestone using seawater as a wettability modifier in spontaneous imbibition nor in a forced imbibition process even at 130°C (Ravari 2011).

B. Purpose

The purpose of this study is to investigate alternate methods of testing outcrop limestone cores compared to the methods used in the study mentioned above by Ravari. The intent is to see if it is possible to alter the wettability of carbonate outcrop cores that have been dynamically aged in crude oil to a slightly oil wet condition to water wet or slightly water wet based on the Amott-Harvey Displacement Index (IAH). The high cost and low availability or reservoir samples make the use of outcrop limestone cores attractive for studies and for testing.

C. Content of the assignment

This paper is presented in the following manner. Chapter three is an overview of general theory that was part of a literature study to prepare for the experiments. It is non-specific and does not describe the study itself. This chapter was very useful as a reference once the study began.

Chapter four provides an overview of the actual materials chosen for the study and a description of their petro-physical properties. The chapter includes the hydrocarbons, brine compositions and carbonate rock chosen for the study.

A chronological description of the experiments conducted in the study are provided in chapter five. The chapter details the equipment, procedures and formulas used. Comments regarding difficulties that occurred are mentioned to give light into why certain procedures were taken or modified, but the chapter does not provide the results of the experiments.

Chapter six contains the results of the experiments. The chapter starts with tables listing the most relevant data obtained from the core studies. This is followed by charts with detailed explanations of the data and comments regarding how the experiments compare with expected results.

A summary of the conclusions is presented in chapter seven. An assessment of the data is compared to the problem definitions and objectives listed below.

Amplifying information such as uncertainty calculations and PHREEQC program code are listed in the appendices.

2) Problem definition and objectives

Question 1

Will increasing the concentration of potential determining ions (PDI) such as calcium (Ca^{2+}), magnesium (Mg^{2+}) and sulfate (SO_4^{2-}) to concentrations 1 ½ times the concentrations found in sea water improve the wettability characteristics of Edwards outcrop limestone cores by shifting the wettability of the core from intermediate oil wet to slightly water wet on the Amott-Harvey displacement index (IAH)?

Question 2

Will increasing the pH level of the brine containing PDI to approximately nine have any effect on the wettability alteration of the core samples?

Question 3

Does adjusting the temperature from 130°C to 90°C improve the outcome of wettability tests.

Question 4

Can the program PHREEQC be used to predict precipitation of minerals and predict final wettability using surface complexation modeling (SCM)?

3) Theory from literature study - Overview of relevant theory, existing methods and models

A. Porosity

Porosity (Ø) is the void volume of a rock expressed as the percentage of the rock's total volume, and it represents the fluid storage capacity of the rock. Absolute porosity ($Ø_a$) is the ratio of the total void volume (V_{pa}) to the bulk volume (V_b) of a rock sample, where effective porosity ($Ø_{eff}$) refers only to the ratio of interconnected pore volume (V_p) to the bulk volume.

$$Ø_a \overset{\text{def}}{=} \frac{V_{pa}}{V_b} \tag{3.1}$$

$$Ø_{eff} = \frac{V_p}{V_b} \tag{3.2}$$

The bulk volume is the sum of the rock's pore space plus the volume of all the solid grains referred to as matrix volume (V_m). In a cylindrical core V_b is the length (l) of the core times its cross-sectional area (A).

$$V_b = V_p + V_m = l \cdot A \tag{3.3}$$

In this study porosity refers to $Ø_{eff}$.

B. Permeability

Permeability (k) is a proportionality coefficient that defines a porous medium's capability to transmit fluids through its network of interconnected pores. In flow experiments, k can be calculated using the generalized form of Darcy Law for the linear, horizontal flow of an incompressible fluid in terms of its viscosity (μ) and flow rate (q) that is being subjected to a pressure differential (ΔP) across a porous medium with length (Δl) and cross-sectional area (A).

$$k = \frac{\mu \, q}{A} \frac{\Delta l}{\Delta p} \tag{3.4}$$

Permeability has the dimension of surface area (l^2), which is not a convenient way to express fluid-transmission capacity of a porous medium. Therefore the Darcy (D) is used. The

permeability (k) of a porous medium is $1\ D$ if a fluid with viscosity (μ) of $1\ cP$ and a pressure difference (Δp) of $1\ atm/cm$ is flowing through the medium's cross-section (A) of $1\ cm^2$, at a rate (q) of $1\ cm^3/s$. Converting to SI units gives $1D\ = 0.987 \cdot 10^{-12}\ m^2 = 0.9869 \cdot (\mu m)^2$.

If flow is non-horizontal, equation 3.4 is written to include the density of the displacing fluid (ρ) and the angle of incidence from horizontal (θ).

$$k = \frac{\mu\ q}{A\left(\frac{\Delta p}{\Delta x} - \rho\ g\ sin\ \theta\right)} \tag{3.5}$$

Absolute permeability (k_a) occurs when only one fluid is flowing through the porous medium. If more than one fluid is present, then the flow capacity of each fluid will be hindered by the other fluid. This is termed as effective permeability (k_e). The ratio of the rock's effective permeability (k_e) to a particular fluid and its absolute permeability (k_a) is called a relative permeability (k_r) to that fluid. In a multi-phase system the sum of the respective k_r values is always less than one.

$$k_r = \frac{k_e}{k_a} \tag{3.6}$$

C. Saturation

Saturation (S_i) is the fraction of the pore volume (V_p) occupied by a particular fluid (V_i) in a porous medium containing a number (n) of fluid phases.

$$S_i \stackrel{\text{def}}{=} \frac{V_i}{V_p}, \qquad i = 1, \ldots, n \tag{3.7}$$

The fluid saturations will be distributed unevenly in the pore space of a reservoir due to factors like wettability preferences and vertical distance above the water-oil contact. The saturation values will also change during production. The sum of the individual saturations (S_i) will always equal 100% of the total pore volume (V_p).

$$\sum_{i=1}^{n} S_i = 1 \tag{3.8}$$

The percentage of oil that is not recoverable from the reservoir during production is called residual oil saturation (S_{or}). It is the difference between initial oil volume (V_{oi}) and displaced or recovered oil volume (V_o) divided by the total pore volume (V_p).

$$S_{or} = \frac{V_{oi} - V_o}{V_p}$$
(3.9)

During a drainage process in a water-wet rock, oil (the non-wetting fluid) displaces water (the wetting fluid). The water saturation (S_w) will continue to decrease until it reaches a point called irreducible water saturation (S_{wir}). This occurs when the hydraulic continuity of the pore water becomes disconnected and water no longer flows through the pores.(Anderson 1987)

D. Viscosity

Viscosity (μ) is a parameter that defines the internal resistance of a fluid to shear flow.

In the Newton model (Figure 1), μ is a proportionality coefficient linking the tangential, or applied shear stress tensor (τ) with the

Figure 1 Longitudinal cross-section of a Newtonian fluid flow in an open channel.

resulting shear rate $\left(\frac{dv_x}{dy}\right)$, where v_x is the fluid flow velocity in the x-direction and y is the vertical direction.

$$\tau = \mu \frac{dv_x}{dy}$$
(3.10)

The SI unit of viscosity is the Pascal-second ($Pa \cdot s$), and the centimeter-gram-second (CGS) unit is the poise (P) or centipoise ($cP = 10^{-2}P = 10^{-3}Pa \cdot s$).

Water and most oils are Newtonian fluids. The viscosity of a Newtonian fluid is constant, meaning there is a linear relationship between τ and $\frac{dv_x}{dy}$. The Viscosity does however vary directly with pressure and inversely with temperature (Reid 1987). If only one viscosity-

8

temperature point of a liquid is known then the viscosity change with temperature can be estimated using a formula adapted by Gambill (1959) of the Lewis and Squires (1934) liquid viscosity correlation (Reid 1987).

$$\mu = \mu_0^{-0.2661} + \left(\frac{T - T_0}{233}\right)^{\frac{-1}{0,2661}} \tag{3.11}$$

Where μ and T are the desired viscosity and temperature values and μ_0 and T_0 are the initial viscosity and temperature.

E. Interfacial tension

Interfacial tension ($IFT\ or\ \sigma$) describes the work or energy which must be extended to keep two immiscible fluids apart in a pressure equilibrium state, and to increase the surface area where the fluid phases meet. The magnitude of IFT is expressed using energy per unit area or force per unit length and it has the SI unit Newton per meter $\left(\frac{N}{m}\right)$. The IFT between a liquid and its vapor phase is referred to as surface tension.

Cohesion is the electrostatic attraction of similar molecules to one another, while adhesion refers to the electrostatic attraction of dissimilar molecules to one another. Both cohesive and adhesive attractions are the result of van der Walls forces. Immiscible fluids will not readily combine because the cohesive forces between like molecules are greater than the adhesive forces between the dissimilar molecules ($\sigma > 0$). The area of the contact surface is minimized and one of the fluids will occur as spherical droplets in the other. Miscible fluids will readily mix because the adhesive and cohesive forces are nearly equal ($\sigma \approx 0$).

i.   Van der Walls

The atoms in a molecule or ion are held together by strong interatomic (covalent or ionic) forces existing between the atoms. The weaker cohesive forces that exist between molecules or ions are called van der Walls forces. These electrostatic forces are short range and exist between all types of atoms, molecules and ions and are responsible for the formation of liquids and solids. (Indira and Chatwal 2010)

There are different types of van der Walls forces. Dipole-dipole interactions exist between polar molecules with permanent dipole moments. As the molecules approach one another they align themselves so the positive dipole (δ^+) end of one molecule attracts the negative dipole (δ^-) end of the other. When a polar molecule approaches a non-polar molecule the δ^+ end of the polar molecule attracts the electron cloud of the non-polar molecule resulting in molecular attraction due to this induced dipole interaction. Similarly, an induced dipole interaction can form between non-polar molecules. The movement of electrons causes the electron cloud to be momentarily negative on one side. This unsymmetrical electron cloud induces an electric dipole in the neighboring non-polar molecule. (Indira and Chatwal 2010)

ii.   Equation based calculation of IFT

Although it is preferred to use techniques such as the pendant drop method, it is not always possible to determine IFT experimentally. In this case formulas can be used to make an estimate. Jennings (1967) measured the IFT between normal decane and water $\left(\sigma_{dec/w}\right)$ using the pendant drop method in the interval 25 to 176 °C and 1 to 817 atmospheres to an accuracy of 0.001 dyne/cm. Using this data, he proposed the following general equation

$$\sigma_{dec/w} = 50.066 + 0,0027247\ P - 0.12050\ \Delta T \qquad (3.12)$$

Where pressure (P) is in atmospheres and (ΔT) is the difference in temperature in degrees Celsius $(T - 25\ °C)$. The formula has a maximum error of 4% and it does not take into account variations due to differences in salinity.

Buckley and Fan (2007) conducted a study on crude oil/brine using the pendant drop method to measure the IFT between forty-two different crude oil samples and three brines: double-distilled water, 0.1 M NaCl, and synthetic sea water (SW). The pH of the brines was adjusted using HCl and NaOH. The study revealed a general trend for IFT to increase with base number (BN), viscosity (μ) and the amount of asphaltenes (As) of the crude oil. Conversely, IFT decreases with increasing pH and acid number (AN). On average IFT decreases $4.7 \pm 2.9\ mN/m$ (about 23%) from initial values when the crude oil/brine make first contact until equilibrium at 2000 s. the following equilibrium IFT formula is given in the paper

$$\sigma_{co/brine} = 21.7 - 1.14\,pH + 0.745\,A_s - 1.21\,AN + 1.15\,BN + 0.0073\,\mu \qquad (3.13)$$

Due to scatter in the data, the formula is presented to show the relationship between the variables and not for calculating IFT, but it does provide a general value for IFT when no other data are available.

F. Wetting

In the presence of more than one immiscible fluid and a solid, the fluid with the greater adhesive attraction to the solid becomes the wetting fluid (WF) and it will preferentially spread over the surface. Craig (1971) defines Wettability as "the tendency of one fluid to spread on or adhere to a solid surface in the presence of other immiscible fluids."

Contact angle (Figure 2) is a common measure of wettability (Craig 1971), and it can be described in a water-oil-solid system using the Young-Dupre equation (Craig 1971).

$$\sigma_{os} - \sigma_{ws} = \sigma_{ow}\cos\theta_c \qquad (3.14)$$

Where $\sigma_{os}, \sigma_{ws}, \sigma_{ow}$ represent the interfacial energy between the oil and solid, water and solid, and oil and water respectively. The angle at the oil-water-solid interface (θ_c) is measured through the water in degrees.
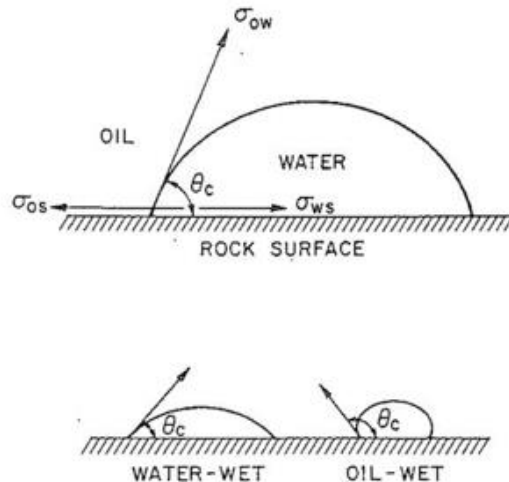
Figure 2 Wettability of oil-water-solid system (Craig 1971)

Table 1 Arbitrary wettability classes for an oil-water-solid system. (Craig 1971, Anderson 1986)	
Wetting angle (degree)	Wettability preference
0-60	Water-wet
60-75	Preferentially water-wet
90	Neutral wettability
105-120	Preferentially oil-wet
120-180	Oil-wet

The system is considered water wet if the contact angle in Figure 2 is less than 90°, oil wet if he contact angle is greater than 90° and neutral (or intermediate) wet if the angle is equal to 90° (Craig 1971, Anderson 1986). Arbitrary classes for an oil-water-solid system are generalized in Table 1. In a rock/oil/brine system the preferential WF will tend to contact the rock surface and occupy the smaller pores while the non-wetting fluid (NWF) will occupy the centers of the larger pores and form globules that extend over several pores (Anderson 1986). Fractional wettability is used to indicate that different wetting preferences exist throughout the rock (Anderson 1986). A subset of fractional wettability introduced by Salathiel (1973) is mixed wettability where the smaller pores remain water wet while the larger pores form continuous path of oil-wet surfaces. There are a variety of methods used to measure contact angle, but in petroleum industry the *sessile drop* and *modified sessile drop* methods are the most common (Anderson 1986).

G. Capillary Pressure

Capillary pressure (P_c) is the driving force behind the Amott-Harvey wettability test (discussed later). If two immiscible fluids are in contact with one another in a narrow capillary tube, the stronger adhesive forces of the WF to the capillary walls will cause the interface between the WF and NWF to curve convex toward the WF. The pressure differential that exists across the interface separating the two immiscible fluids is called the capillary pressure (P_c) which can be solved for using the Laplace equation (Craig 1971, Anderson 1987).

$$P_c \equiv p_{nwf} - p_{wf} = \sigma \left(\frac{1}{r_1} - \frac{1}{r_2} \right) \tag{3.15}$$

Where p_{nwf} and p_{wf} are the pressures of the non-wetting fluid and wetting fluid respectively. The interfacial tension between the NWF and WF is given by σ. The terms r_1 and r_2 are the

radii of curvature of the interface, measured perpendicular to each other. The elements of the Laplace equation can be derived using the terms in Figure 3, where θ is the contact angle through the NWF, r_t is the radius of the tube and r_s is the radius of the sphere (assuming $r_s = r_1 = r_2$). The relationship between the two radii can be expressed as

$$\frac{r_t}{r_s} = \cos\theta \Rightarrow \frac{1}{r_s} = \frac{\cos\theta}{r_t} \tag{3.16}$$

This expression can be substituted into the Laplace equation to give an expression of P_c in terms of tube radius and the interfacial forces (Anderson 1987)

$$P_c = \frac{2\,\sigma\cos\theta}{r_t} \tag{3.17}$$
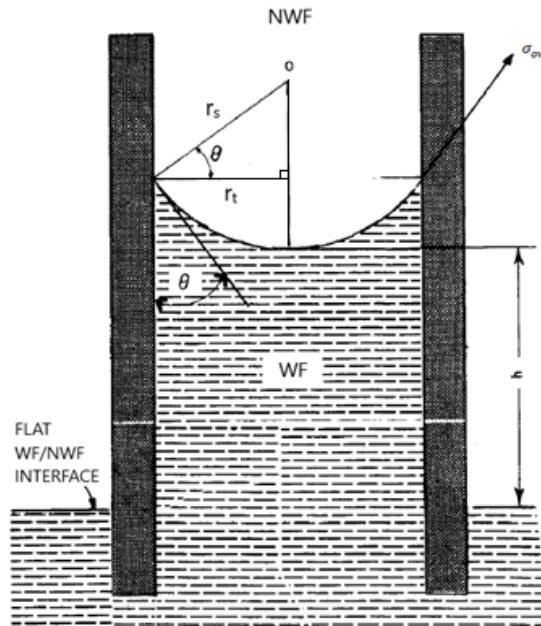
Figure 3 NWF/WF interface in a capillary tube (Anderson 1987)

The method of fluid displacement in the rock will affect the P_c process. In a drainage process (curve 1 in Figure 4) the NWF displaces the WF (Anderson 1987). The pressure of the NWF must exceed a threshold pressure before it can enter the 100% WF saturated core (Craig 1971). As the pressure of the injected NWF increases, the saturation level of the WF decreases until irreducible wetting-phase saturation when the WF becomes disconnected as indicated when

13

curve 1 is nearly vertical (Anderson 1987). In an imbibition process the WF displaces the NWF. After measurement of the drainage P_c curve, the spontaneous imbibition (curve 2 in Figure 4) is developed by allowing the core to imbibe the WF. The P_c curve decreases to zero as the WF saturation increases. In the forced imbibition process the NWF is forcibly displaced by injecting the WF. Curve 3 in Figure 4 shows the development of P_c during this process as saturation of the WF is forced to increase until the NWF becomes hydraulically disconnected and stops flowing as indicated by the near vertical P_c curve. This is referred to as the irreducible nonwetting-phase saturation (Anderson 1987). Curves one and two in Figure 4 follow different paths due to a phenomenon called hysteresis which is a term used to indicate the difference in multiphase rock properties that depends upon the direction of saturation change (Craig 1971). The work required for one fluid to displace the other from the core is proportional to the area under the capillary pressure curve (Anderson 1987).
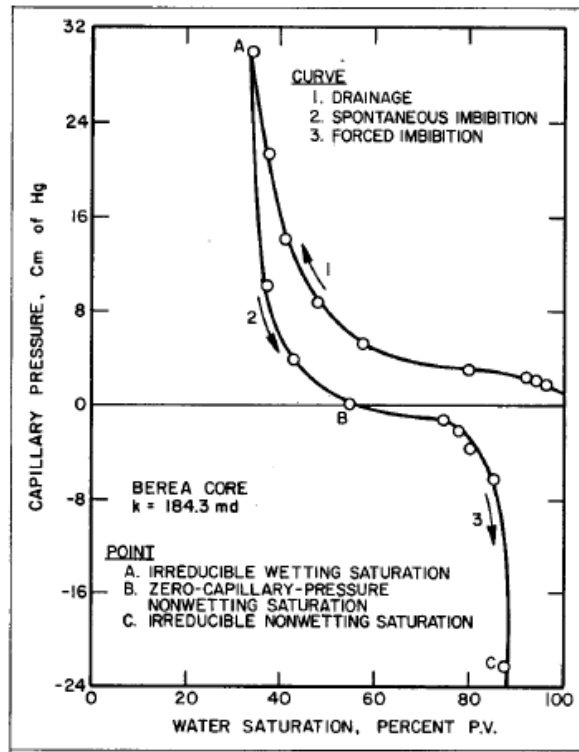
Figure 4 Oil/water capillary pressure curve measured
on a water-wet Brea core (Anderson 1987)

H. Crude oil

i. Crude Oil Composition

Petroleum is a complex mixture of hydrocarbons containing small amounts of organic compounds such as sulfur, oxygen and nitrogen, as well as compounds containing metallic constituents like vanadium nickel, iron, and copper (Speight 2007). Despite the method of generation or the variation in physical properties between light (mobile) and heavy (asphaltic) crude oils, the composition of petroleum generally falls within a narrow window (Speight 2007):

Carbon   83.0% to 87.0%

Hydrogen   10.0% to 14.0%

Nitrogen   0.1% to 2.0%

Oxygen   0.05% to 1.5%

Sulfur   0 .05% to 6.0%

Metals (Ni and V) <1000 ppm

ii. Crude Oil Classification

The hydrocarbons found in petroleum are classified into paraffins, cycloparaffins and aromatics. Paraffins, also known as alkanes or aliphatic are saturated hydrocarbons with straight or branched chains, but no ring structure. The alkanes contain only carbon and hydrogen with single covalent bonds between the atoms making them insoluble in water, stable, non-polar and unable to undergo addition reactions (Speight 2007, McMurry 2012) (Boye, Keeping et al. 2009) (Smith 2010).

Cycloparaffins also known as cycloalkanes are saturated hydrocarbons containing one or more rings, each of which may have one or more paraffin side-chains (Speight 2007, McMurry 2012). Although cycloparaffins are single bonded and saturated, they are unstable because the ring structure forces the bond to deviate from the ideal 109° (McMurry 2012).

The third class, aromatics contain one or more six-membered rings with three alternating double bonds. A single ring is referred to as benzene and can be linked to other rings or paraffin side-chains (Speight 2007, McMurry 2012).

15

A common classification system divides the crude oil by the fraction of the components found in the saturate, aromatic, resin and asphaltene ($SARA$) categories. The first category contains the saturates. These consist of the non-polar linear, branched or cyclic saturated hydrocarbons. Aromatics contain one or more aromatic rings and are polarized. The resins and asphaltenes are compounds bearing heteroatoms (Speight 2007). A heteroatom occurs when an atom other than carbon or hydrogen such as sulfur, oxygen, or nitrogen bonds to the carbon (Noller, Norman et al. 2016). The resins are large and complex polymeric molecules with non-crystalline structure that contain polar constituents and are soluble in heptane or pentane. Asphaltenes are similar in structure to resins but are insoluble in heptane and pentane (Fan, Wang et al. 2002, Page visited 02 Feb 2018, Schlumberger 2017).

iii. Polar Nature of Oil

Atoms bind together to fulfill the eight-electron octet in their outer valence shell. Atoms in the middle of the periodic table need to gain or lose three or four electrons to fill the octet. This is accomplished through covalent bonds where atoms bind together to form molecules by sharing electrons. Generally, covalent bonds occur between similar atoms whose electronegativity[1] (EN) difference is less than 0.5 allowing the boned electrons to be equally and symmetrically shared between the atoms. However, when unlike atoms bind together the shared electrons are distributed unevenly, favoring the atom with the higher EN to form polar covalent bonds. This leads to the development of van der Walls forces where the side of the molecule with the lower EN becomes partial positive (δ^+) while the other side becomes partial negative (δ^-) (McMurry 2012). Polarizability refers to the ease with which the electron cloud of an atom or molecule is distorted by an outside influence to induce a dipole moment (Brown, LeMay et al. 2017).

The bonds between carbon ($EN = 2.5$) and hydrogen ($EN = 2.1$) are covalent due to their similar EN, however polar covalent bonds are formed when carbon bonds with oxygen ($EN = 3.5$) or Nitrogen ($EN = 3.0$) (McMurry 2012). In alcohols the OH functional group

---

[1] Electronegativity is the intrinsic ability of an atom to attract the shared electrons in a covalent bond. Fluorine has the highest EN of 4.0 and cesium the least, 0.7 McMurry, J. (2012). Organic chemistry. Belmont, Calif., Brooks Cole..

creates strong polar bonds due to the large 1.4 EN difference between oxygen and hydrogen. These strong polar bonds lead to increased boiling points and water solubility as compared to alkanes (Boye, Keeping et al. 2009).

<div align="center"><i>iv.   Carboxylic Acids and Acid Number (AN)</i></div>

Carboxylic acids ($RCOOH$) (Figure 5) are common in organic material and serve as the starting material for many carboxylic derivatives (McMurry 2012). Like alcohols, carboxyl groups ($COOH$) form strong polar bonds due to the OH group. These polar bonds result in even higher boiling points and water solubility than in the corresponding alcohol (Boye, Keeping et al. 2009). In the presence of water the carboxylic acid can deprotonate to produce salts consisting of hydronium (H_3O^+) and carboxylate groups ($RCOO^-$) (Boye, Keeping et al. 2009).

$$RCOOH + H_2O \rightleftharpoons RCOO^- + H_3O^+ \hspace{3cm} (3.18)$$
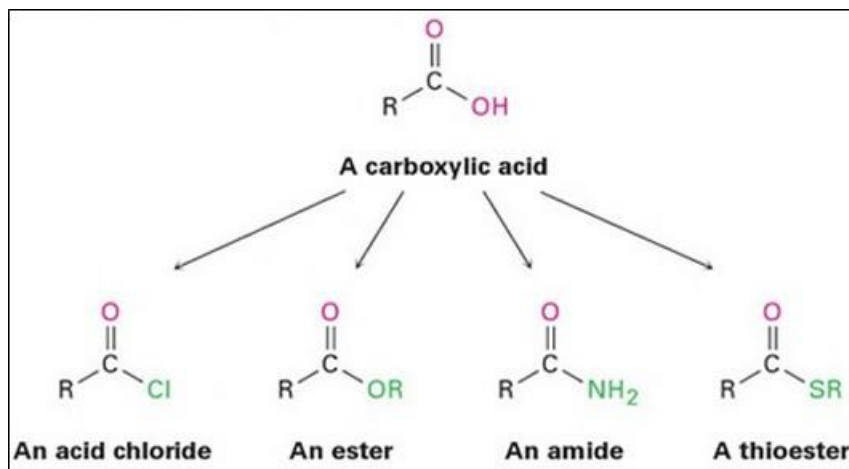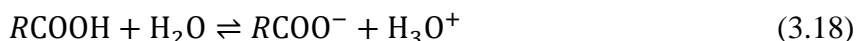
Figure 5 Line-bond structure of carboxylic acid and some common carboxylic acid derivatives

The components in petroleum can be neutral (nonpolar), acidic or basic. The deprotonation of carboxylic acid is an example of a weak organic acid. In addition, petroleum often contains nonorganic acids like carbon dioxide (CO_2) or hydrogen sulfide (H_2S). The common term used to express the amount of acidic components present is a crude oil is called total acidic number (TAN) or simply acidic number (AN). The TAN or AN is normally determined by the mass of the base potassium hydroxide (KOH) in milligrams titrated into a one-gram sample ($mg\ KOH/g$) of oil that is required reach a neutral pH of 7 or some other specified endpoint..

Amines are the basic compounds that form when one or more of the $H - atoms$ in ammonia (NH_3) are replaced by a carbon group (R). Similar to acid number, the base number (BN) is used to express the amount of basic components present is a crude oil. The BN expresses the quantity of acid in milligrams of potassium hydroxide per gram of sample $(mg\ KOH/g)$ that is required to titrate a sample to a specified end point (ASTM 1998 (2003)), i.e. pH 7.

I.   Rock - Carbonates

Rocks are made of minerals, which are solid, homogeneous, crystalline substances (usually inorganic) with a specific chemical composition that occur naturally. Having a crystalline structure implies that the atoms are arranged in an orderly, repeating three-dimensional array, while chemical composition refers to the ratio of atoms that is either fixed or varies within defined limits (Grotzinger and Jordan 2010). The composition of minerals can vary due to cation substitution where cations having similar size and charge can replace each other.

The most abundant chemical minerals are carbonates such as calcite $(CaCO_3)$, which is the main constituent of limestone (Grotzinger and Jordan 2010). Carbon and oxygen atoms join to form the carbonate anion (CO_3^{2-}) (Figure 6a) which is the basic building block of carbonates. Although carbonates can precipitate chemically from seawater, most limestone is composed of calcareous organisms formed in sedimentary basins (Bjørlykke and Avseth 2010). The carbonate ions group together in sheets that are held together by layers of one or more cations (Grotzinger and Jordan 2010). The two most common bonding cations in carbonates are calcium (Ca^{2+}) and magnesium (Mg^{2+}) ions (Bjørlykke and Avseth 2010). In calcite the cation layers are calcium ions (Ca^{2+}) (Figure 6), while dolomite has alternating layers of calcium and magnesium (Mg^{2+}) Other common bonding cations include iron II (Fe^{2+}), manganese (Mn^{2+}), strontium (Sr^{2+}), zinc (Zn^{2+}), barium (Ba^{2+}), lead (Pb^{2+}) (Table 2) (Bjørlykke and Avseth 2010). (Grotzinger and Jordan 2010).
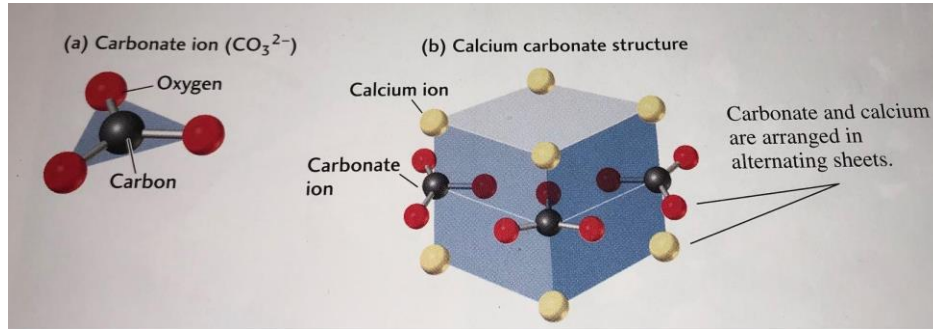
Figure 6 (a) Carbonate ion composed of carbon surrounded by three oxygen atoms in a triangle. (b) View of the alternating layers of calcium and carbonate ions in calcite (Grotzinger and Jordan 2010).

Table 2 Minerology of the most common carbonate minerals (Bjørlykke and Avseth 2010)

Name	Mineral
Low-Mg calcite	$CaCO_3 \ (< 4\% \ MgCO_3)$
High-Mg calcite	$(Ca, Mg)CO_3 \ (> 4\% \ MgCO_3)$
Aragonite	$CaCO_3$
Siderite	$FeCO_3$
Magnesite	$MgCO_3$
Strontianite	$SrCO_3$
Rhodochrosite	$MnCO_3$
Smithsonite	$ZnCO_3$
Witherite	$BaCO_3$
Cerrusite	$PbCO_3$
Ankerite	$Ca(Mg, Fe)(CO_3)_2$
Dolomite	$CaMg(CO_3)_2$
Witherite	$CaMg(CO_3)_2$

The 1962 Dunham classification of carbonates (Figure 7) is based on depositional texture of the limestone and nature of the matrix framework. Mud is defined as carbonate particles with a grain size < 20μm. In the figure as we move from left to right, the quantity of mud decreases as grains increases. Mudstones, wackestones and packstones are generally poor reservoir rocks because of the carbonate mud in the matrix. Grainstones and boundstones tend to have good porosity and permeability if cements precipitation is not too advanced (Bjørlykke and Avseth 2010).
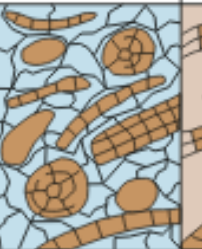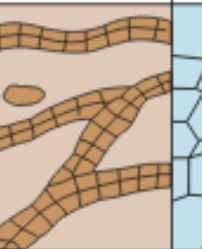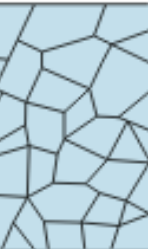
Figure 7 Dunham (1962) classified carbonate rocks according to depositional texture (Bjørlykke and Avseth 2010)

J. Brine Composition and Properties
i. Formation water

All pore water can be referred to as subsurface water while produced water and water analyzed from exploration wells is usually called formation water (FW) or oil field brines (Bjørlykke and Avseth 2010). Subsurface waters are mainly derived from four sources: buried seawater, meteoric water (precipitation that filters into ground water), released water from mineral dehydration, and juvenile water (hydrothermal water from igneous activity) (Bjørlykke and Avseth 2010).

The composition of the subsurface water will be a factor of the water source, the mineral composition of the rock, the burial depth, temperature, and the amount of time the system has had to reach equilibrium. Meteoric waters have the lowest mineral concentrations, usually less than 10,000 ppm dissolved material and may also contain oxygen and bacteria that can

Table 3 Composition of synthetic formation water used in study and synthetic seawater (Austad 2013)

Comp	Ekofisk	Seawater
Na^+	0.685	0.450
K^+	0	0.010
Mg^{2+}	0.025	0.045
Ca^{2+}	0.231	0.013
Cl^-	1.197	0.528
HCO_3^-	0	0.002
SO_4^{2-}	0	0.024

breakdown hydrocarbons (Bjørlykke and Avseth 2010). The composition of meteoric water will change as it travels through the ground and reacts with the soluble minerals in the rock. Sea water normally contains 35,000 ppm of dissolved material consisting of ions like sodium (Na^+), chlorine (Cl^-), magnesium (Mg^{2+}), calcium (Ca^{2+}), bicarbonate (HCO_3^-), and sulfate (SO_4^{2-}) (Bjørlykke and Avseth 2010). The sulfate concentration just below the sea floor reduces due to sulfate reduction with iron (Fe^{2+}). At lower temperatures the negative charge of clay minerals will attract cations like potassium (K^+) and magnesium (Mg^{2+}) to the surface, while the strongly hydrated ions like sodium (Na^+) and lithium (Li^+) will remain mobile (Bjørlykke and Avseth 2010). As temperature increases hydration becomes less effective and the hydrated ions are available to be adsorbed on to the surface. At temperatures from 70-100°C smectite dissolves into illite and water, and from 120-140°C kaolinite dissolves into illite, quartz and water. This process consumes cations, particularly potassium (K^+) leading to reduced salinity in shales (Bjørlykke and Avseth 2010). In most cases the concentration of dissolved solids in pore water increases to 100,000 to 300,000 ppm due to evaporite beds and increasing temperatures that reduce precipitation (Bjørlykke and Avseth 2010). Concentrations of common ions found in the Ekofisk formation and synthetic seawater (SSW) are listed in Table 3.

ii.   *Injected water*

Most oil reservoirs are water flooded today. As a secondary oil recovery process, water flooding improves oil recovery by maintaining the reservoir pressure above the bubble point pressure ($P_{res} > P_b$) and displaces oil from the pores.

As a tertiary recovery process termed "Smart Water", it may be possible to change the wetting properties of the rock by altering the injection water composition so it differs from the composition of the formation (Austad 2013). The concept of Smart Water in central to this study and is therefore discussed in more detail later in the theory section.

K.   Acid-Base Chemistry

Acidity and Basicity are important concepts that describe the polarity and electronegativity interactions in the COBR environment. Two commonly accepted definitions are the Brønsted-Lowry and Lewis acids and bases. In practice it is common to use the method that best describes the particular process at hand.

Brønsted-Lowry describe acids as the substance donating a hydrogen ion (H^+) and the base as the substance receiving the H^+ (also referred to as a proton). This acid-base reaction is described by the general formula where the reactants are the acid (HA) and the base (B), and the products are the conjugate base (A^-) and the conjugate acid (HB^+), written here as the hydronium ion (H_3O^+)

$$HA + B \rightleftharpoons A^- + H_3O^+ \tag{3.19}$$

Strong acids react almost completely with bases while weak acids only donate some of their protons. The strength of the acid is given by the acidity constant (K_a), where the brackets [ ] around a substance refer to the concentration in molarity (moles per liter) of the species.

$$K_a = \frac{[H_3O^+][A^-]}{[HA]} \tag{3.20}$$

Acid strength can be expressed as the negative common logarithm of K_a called pK_a.

$$pK_a = -\log K_a \tag{3.21}$$

A strong acid has a large K_a and a small pK_a, the inverse is true for weak acids. Additionally, a strong acid has a weak conjugate base, while a weak acid has a strong conjugate base. This means strong acids easily release their proton and the conjugate base has a weak hold onto the proton, resulting in a higher concentration of hydronium ions. For weak acids, both the acid and the conjugate base hold the proton tightly resulting in a low concentration of hydronium ions (McMurry 2012).

The Lewis definition describes acids as a substance that accepts an electron pair and a base as the substance that donates an electron pair. The donated electron pair is shared between the acid and the base in a covalent bond.

i. Hydrogen bonding

An important property of water is hydrogen bonding. When hydrogen bonds covalently with a small highly electronegative (EN) atom (N, O, F) a dipole is formed because the EN atom attracts the electrons more than the hydrogen, resulting in a positive dipole (δ^+) on the hydrogen side and a negative dipole (δ^-) on the EN side. The dipole creates an electrostatic attractive force that binds the hydrogen of one atom with the EN atom of the other molecule. The strength of the hydrogen bond is between $10 - 40 \ kJ \ mol^{-1}$ (Indira and Chatwal 2010) and is the force that gives water a relatively high boiling point, viscosity and surface tension, and also makes water a good solvent for polar substances (Bjørlykke and Avseth 2010)

ii. Auto ionization of Hydrogen

The strong polar nature of water allows it to be amphiprotic, meaning it can act as an acid or a base. Two water molecules can react to form hydronium and hydroxide (OH^-) in an autoionization process (Brown, LeMay et al. 2017)

$$H_2O_{(l)} \rightleftharpoons H_3O^+_{(aq)} + OH^-_{(aq)} \tag{3.22}$$

The concentrations of hydronium and hydroxide produced by the autoionization process of pure water at 25 °C are equal $(10^{-7} \ M)$. The acidity constant of water (K_w) at 25 °C is therefore 10^{-14}, and increases with temperature to $5 \ x \ 10^{-13}$ at 100 °C (Brown, LeMay et al. 2017)

$$K_w = [H_3O^+][OH^-] = 1.006 \cdot 10^{-14} \tag{3.23}$$

iii. pH and pOH

The term p refers to the potential of the hydrogen ion and is used to describe the acidity or basicity of an aqueous solution based on the negative logarithm of hydronium concentration (pH) or hydroxide concentration (pOH) (Brown, LeMay et al. 2017). The range of the scale is determined by the negative logarithm of K_w, which is temperature dependent.

$$pH = -\log[H_3O^+] \tag{3.24}$$

$$pOH = -\log[OH^-] \tag{3.25}$$

$$pK_w = -\log[K_w] \tag{3.26}$$

At 25 °C pK_w is approximately 14, so basic solutions will have a $pH > 7$ and acidic solutions will have a $pH < 7$. As temperature increases pK_w decreases. As a result the shift between acidic and basic solutions occurs at one half pK_w.

The concentration of hydronium can be found using 10^{-pH}. Similarly, hydroxide concentration can be determined by taking 10^{-pOH} or $10^{(pH-pK_w)}$.

L. Equilibrium of Minerals and Water

The following section is a summation from (Appelo 2005, Sheng 2010) describing equilibrium calculations of ion and complex concentrations in aqueous solutions. Consider the following generalized chemical reaction where the capital letters A and B are the reactant species and C and D represent the product species. The small letters, a, b, c, d are the stochiometric coefficients indicating the number of moles of each species.

$$aA + bB \rightleftharpoons cC + dD \qquad (3.27)$$

Most reactions of this type follow the law of mass action (LMA) which states that for a given temperature and pressure the equilibrium of equation 3.27 can be expressed by the equilibrium constant (K) of the mass action equation (MAE).

$$K = \frac{products}{reactants} = \frac{[C]^c[D]^d}{[A]^a[B]^b} \qquad (3.28)$$

The brackets [ ] indicate the concentration or activity of each species in molarity $\left(C_i, \frac{mols\ of\ solute}{unit\ volume\ of\ solution}\right)$ or the molality $\left(m_i, \frac{mols\ of\ solute}{unit\ weight\ solvent}\right)$. Note that the concentrations for water and solids are assumed as one and cancel out.

Ionic strength (I) is a brine parameter that measures the strength (amount of charged species) of a solution based on the molar concentrations (C_i) of all the ions in the solution (n).

$$I = \frac{1}{2}\sum_{i=1}^{n} C_i z_i^2 = \frac{1}{2}\sum_{i=1}^{n} \frac{m_i}{m_o} z_i^2 = \frac{1}{2}\sum_{i=1}^{n} m_i z_i^2 \ [dimensionless] \qquad (3.29)$$

The term m_i is divided by a standard state molality (m_o) to render I dimensionless. The valance (z) is the charge of each ion. Activities $[i]$ indicate the effective concentrations of each species dependent on the I of the solution. The activities are calculated by multiplying C_i or m_i by an activity coefficient (γ_i).

$$[i] = \gamma_i \frac{m_i}{m_o} = \gamma_i\, m_i\ [\text{dimensionless}] \tag{3.30}$$

There are three common conventions used to determine the activity coefficient (γ_i): Debye-Hückel formula, Davies equation and Truesdell and Jones. The Debye-Hückel formula is used for specific ions when $I < 0.1$.

$$\log \gamma_i = -\frac{A(T)\, z_i^2\, \sqrt{I}}{1 + B\, å_i\, \sqrt{I}} \tag{3.31}$$

The terms A and B are temperature dependent constants; $A(25°C) = 0.5085$ and $B(25°C) = 0.3285 \cdot 1010\ m$. The term $å_i$ is a value found in tables indicating the effective diameter of the hydrated ion and is multiplied by $10^{10}\ m$.

The Davies equation can be used for I between 0.1 and 0.5. This convention is not ion-specific and provides the same value for all ions with the same absolute valance $|z|$.

$$\log \gamma_i = -A(T)\, z_i^2 \left(\frac{\sqrt{I}}{1 + \sqrt{I}} - (0.3 \cdot I) \right) \tag{3.32}$$

The Truesdell-Jones/Parkhurst convention is a modified version of the Debye-Hückel formula with the addition of table generated ion specific parameters a_i and b_i, and the term $å_i$ is excluded. This convention is used when I is between 0.5 and 2.0.

$$\log \gamma_i = -\frac{A(T)\, z_i^2\, \sqrt{I}}{1 + B\, a_i\, \sqrt{I}} + b_i I \tag{3.33}$$

In an aqueous solution some ions will be "free" while others may attach to one another to form aqueous complexes like $CaSO_4^0, CaCl_2^0, CaCl^+$. The complex is termed outer sphere if water molecules exist between the constituent ions and inner sphere if the ions expel the water between them to form covalent bonds with each other.
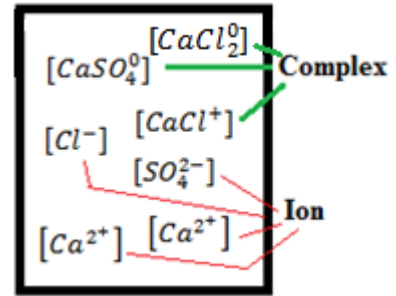
MAE are applicable to aqueous complexes. The equilibrium constant (K) is termed stability constant (K_1) for ion-association equations and dissociation constant (K_2) if the equation is reversed and whereby $K_2 = 1/K_1$.

Mass balance equations (MBE) are written for each species in the aqueous solution in the form

$$C_i = m_i + \sum_j n_{ij} \qquad (3.34)$$

Here (C_i) represents the total concentration an atom, ion or species (i); m_i is the concentration of free species; and n_{ij} is the concentration of complex j that contains the free species i. Both m_i and n_{ij} are given in molal units.

Complexation lowers the activity of the "free" ion in water, thereby increasing the solubility of minerals and mobility of trace metals. This necessitates computing their combined effect using an iterative process to solve several unknowns at once.

The first step is to write a MAE in the form of equation 3.27 for each mineral and determine the concentration of each species. Use these concentrations in equation 3.29 to compute an initial ionic strength (I) of the solution. Based on the value of I, choose the appropriate equation (3.31, 3.32 or 3.33) to calculate the activity coefficients (γ_i) and then use equation 3.30 to determine the activities $[i]$ for each species. Now determine which complexes will form in the solution and write an MBE for each species in the form of equations 3.34 and an MAE for each complex in the form of equation 3.27. It is necessary to formulate at least as many equations as there are

unknown m_i and n_{ij}. The MBE are then solved simultaneously in excel, PHREEQC or by another means to determine the unknown molar (m_i) and total concentrations (C_i) of each species. Following each iterative step the values for γ_i and I are updated and the process continues until no significant improvement in molar concentration occurs.

M. Saturation states

The saturation state of a solution can be expressed using the saturation index (SI), which is the log of ion activity product of the mineral (IAP_{min}) divided by the solubility product of the mineral $(K_{SP,min})$ (equation 3.35) (Appelo 2005). Both the IAP_{min} and $K_{SP,min}$ are applications of the LMA in the form of equation 3.28. The IAP_{min} is obtained by inserting the actual concentrations or activities of the species into equation 3.28, while the $K_{SP,min}$ is a temperature dependent constant that occurs when the mineral is in equilibrium with the aqueous solution. When $IAP_{min} = K_{SP,min}$ the solution is at equilibrium and the maximum amount of mineral will be dissolved into the solution as indicated by an SI of zero. If SI is less than zero, the solution is undersaturated and the mineral will dissolve into the solution. The mineral will precipitate out of the solution when SI is greater than zero.

$$SI = \log\left(\frac{IAP_{min}}{K_{SP,min}}\right) \tag{3.35}$$

i. Calculation of mass action constants

It is possible to calculate $K_{SP,min}$ using the change in Gibbs free energy $\left(\Delta Gr\,\frac{KJ}{mol}\right)$ and table data (Appelo 2005).

$$\Delta G_r = \Delta G_r^o + RT\ 2.303 \log\frac{[C]^c[D]^d}{[A]^a[B]^b} \tag{3.36}$$

Where T is the absolute temperature in Kelvin (K), R is the gas constant $\left(8.314 \cdot 10^{-3}\,\frac{KJ}{mol \cdot K}\right)$, and ΔG_r^o is the standard Gibbs free energy of the reaction when the activity product in the log term is equal to one in which case $\Delta G_r = \Delta G_r^o$ at a specified standard state (25°C and 1 atm). As discussed in the section on saturation states, the activity product in the log term is equal to $(K_{SP,min})$ at equilibrium and (IAP_{min}) at actual concentrations. It is necessary to use the change in energy because energy can only be measured in relative amounts.

At equilibrium $\Delta G_r = 0$ and equation 3.36 reduces to

$$\Delta G_r^o = -RT\ 2.303 \log K_{SP,min} \tag{3.37}$$

Back substation of equation 3.37 into 3.36 gives

$$\Delta G_r = -RT\ 2.303 \log K_{SP,min} + RT\ 2.303 \log IAP_{min} \tag{3.38}$$

Analogous to the formulation of SI, equation 3.37 can be written to indicate the distance from equilibrium

$$\Delta G_r = RT\ 2.303 \log \left(\frac{IAP_{min}}{K_{SP,min}} \right) \tag{3.39}$$

It is possible to calculate a value for ΔG_r^o using the following equation

$$\Delta G_r^o = \sum \Delta G_{f\ products}^o - \sum \Delta G_{f\ reactants}^o \tag{3.40}$$

The terms ΔG_f^o are the Gibbs free energy of formation taken from tabulated data at that indicate the energy needed to produce one mole of a substance from pure elements in their most stable form at a standard temperature and pressure, usually 25°C and 1 atm. The value obtained for ΔG_r^o is inserted into equation 3.37, which is then solved for $K_{SP,min}$

While variations in pressure usually have little effect, changes in temperature can alter $K_{SP,min}$ significantly (Appelo 2005). The Van't Hoff equation can be used to estimate $K_{SP,min}$ as temperature changes.

$$\frac{d \ln K_{SP,min}}{dT} = \frac{\Delta H_r}{RT^2} \tag{3.41}$$

Integration of equation 3.41 from temperature T₁ to T₂ gives the following relationship.

$$\log K_{SP,min}(T_1) - \log K_{SP,min}(T_2) = \frac{-\Delta H_r^0}{2.303R}\left(\frac{1}{T_1} - \frac{1}{T_2}\right) \qquad (3.42)$$

Where ΔH_r is the reaction enthalpy, which indicates the heat lost or gained by the chemical reaction. In an exothermic reaction $\Delta H_r < 0$. The system (solution) loses energy causing the surroundings (container) to heat up. In an endothermic reaction $\Delta H_r > 0$ and the system gains energy causing the surrounding to cool. The term ΔH_r^o is the standard state reaction enthalpy and similar manner to ΔG_r^o, it can be calculated from formation enthalpies $\left(\Delta H_f^o\right)$ listed in thermodynamic tables and equation 3.43.

$$\Delta H_r^o = \sum \Delta H_{f\ products}^o - \sum \Delta H_{f\ reactants}^o \qquad (3.43)$$

ii.   Equilibrium with dissolved calcite

In a closed system consisting of only calcite crystals dissolved in pure water the solution will not be influenced by complexes nor CO_2 in the atmosphere, and the process can be described by the simple dissolution equation (Appelo 2005)

$$CaCO_3(s) \rightleftharpoons Ca^{2+}(aq) + CO_3^{2-}(aq) \qquad (3.44)$$
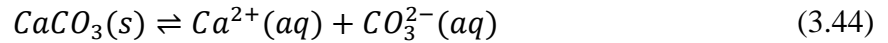
Applying the LMA in the form of equation 3.28 gives the following relationship where the concentrations of calcium and carbonate are the same at equilibrium

$$K_{SP,Calcite} = [Ca^{2+}][CO_3^{2-}] = [Ca^{2+}]^2 = 10^{-8.48} \qquad (3.45)$$

From equation 3.44 the calcium and carbonate concentrations can be predicted by taking the square root of the solubility product

$$[Ca^{2+}] = [CO_3^{2-}] = \sqrt{10^{-8.48}} = 10^{-4.24} \qquad (3.46)$$

In an open system the concentration of carbon dioxide (CO_2) in water has a significant influence on pH and the solubility of carbonates, and thereby the carbonate reactions. CO_2 gas from the atmosphere dissolves in water to form aqueous CO_2. Some of the CO_2 will associate with water to form carbonic acid (H_2CO_3), which dissociates into bicarbonate (HCO_3^-), and eventually

carbonate (CO_3^{2-}) and protons (H^+). (Bjørlykke and Avseth 2010). According to Le Châtelier principle an increase in CO_2 will force equilibrium to the right and increase $[H^+]$ thereby reducing pH.

$$CO_{2(aq)} + H_2O \rightleftharpoons H_2CO_3 \rightleftharpoons HCO_3^- \rightleftharpoons CO_3^{2-} + 2H^+ \tag{3.47}$$
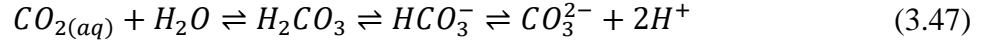
Looking at an open system with calcite a similar process occurs

$$CO_{2(aq)} + H_2O + CaCO_{3(s)} \rightleftharpoons Ca^{2+} + 2HCO_3^- \rightleftharpoons Ca^{2+} + 2CO_3^{2-} + 2H^+ \tag{3.48}$$
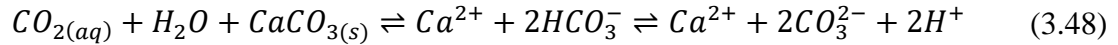
Applying the Le Châtelier principle to the above equation shows that an increase CO_2 concentration or an increase in pH (reduced $[H^+]$) will cause equilibrium to shift to the right thereby increasing the solubility of calcite. Conversely, calcite will precipitate out of solution if CO_2 is removed from the system or pH is reduced. The solubility of CO_2 in water is greatest at low temperatures and high pressures (Bjørlykke and Avseth 2010).

iii.   The carbonic acid system

In an open system without calcite, CO_2 from the atmosphere will dissolve in pure water to form aqueous CO_2.

$$CO_{2(g)} \rightleftharpoons CO_{2(aq)} \tag{3.49}$$

Some of the aqueous CO_2 will associate with water to form carbonic acid.

$$CO_{2(aq)} + H_2O \rightleftharpoons H_2CO_{3(aq)} \tag{3.50}$$

The activity of a gas $[P_i]$ is given by its partial pressure (P_i). In an open system the P_{CO_2} for atmospheric CO_2 is $10^{-3.5}$ (Appelo 2005) and is used to represent the concentration of CO_2 gas in equations.

$$P_i = \frac{pressure\ of\ gas\ i}{total\ pressure} = [P_i] \tag{3.51}$$

Because $CO_{2(aq)}$ is typically 600 times more abundant than H₂CO₃ at 25°C (Appelo 2005), the following convention is used to facilitate calculations

$$CO_{2(g)} + H_2O \rightleftharpoons H_2CO_{3(aq)}^* \qquad (3.52)$$

where

$$H_2CO_{3(aq)}^* = CO_{2(aq)} + H_2CO_{3(aq)} \qquad (3.53)$$
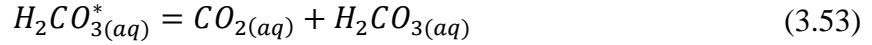
Dissolution of carbonic acid releases two protons, which will decrease the pH of the system thereby affecting the concentration of dissolved carbonates. Equations 3.52 and 3.53 will be forced to the left in accordance with the Le Châtelier principle. The reactions in Table 4 occur simultaneously and can be used along with the mass action constants to make manual calculations of the solution composition

Table 4 Equilibria in the carbonic acid system with approximate equilibrium constants at 25 °C		
$H_2O \rightleftharpoons H_{(aq)}^+ + OH_{(aq)}^-$	$K_w = [H^+][OH^-] = 10^{-14.0}$	(3.54)
$CO_{2(g)} + H_2O \rightleftharpoons H_2CO_{3(aq)}^*$	$K_H = [H_2CO_3^*]/[P_{CO_2}] = 10^{-1.5}$	(3.55)
$H_2CO_{3(aq)}^* \rightleftharpoons H_{(aq)}^+ + HCO_{3(aq)}^-$	$K_1 = [H^+][HCO_3^-]/[H_2CO_3^*] = 10^{-6.3}$	(3.56)
$HCO_{3(aq)}^- \rightleftharpoons H_{(aq)}^+ + CO_{3(aq)}^-$	$K_2 = [H^+][CO_3^-]/[HCO_3^-] = 10^{-10.3}$	(3.57)

The pH of a solution is the negative log of the H^+ concentration

$$pH = -\log[H^+] \qquad (3.58)$$

Therefore $[H^+]$ can be expressed as

$$[H^+] = 10^{-pH} \qquad (3.59)$$

Using equation 3.59 for hydronium concentration the equations in table 3.x can be rearranged and simplified using back substitution to generate the following equations

$$[H_2CO_3^*] = K_H \cdot [P_{CO_2}] \qquad (3.60)$$

$$[HCO_3^-] = \frac{K_1 \cdot [H_2CO_3^*]}{[H^+]} = \frac{K_1 \cdot K_H \cdot [P_{CO_2}]}{10^{-pH}} \qquad (3.6161)$$

$$[CO_3^{2-}] = \frac{K_2 \cdot [HCO_3^-]}{[H^+]} = \frac{K_2 \cdot K_1 \cdot K_H \cdot [P_{CO_2}]}{10^{-2pH}} \qquad (3.6262)$$

Total inorganic carbon (TIC) is a term used to express the mass of all carbon species in molal concentrations that are dissolved in a brine solution. In a closed system TIC is constant, but in an open system it is variable due to the formation of carbonic acid from atmospheric CO_2 and water.

$$TIC = m_{H_2CO_3^*} + m_{HCO_3^-} + m_{CO_3^{2-}} \qquad (3.6363)$$

If the activity coefficients (γ_i) are assumed 1, it is possible to express TIC in terms of $K_{SP,min}, pH,$ and P_{CO_2} using substitution and equations 3.51, 3.55, 3.56, 3.57 and 3.59 to obtain

$$TIC = P_{CO_2} \cdot K_H \left(1 + K_1 \frac{1}{10^{-pH}} + K_2 \cdot K_1 \frac{1}{10^{-2pH}}\right) \qquad (3.64)$$

Equations 3.62-3.64 show that if P_{CO_2} remains constant then the concentrations of H_2CO_3 and P_{CO_2} will remain constant regardless of pH. On the other hand, both bicarbonate and carbonate concentrations will be influenced by pH. The concentrations of the three carbonate species divided by TIC are plotted in figure Figure 8.
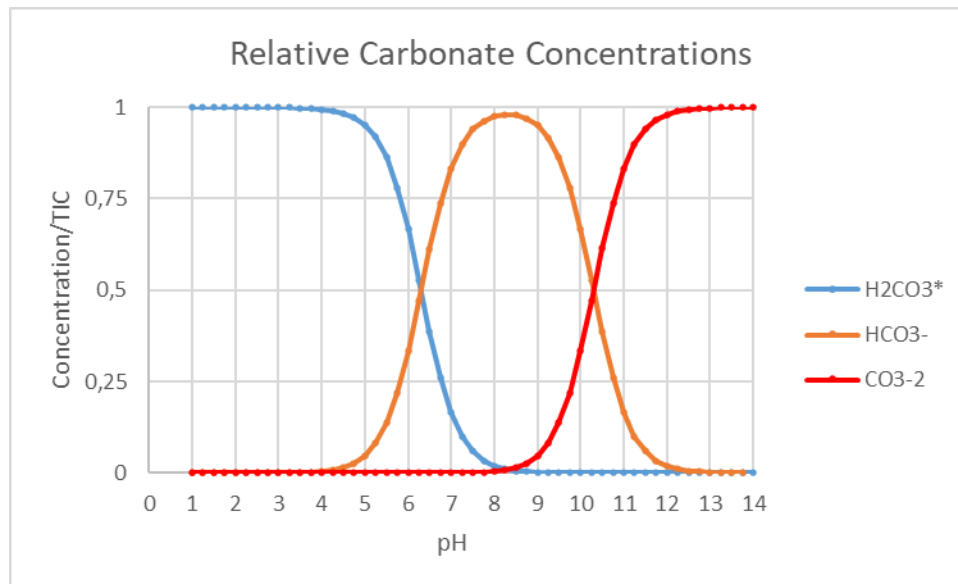
Figure 8 The relative concentrations of carbonate species in an open system as a function of pH. At low pH carbonic acid and P_{CO_2} dominate, while carbonate dominates at high pH. The concentration of bicarbonate dominates when pH is between 6.3 and 10.3.

N. Ion exchange

The following section is summarized from Sheng (2010). Ions in a solution that is in contact with a solid may undergo sorption processes where the ions can adsorb to the surface, absorb into the solid or exchange place with another ion on the surface. In a reservoir, the formation will likely have reached a state of equilibrium with the surrounding brine and oil. Introduction of a new brine with a different composition may initiate a sorption process.

In an EOR process ion exchange at surface sites normally occurs between cations. Species with higher charge densities (multivalents or small ionic radii) have a higher affinity to clay and occur in the following order

$$Li^+ < Na^+ < k^+ < Rb^+ < Cs^+ < Mg^{2+} < C^{2+} < Sr^{2+} < Ba^{2+} < H^+$$

The capacity for a given rock to exchange cations is expressed in terms of cation exchange capacity (CEC). The units for CEC are usually given in milliequvalent per kiologram of rock (meq/kg) or milliequvalent per liter pore volume (meq/L PV). Generally the value of CEC increases linearly with the surface area per gram of rock. CEC also increases with clay content and inorganic carbon. The pH in the system will affect CEC. If protons adsorb onto the surface the CEC will increase, but CEC will decrease if the surface is dissolved by the protons.

$$CEC \left[\frac{meq}{kg} \right] = \frac{\sum n_i z_i}{m_{rock}} \tag{3.65}$$

Where n_i is the number of millimoles of species i, z_i is the valence of the cation and m_{rock} is the mass of the rock in kg. Using the rock density (ρ_r), porosity ($\emptyset$) and liters of pore volume (L PV) the CEC can be converted to (meg/LPV) using the following conversion:

$$CEC \left[\frac{meq}{kg} \right] / \left(\frac{\emptyset}{\rho_r (1 - \emptyset)} \right) = CEC \left[\frac{meq}{L\ PV} \right] \tag{3.66}$$

The LMA can be modified for application to ion exchange where the solute species (A) with valance (a) replaces another species (B) with valance (b) at an adsorption site (X) with a charge of one. It is assumed that a cation will occupy an equal number of sites as its valance and that all sites on the surface are always occupied.

$$\frac{1}{a}A^a + \frac{1}{b}(B\text{-}X_b) \rightleftharpoons \frac{1}{a}(A\text{-}X_a) + \frac{1}{b}B^b \tag{3.66}$$

$$K_{A-B} = \frac{[A\text{-}X_a]^{\left(\frac{1}{a}\right)}[B^b]^{\left(\frac{1}{b}\right)}}{[B\text{-}X_b]^{\left(\frac{1}{b}\right)}[A^a]^{\left(\frac{1}{a}\right)}} \tag{3.67}$$

The subscript of the equilibrium constant ($K_{A\text{-}B}$) (more appropriately called selectivity or exchange coefficient) is written so the first species to be a solute (A) precedes the adsorbed species (B). The magnitude of $K_{A\text{-}B}$ indicates the reactiveness or affinity of the two ions toward the solid. The larger the value of $K_{A\text{-}B}$ the greater tendency of species A to attach to the surface.

Note that the brackets [ ] now indicate activities instead of concentrations, however there are several methods to calculate exchange activities and they are not the same as previously discussed in the section on "Minerals and Water". For ion exchange the terms β_I (Gaines-Thomas convention) or β_I^m (Vanselow convention) are used to denote activities at the exchange site and they represent the fraction of all available exchange sites that are occupied by a specific ion. In a standard state all exchange sites are occupied by the same species so $\beta_I = \beta_I^M = 1$, otherwise we have the condition that $\sum_{I,J,K} B_I = \sum_{I,J,K} B_I^M = 1$ (where I, J, K,… are the exchangeable cations with charges i, j, k,…). For ion I^{i+} the Gaines-Thomas convention calculates the equivalent fraction (β_I) of ion i in relation to CEC, or the total charge of the surface

$$\beta_I = \frac{meq\ I\text{-}X_i\ per\ kg\ sediment}{CEC} = \frac{meq_{I\text{-}X_i}}{\sum_{I,J,K\dots}meq_{I\text{-}X_i}} = \frac{n_i z_i}{\sum n_i z_i} \tag{3.68}$$

In the Vanselow convention the molar fraction (β_I^m) of ion I is calculated in relation to total exchangeable cations (TEC), or the total number of available sites

$$\beta_I^M = \frac{mmol\ I\text{-}X_i\ per\ kg\ sediment}{TEC} = \frac{(meq_{I\text{-}X_i})/i}{\sum_{I,J,K\dots}(meq_{I\text{-}X_i})/i} = \frac{n_i z_i \frac{1}{z_i}}{\sum n_i z_i \frac{1}{z_i}} \tag{3.7069}$$

The convention used is a matter of choice. For homovalent exchange (exchange ions have the same valance) both conventions provide similar results, however the difference is quite significant for heterovalent exchanges, and the Gaines-Thomas convention appears to be a better choice. Using the exchange term β_I, the LMA can be written as follows

$$K_{A-B} = \frac{[A\text{-}X_a]^{\left(\frac{1}{a}\right)} [B^b]^{\left(\frac{1}{b}\right)}}{[B\text{-}X_b]^{\left(\frac{1}{b}\right)}[A^a]^{\left(\frac{1}{a}\right)}} = \frac{\beta_A^{\left(\frac{1}{a}\right)} [B^b]^{\left(\frac{1}{b}\right)}}{\beta_B^{\left(\frac{1}{b}\right)}[A^a]^{\left(\frac{1}{a}\right)}} \tag{3.7170}$$

In table data the values for K_{A-B} are often given in relation to one solute, i.e. Na^+. To find the value for K_{A-B} involving the exchange of two cations listed in the (B) portion K_{A-B}, divide the K_{A-B} of the solute cation by the K_{A-B} of the cation on the exchange site. For example, if $K_{Na-Ca} = 0.40$ and $K_{Na-Al} = 0.70$ then

$$K_{Ca-Al} = \frac{K_{Na-Ca}}{K_{Na-Al}} = \frac{0.40}{0.70} = 0.57 \tag{3.7271}$$

In a system consisting of only monovalent and divalent cations where the brine concentration and exchange coefficients (K_{A-B}) are known, it is possible to calculate the exchange compositions (β_I) of each cation on the surface. Begin by writing general reaction (in the form of equation 3.71) and exchange coefficient (in the form of equation 3.72) for each exchange ion. Rearrange each of the exchange coefficient formulas to form expressions for β_I and substitute those expressions into the following equation and solve using the quadratic equation

$$\beta_I + \beta_J + \beta_K + \cdots = 1 \tag{3.7372}$$

An example of the process to calculate exchanger composition is given in example 6.4 in (Appelo 2005)

Exchanger compositions can be calculated using the program PHREEQC discussed under surface complexation modeling.

O. COBR interactions in carbonates

The carbonate surface at reservoir conditions tends to be positively charged and will strongly attract heavy end crude oil components (resin and asphaltene fractions) that contain the negatively charged carboxylate group ($RCOO^-$). The degree of crude oil adsorption on the carbonate surface increases with increasing AN and will alter the wettability toward strongly oil wet, which drastically reduces water imbibition rates and
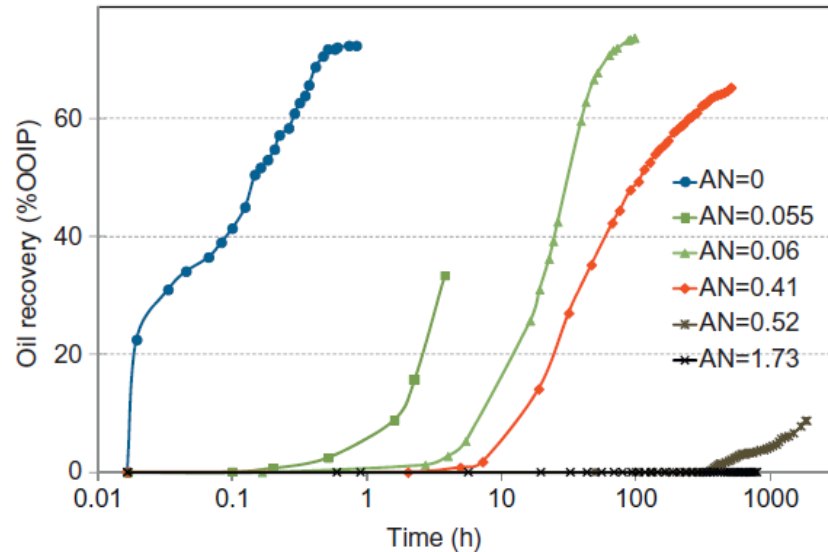
Figure 9 Spontaneous imbibition into chalk cores saturated with different oils (Austad 2013)

hence oil recovery (Figure 9). Conversely, an increase in BN tends to improve water wetness. (Austad 2013)

Wettability alteration is also influenced by other conditions in the reservoir. Increasing temperatures appear to increase water wetness by decreasing AN due to increased decarboxylation of the acidic material. Decreasing pressure toward the bubble point reduces asphaltene solubility causing them to precipitate out of the crude oil and onto the rock. The composition of the FW can also alter wettability, particularly an increase in sulfate concentration will increase water wetness of the system. (Austad 2013)

P. Transport of fluid phases

As a solution is transported away from the injector through a porous medium the effects of retardation (R_C), diffusion (D) and dispersion (D_L) will change the concentration (C) of the solute thereby reducing the effects of smart water with respect to distance. This reduction will be gradually mitigated in time as more solute is transported through the medium. Other pertinent factors affecting the solute concentration include length (l), time (t), speed of the water (v_w),

initial concentration in the medium (C_0), injected concentration (C_{inj}), rate of sorption (dq) of the ion onto or off the mineral surface and temperature (T).
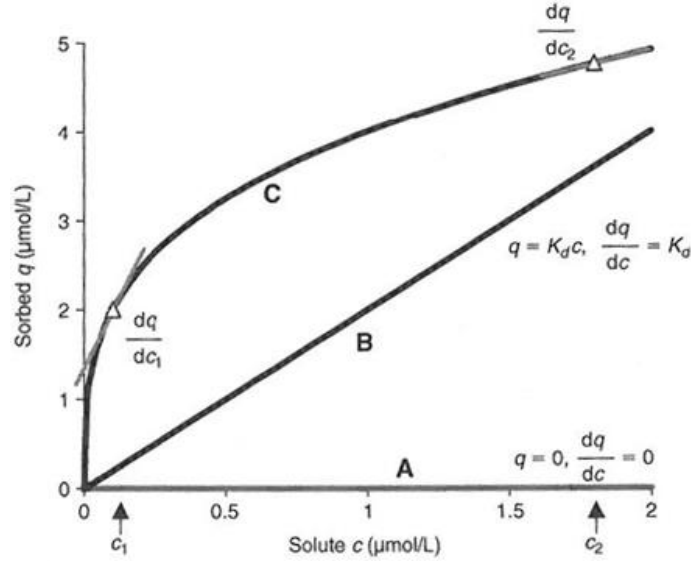
Figure 10 Depiction of sorption isotherms: A no sorption, B linear sorption, C non-linear convex Freundlich isotherm (Appelo 2005)

i. Retardation

The term sorption refers to any process of adsorption onto a surface, desorption from a surface or absorption into a body. Advection is the transport of the ions by the water flow in one direction. The speed of the concentration (v_C) will be equal to or less than the speed of the water (v_w) depending on the rate of sorption with respect to concentration $\left(\frac{dq}{dC}\right)$. The speed of the concentration (v_C) is given by the retardation equation (Appelo 2005)

$$v_C = \frac{v_w}{R_C} \tag{3.73}$$

Where R_C is the retardation factor expressing how much v_C is reduced in comparison to v_w

$$R_C = 1 + \frac{dq}{dC} \tag{3.74}$$

There are three basic advection isotherm scenarios (Figure 10) to describe the rate of sorption with respect to concentration $\left(\frac{dq}{dC}\right)$ (Appelo 2005):

37

A. Non-sorption $\qquad q = 0 \qquad \Longrightarrow \qquad \dfrac{dq}{dC} = 0$

B. linear sorption $\qquad q = c \qquad \Longrightarrow \qquad \dfrac{dq}{dC} = K_d$

C. non-linear sorption $\qquad q = K_F \cdot C^n \qquad \Longrightarrow \qquad \dfrac{dq}{dC} = n \cdot K_F \, C^{(n-1)}$

Where K_d is the distribution coefficient constant for linear sorption and K_F and n are the Freundlich isotherm constants for non-linear sorption processes.

If there is no sorption of species (case A), then $v_c = v_w$. An example is Cl^- which is often used as a tracer since it does not adsorb. If sorption occurs at a constant linear rate (case B) then v_C will travel at a slower, but constant rate in relation to v_w. Most concentrations will follow the non-linear (case C) Freunlich isotherm, and v_C will vary with the rate of sorption as determined by the concentration.

The reactive transport equation describes the change in concentration with respect to time for advection

$$\frac{\partial C}{\partial t} = -v_w \frac{\partial C}{\partial l} - \frac{\partial q}{\partial t} \tag{3.75}$$

ii. Diffusion

Over time, uneven concentrations in a stagnant solution will be equalized through Brownian motion of the molecules. This 3D process is called molecular diffusion and is described by Fick's laws. Fick's first law of diffusion relates the flux of a chemical (F) as a vector quantity that describes the magnitude and direction of the chemical based on the concentration gradient $\left(\frac{\partial C}{\partial x}\right)$ and a diffusion coefficient (D).

$$F = -D \frac{\partial C}{\partial x} \tag{3.76}$$

Fick's second law of diffusion describes how concentrations deteriorate over time due to diffusion.

$$\frac{\partial C}{\partial t} = D \frac{\partial^2 C}{\partial x^2} \qquad (3.77)$$

Larger values of D indicate that concentrations will become uniform quicker.

iii. Dispersion

The tortuosity of a porous medium will force solute traveling by advection to change direction and spread. This is referred to as dispersion. There are two types of dispersion. Longitudinal dispersion (D_L) accounts for the differences in travel time due to the varying lengths of the tortuous pathways. Transverse dispersion (D_T) occurs because diffusion causes the flow to enter adjacent pathways. The spreading of concentration fronts can be mathematically quantified by combining the reactive transport and the diffusion equation

$$\frac{\partial C}{\partial t} = -v_w \frac{\partial C}{\partial l} - \frac{\partial q}{\partial t} + D_L \frac{\partial^2 C}{\partial l^2} \qquad (3.78)$$

This equation is referred to as the ARD equation because the first term describes Advective flow, the second term describes chemical Reactions and the third term describes Dispersion. The ARD equation is difficult to solve mathematically, therefore a statistical approach is normally used. The scope of which is beyond this study.

Q. Smart Water Theory

Spontaneous imbibition (SI) of water into carbonates is a mechanism that can be used to produce oil from the reservoir. It was first introduced in the highly fractured carbonate Spraberry field in west Texas in the early 1950s. The driving force of SI is a positive capillary pressure (Pc), which occurs in water-wet rock. Unfortunately, 90% of carbonate reservoirs are neutral to oil-wet which prevents the occurrence of SI (Ravari 2011). Waterflooding of fractured carbonate reservoirs may therefore be less efficient than expected in recovering oil because the injected water will channel through fractures rather than imbibing in to the matrix.

The basis of "Smart Water" as an EOR process is to alter the composition of the injection water in order to change the wetting properties of the crude oil, brine, rock (COBR) system, thereby

altering Pc and relative permeability of oil and water to increase oil recovery (Austad 2013). In relation to traditional EOR methods, Smart Water is inexpensive and environmentally friendly as no expensive chemicals are added. In addition, there are no injection problems. For best results the smartest water should be used from the start of the water flooding process. (Austad 2013)

Due to the high concentration of Ca^{2+} in FW, the surface of carbonates at reservoir conditions tends to be positive. Deprotonation of the carboxylic group (COOH), which is found mostly in the heavy end fraction of crude oil (resins and asphaltenes), forms negatively charged carboxylic groups (COO$^-$) that are strongly attracted to the positive carbonate surface. (Austad 2013)

Seawater contains potentially determining ions (PDI) such as Ca^{2+}, Mg^{2+}, and SO_4^{2-} that can react with the carbonate surface to alter the surface charge (Austad 2013). At natural pH levels the initial charge of the carbonate reservoir surface is positive due to a high concentration of Ca^{2+} and Mg^{2+} in the FW, while the concentration of negative PDI like SO_4^{2-} and CO_3^{2-} are low or non-existent. Sulfates in the injected brine will be attracted to the carbonate surface thereby reducing the positive charge. This allows the concentration of Ca^{2+} near the surface to increase. The Ca^{2+} ions can then bind to the negatively charged carboxylic groups and free them from the surface (Figure 11a). (Austad 2013) At low temperatures the small Mg^{2+} ion has a strong hydration energy, but as temperature increases it becomes less hydrated and more reactive with the carbonate surface. The Mg^{2+} ions are now available to displace the calcium carbonate complex [RCOOCa]$^+$ from the surface (Figure 11b) (Austad 2013).

In order to achieve wettability modification, the imbibing water must contain either Ca^{2+} and SO_4^{2-} or Mg^{2+} and SO_4^{2-}, but oil recovery increases if all three PDIs are included in the injection brine as the presence of Mg^{2+} hinders the precipitation of $CaSO_4(s)$ (anhydrite). (Austad, Strand et al. 2008)

Temperature plays a significant role on the effectiveness of the process described above. At low temperatures ($\leq 100°C$) increasing the concentration of SO_4^{2-} above that found in sea water can increase oil recovery nearly two-fold. However, at high temperatures (130°C) increasing SO_4^{2-}

concentrations above that found in sea water has little effect on oil recovery and CaSO₄(s) begins to precipitate. (Austad 2013)
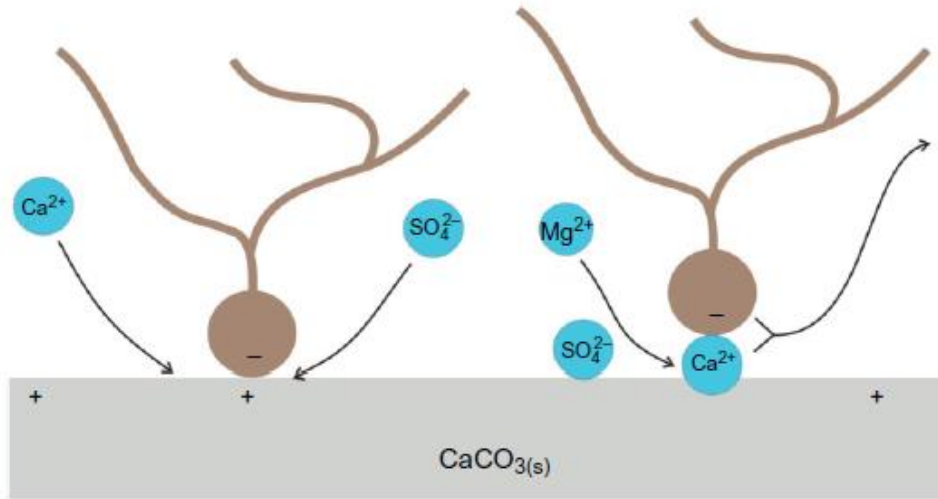
Figure 11 Schematic model of the suggested mechanism for the wettability alteration induced by seawater. (a) Proposed mechanism when main Ca²⁺ and SO₄²⁻ are active at lower temperature and (b) proposed mechanism when Mg²⁺ and SO₄²⁻ are active at higher temperatures. (Zhang, Tweheyo et al. 2007)

Although the reactivity of the PDI to the surface can vary depending on the type of carbonate (chalk, limestone, dolomite), the mechanism described seems to apply. However some studies have shown that the mechanism works on reservoir limestone, but not on outcrop limestone. (Austad 2013)

If the core material contains a small amount of CaSO₄(s) in the matrix then injection of diluted FW can increase oil recovery as $SO_{4(aq)}^{2-}$ is created in situ by the dissolution of anhydrite making available to adsorb to the surface $\left(SO_{4(ad)}^{2-}\right)$ in the following equation

$$CaSO_{4(s)} \rightleftharpoons Ca_{(aq)}^{2+} + SO_{4(aq)}^{2-} \rightleftharpoons Ca_{(ad)}^{2+} + SO_{4(ad)}^{2-}$$
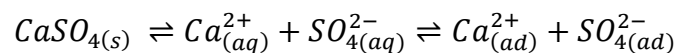
R. Surface Complexation Modeling

The surface complexation model (SCM) proposed by Brady, Krumhansl et al. (2012) provides a means to predict wettability by determining the charge (zeta potential (ζ)) on oil and mineral surfaces as a function of the brine chemistry. Adsorption and desorption of ions into the stern layer are predicted by changes to ζ (Bonto, Eftekhari et al. 2019).

The crude oil and mineral surfaces are simulated using solution analogues consisting of equilibrium equations and temperature dependent surface complexation log Ks. The analogues are processed in conjunction with the brine composition using the program PHREEQC (Parkhurst and Appelo 2013) to determine the resulting molar fractions of charged species on the oil and mineral surfaces. A description and copy of the coding used in PHREEQC in this thesis are included in the appendices B and C. The resulting electrostatic adhesion between the mineral and oil is then estimated using a bond product sum (BPS). The BPS is calculated by multiplying molar fractions of each charged species on the oil $[X_{oil,i}]$ surface by the molar fractions of each oppositely charged species on the mineral surface of the rock $[X_{min,j}]$ (Figure 12). The resulting products are then added together to attain the BPS. If all species on both surfaces have neutral or the same charge the BPS will be zero and no oil will be able to adsorb onto the surface indicating a completely water wet surface. A completely oil wet condition will be indicated by a BPS of one and will occur if all of the species on the oil surface have the same or a neutral charge while all of the species on the mineral have a neutral or the same charge in relation to each other, but opposite of the charge on the oil surface.

$$BPS = \sum_{1}^{i,j} [X_{oil,i}][X_{min,j}] \tag{3.80}$$
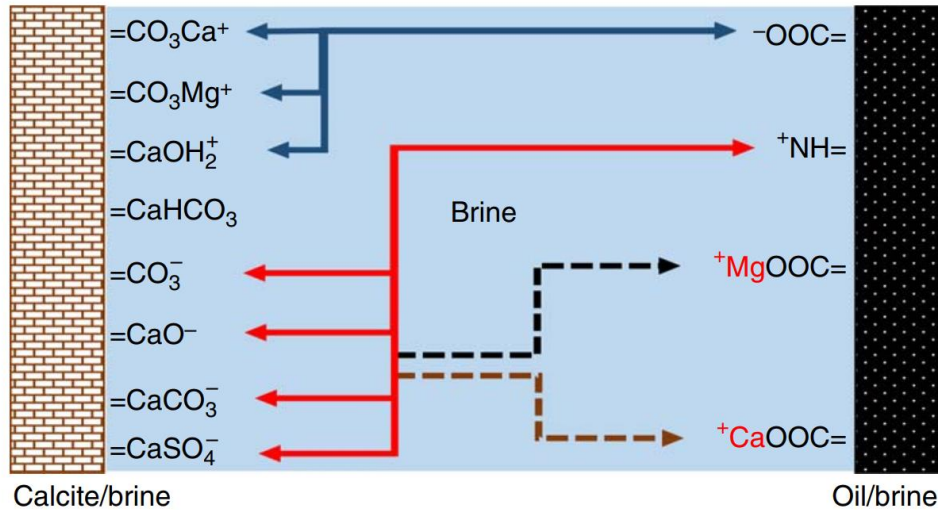
Figure 12 Illustration of the charged species on the calcite and oil surfaces. The bond product is calculated by multiplying the mole fraction of oppositely charged species on each surface. (diagram provided by Erzuah (2017))

The solution analogue for crude oil are the carboxylic acids (_COOH) and amines (_NH$^+$), where the underscore indicates attachment to the surface (Figure 12). The carboxylic acid sites can undergo dissociation or react with divalent cations from the brine. In the model the amin groups can only undergo protonation (Bonto, Eftekhari et al. 2019). For calcite the solution analogues are hydrated carbonate (_CO$_3$H°) and hydrated calcium (_CaOH°) (Wolthers, Charlet et al. 2008). Both of these species can undergo dissociation, protonation and react with divalent cations. The polar components in crude oil can bond directly to oppositely charged exchange sites on the rock surface. Cation bridging via divalent ions provides a means for oil to bond on a mineral with a similar surface charge.

SCM computations are performed using PHREEQC version 3, a freeware program from the USGS used to perform aqueous geochemical calculations through the simulation of chemical reactions and transport processes (Parkhurst and Appelo 2013). The program is based on equilibrium chemistry of aqueous solutions interacting with minerals, gases, solid solutions, exchangers, and sorption surfaces. The program can use Charge Distribution MULtiSIte Complexation (CD-MUSIC) (Wolthers, Charlet et al. 2008) or the diffuse-layer model (Van Cappellen, Charlet et al. 1993) to perform SCM. Modelling allows for multiple binding sites for each surface, and the charge, potential and sorbed species can be distributed over the Stern layer

and the Helmholtz layer (Figure 13). Temperature effects are modeled using the Van't Hoff reaction enthalpy equation. Ion exchange is modeled using the Gaines-Thomas, Gapon or Vanselow conventions.

The electro kinetic measurements rely on the assumption that the zeta potential (ζ) is the potential at the boundary (shear plane) between the immobile and mobile phases near the outer Helmholtz plane (OHP) (Bonto, Eftekhari et al. 2019). At low ionic strength ζ occurs near or at the OHP and can be fitted using the Debye Hückel approximation (Song, Zeng et al. 2017), where ψ_0 is the potential at the shear plane, κ is the Debye length and d_s is the distance of the slipping plane from the OHP.

$$\zeta = \psi_0 \exp(-\kappa d_s) \tag{3.8179}$$

PHREEQC calculates the composition of the electrical double layer (EDL) and ζ through explicit integration of the Poisson-Boltzman equation to determine the concentration of ions in the brine $(n_i(x)\ mol/m^3)$

$$\frac{d^2\psi(x)}{dx^2} = -\frac{F}{\varepsilon\varepsilon_0} \sum_{i=1}^{N} z_i(n_i(x) - n_i^0) \tag{3.8280}$$

$$n_i(x) = n_i^0 \exp\left(-\frac{z_i F\psi(x)}{RT}\right) \tag{3.83}$$

Where $F\ [C/mol]$ is the Faraday constant, $\varepsilon_0 = 8.85\ x\ 10^{-12}\ F/m$ is the vacuum permittivity, ε is the relative permittivity of water, z_i is the ionic valency, ψ is the surface potential and n_i^0 is the bulk concentration $[mol/m^3]$.

Figure 13 shows a description of the generalized double layer model with a surface plane and a diffuse layer. Surface potential is equivalent to the potential at the outer Helmholtz plane
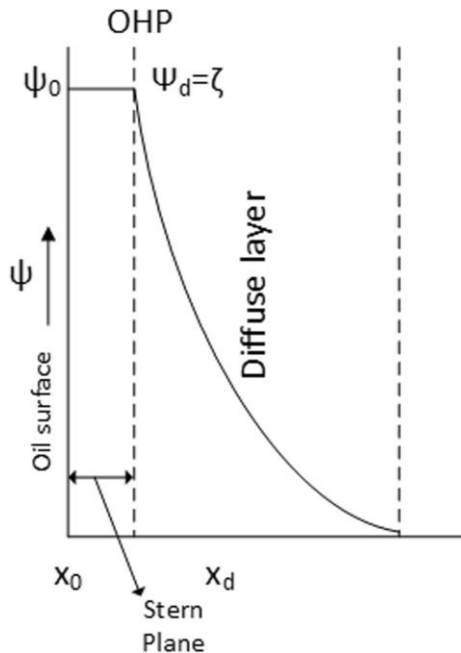
Figure 13 Schematic of the double layer model. The ψ equals ψ_0 up to x_d and then decays exponentially with the distance x. (Bonto, Eftekhari et al. 2019)

$(z = z_d)$ where all ions are considered being absorbed in the same plane. The Poisson-Boltzmann equation is used to establish the relationship of potential and concentration of ions in brine.

1.   Advantages

-    SCM can be used to optimize injection brine composition to promote wettability alteration toward water wet that may encourage dissolution of polar oil components from the rock surface, thereby leading to increased oil production.

-    Low cost as PHREEQC is a publicly available, freeware program

-    The data bases are amendable by the user

2. Disadvantages

-    The PHREEQC databases are not all inclusive

-    The logarithms of equilibrium constants (log Ks) and enthalpies have been taken from literature and not verified experimentally.

-    The default ion-exchange formulation assumes that the activity of an exchange species is equal to its equivalent fraction, which can be multiplied by a Debye-Hückel activity coefficient, but other calculation methods would have to be written into the data base

-    Mole fraction is used in SCM instead of molarity which may increase uncertainties when multidentate surface species are present.

-    Experimental data is often required on material to adjust SCM

45

S. Amott-Harvey

Amott-Harvey is modified from the original Amott method used to determine quantitatively the average wettability of a core using both forced displacement and imbibition. In the following procedures, centrifuging can be replaced by dynamic displacement in a sample core holder. Prior to conducting measurements, the core is cleaned and then centrifuged under brine and then oil to reduce the plug to initial water saturation (S_{wi}) (Figure 14). Step 1, The core is Immersed in brine (Figure 14 left) until imbibition is complete (20 to 480 hours) and the volume of oil displaced as a function of time is measured, which is equal to the volume of water spontaneously imbibed (V_{wsi}). Step 2, Centrifuge the core in brine until residual oil saturation (S_{or}) is reached, and measure the volume of water forcibly imbibed (V_{wfi}), which is equal to the volume of oil displaced. Step 3, the core is immersed in oil (Figure 15 right) until imbibition is complete and the volume of water displaced, which is equal to the volume of oil spontaneously imbibed (V_{osi}) is measured as a function of time. Step 4, Centrifuge the core in oil until irreducible water saturation (S_{wir}) is reached and measure the volume of water displaced, which is the volume of oil forcibly imbibed (V_{ofi}).
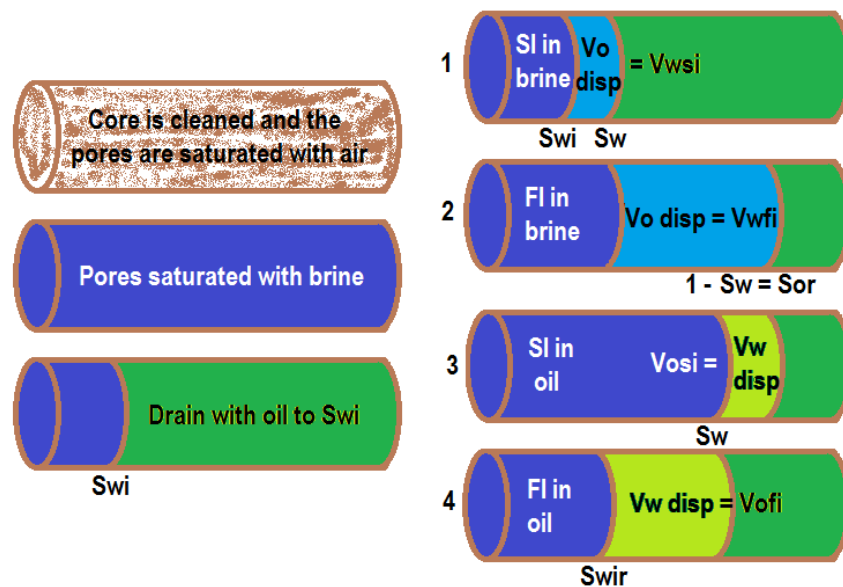
Figure 14 Core saturations during the preparation (left) and four steps of the Amott-Harvey wettability test (right). Dark blue is water, light blue is imbibed water, dark green is oil and light green is imbibed oil.

Determine the displacement-by-oil ratio (δ_o) and displacement-by-water ratio (δ_w) using the following formulas.

$$\delta_w = \frac{V_{wsi}}{V_{wsi} + V_{wfi}}, \qquad \delta_o = \frac{V_{osi}}{V_{osi} + V_{ofi}} \qquad (3.81)$$

The Amott-Harvey relative displacement index (*IAH*) is obtained by taking the difference between the two displacement ratios.

$$IAH = \delta_w - \delta_o \qquad (3.82)$$

The value of *IAH* can vary from +1 indicating complete water wet to -1 indicating complete oil wet. Values between -0.3 and 0.3 are considered intermediate wet (Boneau and Clampitt 1977, Anderson 1986, McPhee, Reed et al. 2015).

1. *Advantages*

- Both reservoir core and fluids can be used in the test (Anderson 1986)
- Can give an indication of non-uniform wettability (Anderson 1986)

2. *Disadvantages*

- Insensitive to near neutral wettability as neither fluid will spontaneously imbibe when the contact angle varies from 60 to 120° (Anderson 1986)

Spontaneous water   Spontaneous oil
imbibition   imbibition
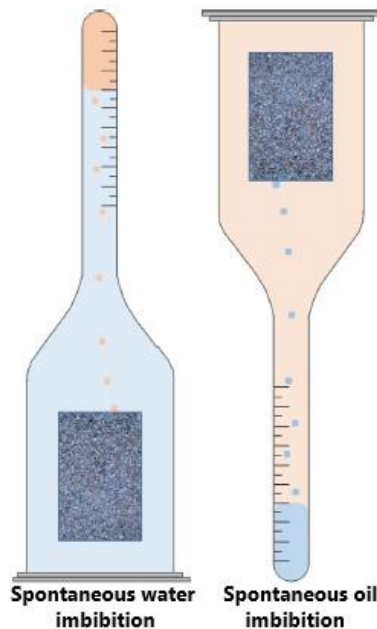
Figure 15 Amott cell schematic for spontaneous imbibition of water (left) and oil (right) (McPhee, Reed et al. 2015)

4) Experimental materials chosen
A. Core Material

The rock material used in this study is from an outcrop in the Edwards formation close to Garden City, West Texas. Edwards limestone was chosen for this study because the outcrop/mineral oil/brine system (initially water-wet) can be altered to oil-wet by aging in crude oil. Both mineral oils and crude oil were used in this study (further described in section C) allowing the investigation of PDI brine influence on wettability in both water-wet and intermediate-wet/weakly oil-wet core plugs. Edwards limestone is a cretaceous limestone also known as West Texas Crème, Cedar Hill Cream, or Valencia Ivory building stone. Based on the Dunham's classification it is a boundstone (its original components were bound together (e.g. by corals or algae) during deposition) (Allaby 2019). The limestone was characterized using thin section and a scanning electron microscope (SEM) micrographs (Figure 16), BET surface area was 0.2 m^2/g and cation exchange capacity (CEC) was 0.00026 meq/100g. Mercury injection and BJH pore structure analysis were used to obtain pore structure data for each rock type. Fractions of micro-, meso-, and macro-porosity (pore radius < 2.1 nm, 2.1 to 53nm, and > 53nm, respectively) have been identified from desorption/adsorption isotherms (Tie and Morrow 2005).

Measurements collected from 12 x 12 x 6-inch blocks showed homogeneous petrophysical data (Table 5 Core properties (Tie and Morrow 2005)). Air permeabilities and porosities of the cores fell in the range of 12.1±1.7 mD, and 21.0±0.3% respectively. This rock is composed mostly of calcite minerals both inside the rock and at the pore walls. Hardly any fine pore structure can be identified by SEM. Mercury injection (for the larger pores) and BJH pore structure analysis (for the very small pores) showed a relatively narrow pore size distribution and almost no pore throats of less than 30 nm radius. A peak in pore throat radii is indicated at around 5 µ by mercury injection. The secondary peak is probably artifact because it coincides with change in the mercury injection cell at 30 psi (Tie and Morrow 2005).

Table 5 Core properties (Tie and Morrow 2005)

Core	L,cm	D,cm	k, md	φ	S_{wi},%	σ , mN/m	Wetting state
Edwards (GC) (EGC)							
1EGC25A	3.74	6.41	11.3	0.206	0	50	VSWW
1EGC25B	3.74	6.45	10.9	0.212	0	50	VSWW
1EGC23B	3.74	6.24	11.4	0.213	19.8	29.7	MXW
1EGC24A	3.73	6.39	13.7	0.210	16.1	29.7	MXW
1EGC05A	3.80	6.26	11.6	0.208	16.0	29.7	MXW
1EGC06B	3.80	6.37	10.4	0.212	16.3	29.7	MXW-F
1EGC06A	3.80	6.38	12.9	0.210	16.3	29.7	MXW-DF
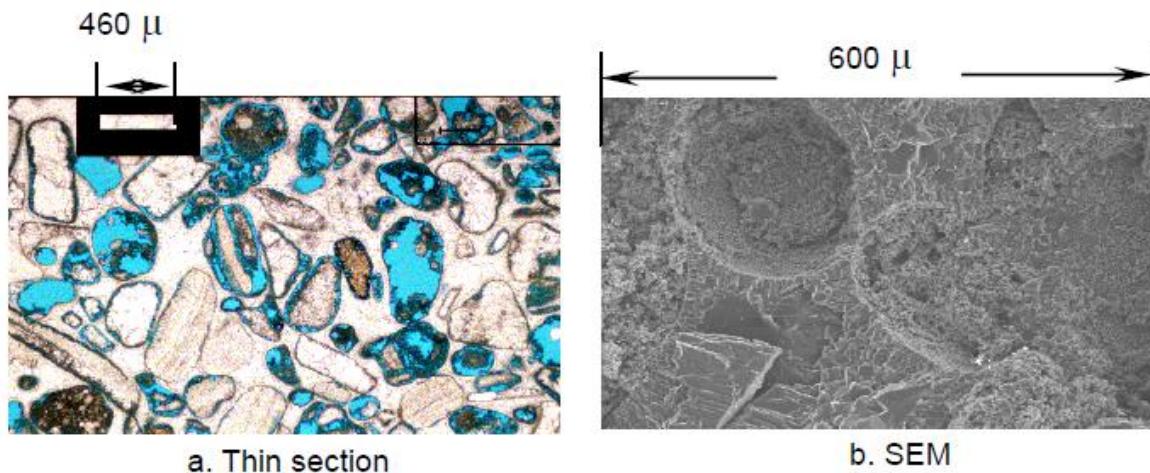
Figure 16 a. Edwards thin section, b. Edwards SEM (Tie and Morrow 2005)

Another thin section of Edwards outcrop core material (Figure 17) was prepared by Minoprep in Sweden with an analysis conducted by Michael R. Talbot at the University of Bergen and James J. Howard at COP Research Center. The pores were saturated with a special blue epoxy. The rock minerals and fragmental organic remains are indicated by the black and grey colors. The organic remains include mussel, snail and sea urchin Mollusca (shellfish). The scale in the bottom right corner is 0.5mm (Tipura 2008).
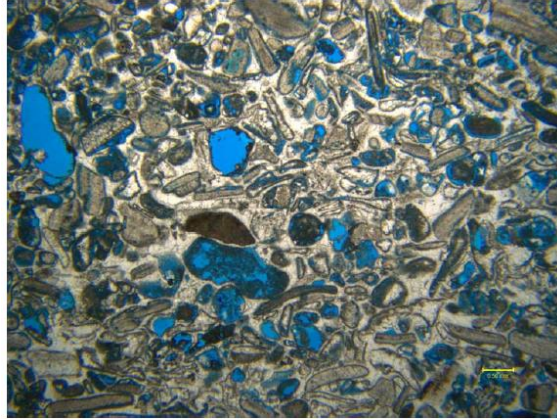
Figure 17 Thin section photo of Edwards limestone (Tipura 2008)

The pores are neither spherical nor very edgy, and their sizes vary with random distribution in the rock. The primary porosity is filled with sparry calcite cement, while the secondary porosity (a consequence of bioclastic dissolution) is dominant. In the sample the pore sizes range from 2 mm (rare) to a few microns (dominant) indicating a heterogeneous sample with varying porosity and permeability values No vugs are present in the sample. The rock was classified as bioclastic grain stone due to the high occurrence of large organic fragments. (Tipura 2008)

A mercury injection experiment performed on three samples in collaboration with ConocoPhillips Research Centre indicated pore throat radius ranged from 90 microns for the large pores to a range of between 0.1 and 0.01 microns for the smaller pores (Tipura 2008).

B. Brines

Three synthetic brines were selected for this study and their influence on wettability established. The compositions are listed in table 6 and given in molality (mol/kg water). The first is a synthetic formation water *(FW)* brine. The other two brines contain a higher concentration of potential determining ions *(PDI)* approximately 1.5 times higher than the levels of Ca^{2+}, Mg^{2+} and SO_4^{2-} found in seawater. The pH level of the first PDI brine was not adjusted. The pH level of the second PDI brine was elevated to approximately 9 (PDI pH~9). using a diluted solution of NaOH. The brines were mixed using deionized *(DI)* water filtered through a Merck Milli-DI filter (Figure 18). The chemicals used to make the synthetic brines were sodium chloride (NaCl), magnesium chloride hexahydrate (MgCl$_2$·H$_2$O), calcium chloride dihydrate (CaCl$_2$·H$_2$O) and sodium sulfate (Na$_2$SO$_4$). The antibacterial, sodium azide was added to each of the brine mixtures in the ratio of 0.5 ml antibacterial per kg of water.

Figure 18 Merck Milli-DI 22 μM filter. Feedwater conductivity = 0.04 S/m and 0 ppm dissolved CO$_2$. DI water quality resistivity > 1MΩ.cm at 25 °C. (Merck 2012)

An ATI model Q45 pH meter (Figure 19) was used to measure brine and effluent pH. The meter is capable of measuring pH in the range of 0.00 to 14.00 in a temperature range of -20 to 60 °C and ambient humidity of 0 to 95%. The accuracy and repeatability are listed as $\pm$ 0.01 pH. Instrument response time is 6 seconds to 90% of step input at the lowest setting. The operator's manual recommends cleaning the salt bridge and measuring electrode glass sensor using deionized or distilled water and a soft cloth. A mild, non-abrasive soap solution such as dishwashing liquid can be used. Soaps containing any oils such as lanolin can coat the glass electrode and harm sensor performance.

All cores were initially saturated with FW. After draining and fracturing as discussed in chapter five, the cores were subjected to a modified spontaneous imbibition (mod SI) process using one of three different brines: FW, PDI, and PDI pH~9. Cores were not tested using synthetic seawater (SSW), but a comparison was included in the SCM using PHREEQC. An ATI model Q45 pH meter (Figure 19) was used to measure the pH of brine samples taken from the bottle at 25°C just prior to filling the piston valve, and from the 90°C core holder injection end fitting after letting the brine cool due to pH meter limitations.

Figure 19 ATI model Q45 pH meter and sensor used to measure injection brine and effluent pH.

A preliminary test of the four brines listed in Table 6 was run in PHREEQC to estimate expected pH and precipitation of minerals at 25°C and 90°C in a closed system (no CO_2) and an open system (CO_2 partial pressure of $10^{-3.5}$ atmospheres). The saturation index (SI) for the various brines was calculated for the standalone brine and the brine in contact with the rock and crude oil surfaces. A negative SI indicates that the mineral is soluble in the solution and no precipitation is expected.

Table 6 Compositions of brines used in this study given in molality (mol/kg water). The antibacterial sodium azide was added to each brine in the ratio of 0.5 ml/kg of water. Synthetic seawater (SSW) from Austad (2013)

Brine	Cl^-	SO_4^{2-}	Mg^{2+}	Ca^{2+}	Na^+	TDS (g/l)	pH
FW	1.196	0	0.025	0.231	0.684	68.02	
SSW	0.528	0.024	0.045	0.013	0.450	33.39	
PDI	0.610	0.030	0.090	0.020	0.450	49.41	6.7
PDI pH~9	0.610	0.030	0.090	0.020	0.450	49.41	9.0

No precipitation was predicted by the PHREEQC analysis of the four standalone brines. The brines were mixed and checked at 25°C and 90°C in semi-open beakers with no visual evidence of precipitation. The SI values for all minerals tested (except anhydrite and gypsum) were lower than -2. The danger of precipitation is greatest for anhydrite in the PDI and PDI~9 brines at 90°C

for both open and closed systems. Here the SI values are slightly less than -0.2. There is a significant trend in in the SI values of aragonite, calcite and dolomite when going from an open to a closed system. Here the SI values go from minus infinity to a range between -2 and -10. The shift in SI values for sulfur when going from a closed to an open system shows a decrease in the risk of precipitation (Figure 20).

Another simulation was run in PHREEQC to test the brines in contact with the crude oil and carbonate surfaces. Figure 20 only contains the minerals that had an SI value greater than -2 indicating they are closer to precipitation. The conditions for the first three minerals: anhydrite, gypsum and dolomite are in an open system at 25°C or 90°C and in contact with either SSW, PDI or PDI pH~9 brine. Except for sulfur, closed system data is not included because the SI values were similar to the 25°C open system. Additionally, FW brine is not included because all SI values using FW were less than -2.
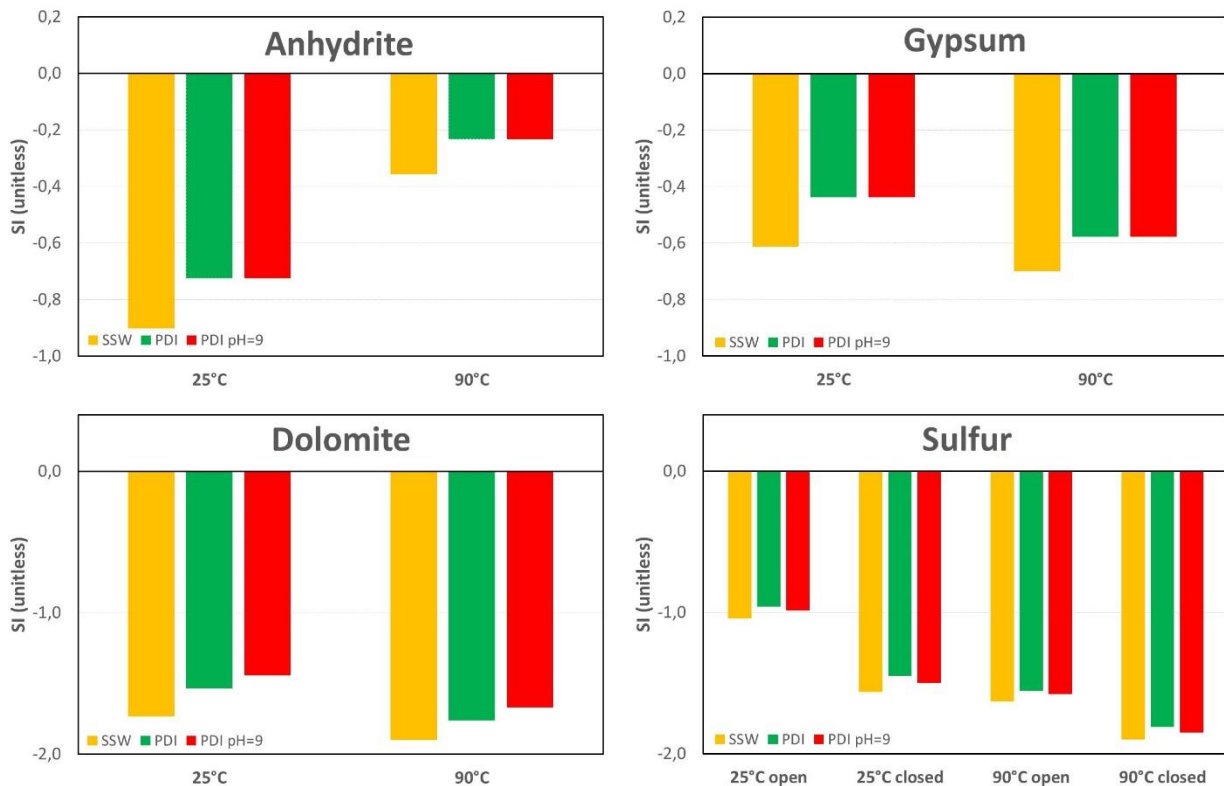
Figure 20 Diagrams showing the PHREEQC calculated saturation index (SI) for anhydrite, gypsum, dolomite and sulfur at 25°C or 90°C for the crude oil, carbonate system in the presence of SSW, PDI or PDI pH~9 brines. Precipitation is expected when SI increases above zero, so a line protruding further downward is preferred.

In Figure 20 (except for anhydrite) the risk of precipitation decreases with temperature. As expected, the risk of precipitation increases with ion concentration for all minerals. This was a concern in brine selection and limited the concentration of divalent cations that could be added to the brine. Although there is a slight decrease in the SI of dolomite, the increase in pH did not have a significant effect on the risk of precipitation. The addition of CO_2 in an open system has a detrimental effect on the solubility of sulfur, especially at lower temperatures.

C. Oil

Two types of oil were chosen for this study, n-decane and crude oil (table 9). Empirical formulas presented in chapter three were used to make temperature adjustments to the viscosity and IFT data in table 9. Densities for n-decane were adjusted using linear transformation for temperature.

Table 7 (a) Mineral and Crude Oil Properties from (Fernø, Torsvik et al. 2010)

	Density at 20°C (g/cm³)	Density at 90°C (g/cm³)	Viscosity at 20°C (cP)	Viscosity at 20°C (cP)
n-decane	0.73	0.68	0.92	0.40
Crude oil	0.85	0.85	14.3	2.7

(b) Crude Oil Composition

AN (mg of KOH/g of oil)	BN (mg of KOH/g of oil)	RI	API (deg)	Saturates (%)	Aromatics (%)	Resins (%)	Asphaltenes (%)
0.41±0.02	1.4 ±0.1	1.4834	27±3	61±3	20±1	19±1	0.59±0.03

D. Calculation of bond product sum (BPS) using PHREEQC

Table 8 Bond product sum (BPS) determined using the program PHREEQC. The BPS is calculated for synthetic seawater and the brines selected for the study. The brines are in contact with the crude oil and carbonate surfaces. The calculations were made at 25°C and 90°C. A BPS of zero is completely water wet and values near one indicate oil wet.

	25°C Open	25°C Closed	90°C Open	90°C closed
FW	1.30	1.31	1.01	1.03
SSW	1.19	1.13	1.01	1.02
PDI	1.20	1.12	1.01	0.94
PDI pH~9	1.19	1.12	1.01	1.02

A prediction of wettability was made using surface complexation modeling (SCM) and the program PHREEQC. A summary of the PHREEQC code is provided in appendix B and the actual code in appendix C. Although SSW was not used in the tests, it was included in the PHREEQC analysis as a reference. The higher BPS at 25°C indicate the system is more oil wet at lower temperatures. This would be expected as the heavier components in the crude oil will precipitate as temperature decreases. At 25°C the BPS for the open systems are also higher indicating a more oil wet system. At 90°C, with the exception of PDI brine there is a general trend for BPS to improve in the open system. According to the BPS data we would expect to see the greatest shift toward water wetness using the PDI brine at 90°C in a closed system.

5. Experimental procedures

A. Uncertainties

Methods used to calculate uncertainties are outlined in appendix A.

B. Filtering of oil

Cores selected to be water wet were drained using n-decane that had been filtered through silca gel 60, aluminum oxide and glass wool to remove polar components (Figure 21). The use of filtered decane results in water wet cores with an $IAH \sim 0.7$. The use of non-polar oil provides a reference to measure the effectiveness of the selected brines in the cores drained with crude oil containing polar components.
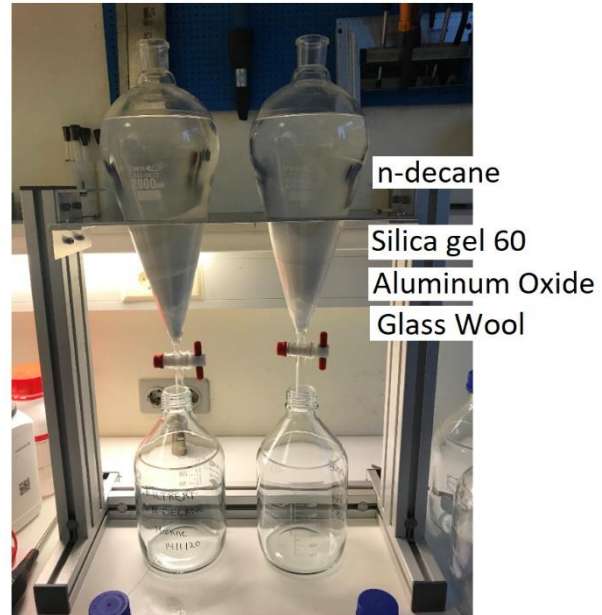
Figure 21 Setup for filtration of n-decane

Cores chosen to be oil-wet were dynamically aged using filtered crude oil and as outlined in (Fernø, Torsvik et al. 2010). Prior to aging the cores, the crude oil was filtered through a thin section of limestone core in the aging cabinet (Figure 22). The aging cabinet consists of two Quizix QX-1500 pumps, two Hassler core holders, two piston valves and two Equilibar EB1ZF1 series backpressure regulators (BPR). The filter was aged by injecting crude oil at 80°C through the section at 1 ml/hr for 48 hours in one direction and 48 hours in the other. The oil used to age the filter was discarded. Unfiltered crude oil was then injected from one piston cell through the aged filter and into another piston cell for storage.
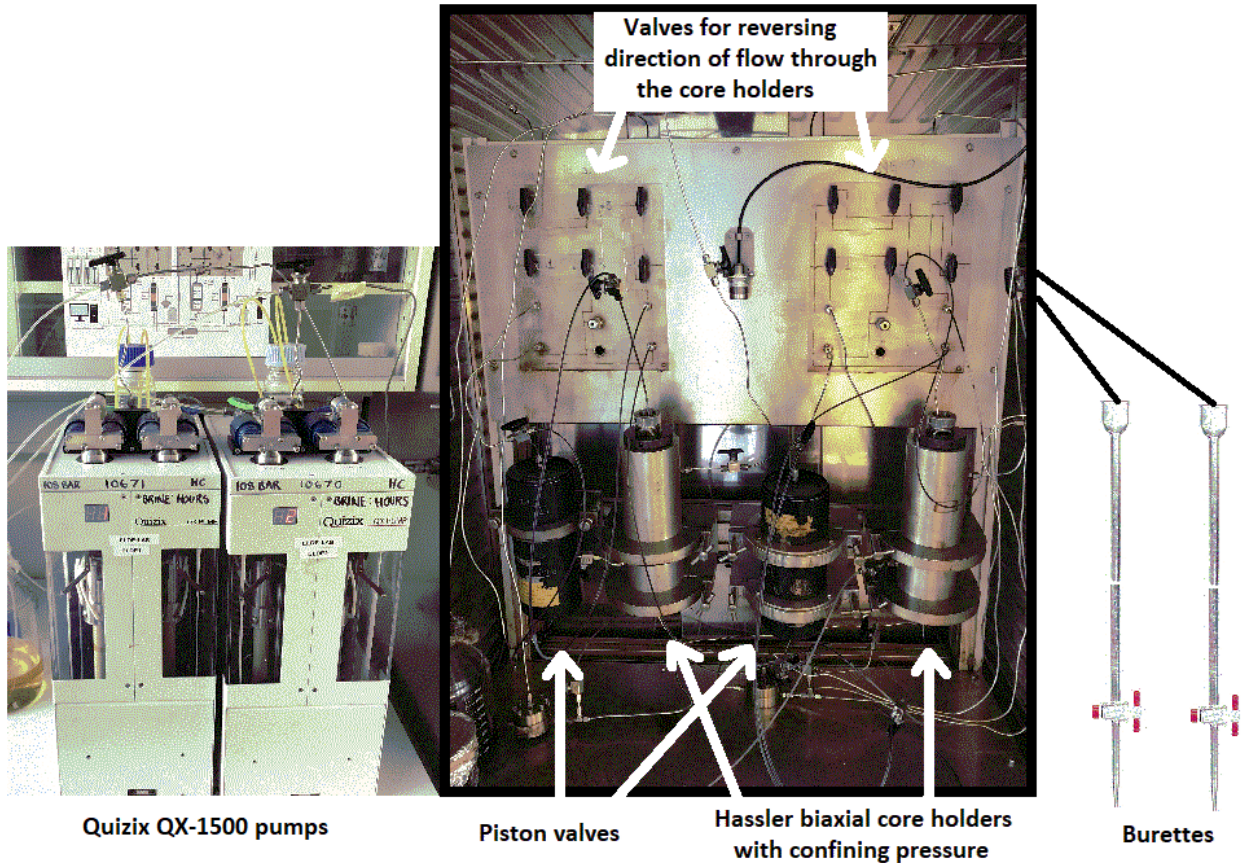
Figure 22 Aging cabinet set-up for filtering crude oil, draining cores with crude oil and establishing oil wet cores through dynamic aging.

C. Porosity

The core length (l) and diameter (d) were each measured three times at different locations on the core using a slide caliper. Core bulk volume (V_b) was calculated using the average l and d measurements

$$V_b = \pi * l * \frac{d^2}{4} \tag{5.1}$$

After gentle cleaning with tap water the core samples were dried at room temperature for 24 hours and then placed in a heating cabinet at 65°C for at least 96 hours. The dried cores were weighed (W_{dry}) on an AND GF-3000 digital scale. The cores were then vacuum evacuated in an air evacuation apparatus with less than 1 mbar for one hour. Then the FW brine was vacuum evacuated for 10 minutes to remove air from the brine. After this the evacuated brine was released into the closed beaker containing the evacuated cores allowing the brine to enter through

all core faces. The cores were left to saturate for 24 hours. The next day the brine saturated cores were weighed (W_{sat}) and then stored in U-FW brine in closed containers. The interconnected core pore volume (V_p) was calculated by dividing the difference between (W_{sat}) and (W_{dry}) by the density of the saturated brine (ρ_{brine}).

$$V_p = \frac{W_{sat} - W_{dry}}{\rho_{brine}} \tag{5.2}$$

The values for V_p and V_b were used to calculate effective porosity (Ø) using the formula

$$Ø = \frac{V_p}{V_b} \tag{5.3}$$

D. Absolute permeability

Absolute permeability (k_a) was measured for each core using FW brine, a Quizix QX-1500 pump, ESI-USB Dynamic inlet and outlet pressure transducers, Hassler core holder and a TESCOM 54-2100 series liquid backpressure regulator (BPR) (Figure 25). The core holder was horizontal and confining pressure (P_{conf}) was adjusted to 10 bar plus inlet injection pressure (P_{inj}) to ensure flow only occurred through the end faces and not around the core.

$$P_{conf} = P_{inj} + 10 \, [bar] \tag{5.4}$$

Brine with a viscosity (μ_{brine}) was injected at three different flow rates (q) in both directions (Figure 23). The BPR was connected to the outlet line downstream of the outlet pressure transducer to assist in removing air from the core. The BPR was set to approximately two bar at the lowest flow rate. The backpressure increased automatically with flow rate and on most cores it exceeded five bar at the highest flow rate. It was necessary to adjust P_{conf} with each change in P_{inj} or P_{BPR} changed. Once the pressure stabilized for a given q, the pressure differential (ΔP) between the inlet and outlet pressure transducers was recorded every second for a minimum of two minutes to provide an average ΔP across a core with length (l_{core}) and cross sectional area (A_{core}). The ΔPs were plotted in excel against flow rate (Figure 24). Excel uses the least squares method to perform linear regression and calculate an equation for the trend line. Due to offset caused by the pressure transducers, each value for ΔP was adjusted by subtracting the y-intercept

of the trend line formula to parallel displace the pressure differential trend line through the origin.
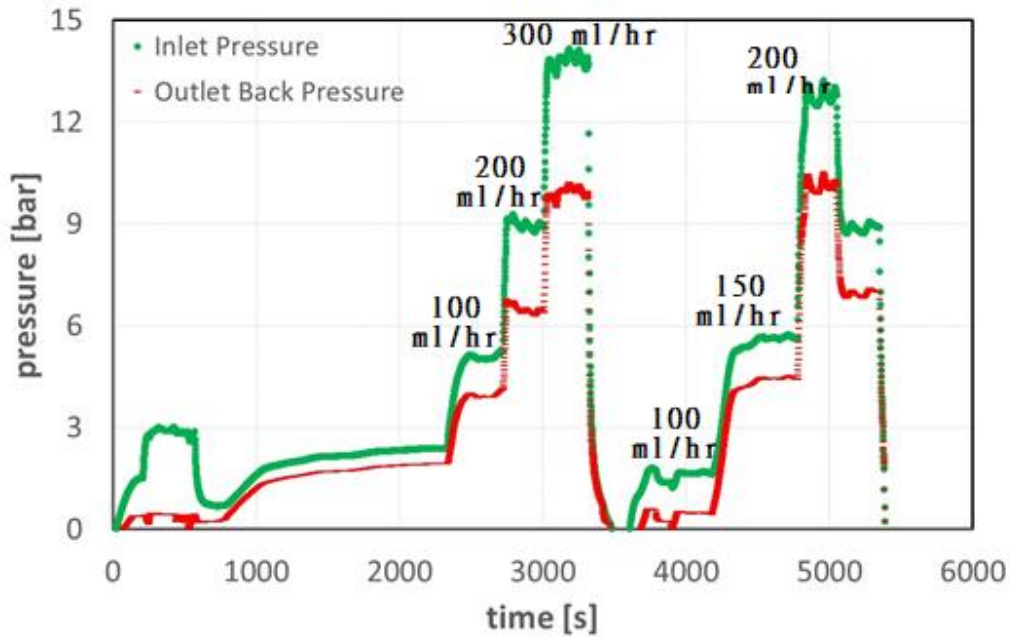
Figure 23 Pressure profile with respective flow rates used in determining absolute permeability for core B. The pressure differential lies between the inlet pressure and outlet back pressure lines. The first series between 2500-3500 seconds represents flow in the forward direction and the second series is flow in the reverse direction.

The measured parameters were set into Darcy's equation (equation 5.5) and multiplied by a conversion factor (α) equal to 0.2815 to convert bar to atmosphere, Darcy to mili Darcy, and hours to seconds. All other parameters were measured using the standard units listed in paragraph 3.b. The value recorded for k_a is the average of k_a measured in using forward and reverse flow.

$$k_a = \alpha \cdot \frac{\mu_{brine} \cdot q}{A_{core}} \frac{l_{core}}{\Delta p} \tag{5.5}$$
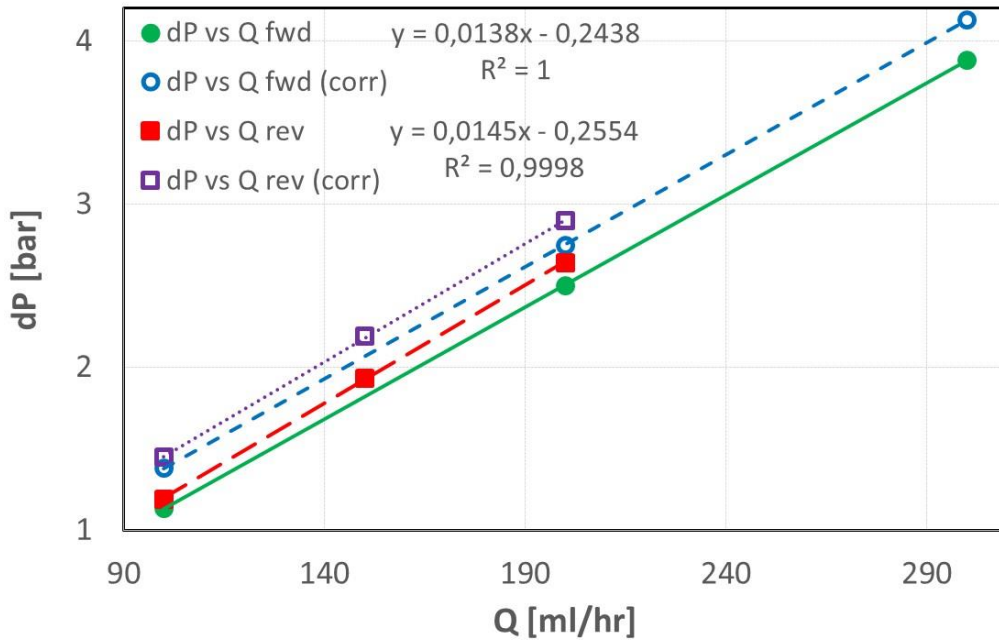
Figure 24 Pressure differentials used in equation 5.5 were adjusted for each flow rate by subtracting the y-intercept of the respective linear equation from the average pressure. The figure depicts the parallel displacement procedure for core B.
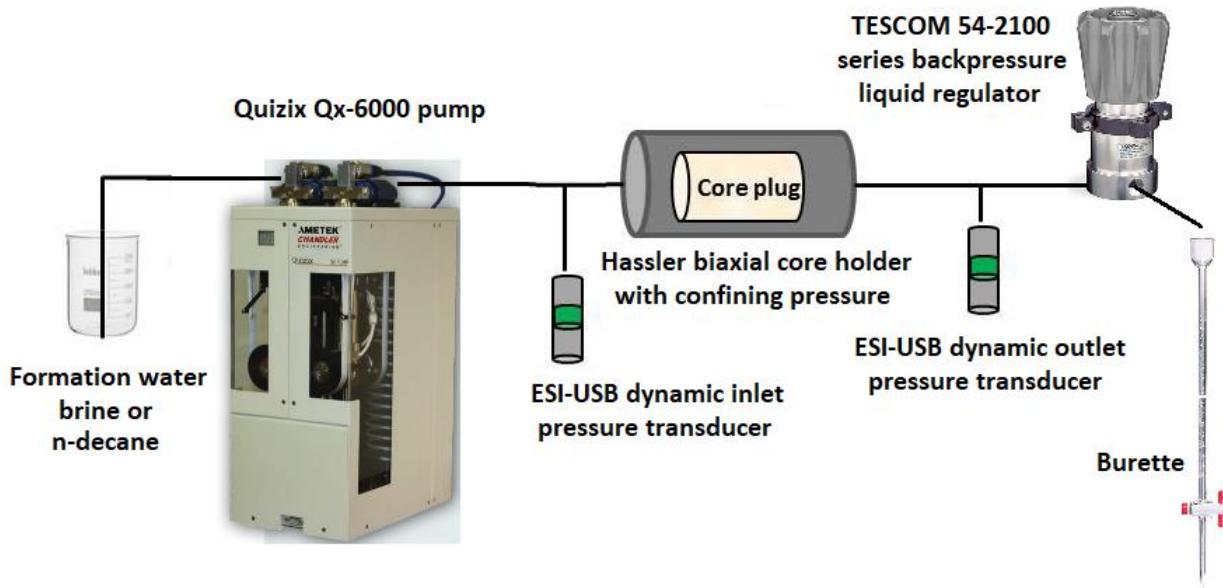
Figure 25 Experimental set-up for determining absolute permeability and draining water wet cores

E. Draining the water wet cores with n-decane

Cores B, C, G and 29 were selected to be water wet. The weights of the core plugs were recorded before the drainage procedure. The brine saturated cores were drained horizontally at 25°C to irreducible water saturation (S_{wir}) by injecting 2.5 V_p of filtered n-decane through the core (Figure 25) at a flow rate high enough to produce an injection pressure (P_{inj}) equal to two bar per cm times the core length (l_{core}) in cm plus backpressure in bar.

$$P_{inj} = l_{core}\ [cm] \cdot 2 \left[\frac{bar}{cm}\right] + P_{BPR}\ [bar] \tag{5.6}$$

The pressure transducers were zeroized prior to inserting the core into the core holder. Equation 5.4 was used to calculate P_{conf}, and a minimum of two bar was set into the BPR. Effluent was collected in a graduated burette and the volumes of brine in the effluent were recorded against time to provide insight on the changes in average water saturation during displacement until oil breakthrough. The total volume of brine recovered (V_{brine}) was recorded after flowing 2.5 V_p of n-decane through the core in both directions. The V_{brine} was divided by V_p and subtracted from one to calculate S_{wi}

$$S_{wi} = 1 - \frac{V_{brine}}{V_p} \tag{5.7}$$

F. Relative oil permeability of water wet (WW) cores

Upon completion of the drainage procedure the endpoint effective permeability of oil (k_o) was calculated as described in paragraph 6.b with the following exceptions: flow occurred in only one direction, flow began at P_{inj} and was stepped down and μ_{brine} was replaced with the viscosity of decane (μ_{dec}) in equation 5.8.

$$k_o = \alpha \cdot \frac{\mu_{dec} \cdot q}{A_{core}} \cdot \frac{l_{core}}{\Delta p} \tag{5.8}$$

The endpoint relative permeability of oil $(k_{r,o})$ was then determined by dividing k_o by k_a

$$k_{r,o} = \frac{K_o}{K_a} \tag{5.9}$$

G. Draining the intermediate wet cores with crude oil

Cores I, A, J and 28 were selected to be oil wet and were drained to S_{wi} using filtered crude oil at 80°C in the aging cabinet (Figure 22). The weights of the core plugs were recorded before draining and after measuring $k_{r,o}$. A brine saturated core was inserted into the aging cabinet vertical core holder from the bottom. A total of 2.5 V_p of filtered crude oil was injected through the core at a flow rate high enough to produce an injection pressure (P_{inj}) equal to two times the core length in bar plus backpressure (equation 5.6). The aging cabinet does not have an ESI-USB pressure transducer, so P_{inj} was monitored and recorded using the pressure readings directly from the Quizix pump.

Equation 5.4 was used to calculate P_{conf}, and two bar was set into the BPR. Effluent was collected in a graduated burette. The initial mixing of crude oil and brine in the effluent prevented reading the brine volumes against time. After draining the core in the forward direction, the core was dynamically aged using the procedure in the next paragraph. Then flow was reversed to drain and age the core in the reverse direction. The total volume of brine recovered (V_{brine}) was recorded after flowing 2.5 V_p of filtered crude oil in both directions, and equation 5.7 was used to calculate S_{wi}.

H. Aging to alter core wettability

The process to age cores I, A, J and 28 began immediately following the drainage procedure outlined in paragraph 6.d above. The flow rate was reduced to 1.5 ml/hr for 96 hours and then reversed. The core was drained in the reverse direction and then flow was reduced to 1.5 ml/hr for another 96 hours. A system of valves mounted inside the aging cabinet allowed flow to be reversed without removing the cores from the core holder. It was necessary to adjust P_{conf} using equation 5.4 to compensate for the reduced P_{inj}.

I. Relative oil permeability of oil wet cores

Upon completion of the aging process the endpoint effective permeability of oil (k_o) was calculated as described in paragraph 6.b with the following exceptions: flow occurred in only one direction and due to the vertical position of the core holder, equation 5.10 was used to calculate k_o. The parameters in equation 5.10 are the same as in equation 5.5 with the addition of

the crude oil viscosity (μ_{CO}), crude oil density (ρ_{CO}) and gravity constant (g) ($980\ dyne/g$). It was necessary to convert bar to pascal by multiplying Δp by 10^5, and then return to bar by multiplying α by 10^5. The inclination term is multiplied by 10^{-1} to convert $dyne/cm^2$ to pascal. The BPR in the aging cabinet is set using an analog dial. The lack of an outlet pressure transducer increased the uncertainty of the k_o measurements. In addition, the logging periods of the Quizix pumps in the aging room are defaulted to every minute vice every second. As a result, only two or three pressure readings were recorded for each flow rate further increasing the uncertainty of the k_o measurements. Equation 5.9 was used to determine the endpoint relative permeability of oil $\left(k_{r,o}\right)$.

$$k_o = \alpha \cdot 10^5 \cdot \frac{\mu_{CO} \cdot q}{A_{core} \cdot \left(\dfrac{\Delta p \cdot 10^5}{l_{core}} - (10^{-1} \cdot \rho_{CO} \cdot g \cdot \sin\theta) \right)} \tag{5.10}$$
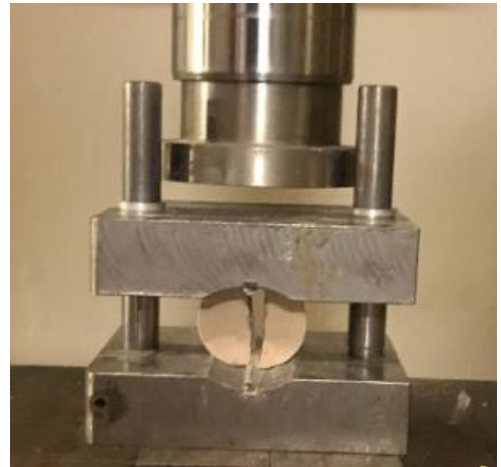
Figure 26 Cores were fractured along the longitudinal axis.

J.   Fracturing the cores

After aging and draining, all the cores used in the study were fractured along the longitudinal axis (Figure 26). The following measures were taken to limit cooling of the cores saturated with crude oil: only one core was fractured at a time, the cores were transported in their container of crude oil which was also placed inside of a closed cardboard box and the all preparations were made in the fracturing room prior to removing the core from the oven to reduce the amount of

time the core was outside of the oven. The weights of the cores were recorded before (W_{before}) and after (W_{after}) fracturing to determine the percentage of material lost (W_{decr}) as a result of the fracturing process.

$$W_{decr} = \frac{W_{before} - W_{after}}{W_{before}} \qquad (5.11)$$

It is assumed that the amount of oil, brine and rock lost during the fracturing process is equal to the respective value times W_{decr}. The following formula was used to calculate bulk volume after fracturing $(V_{b,frac})$, pore volume after fracturing $(V_{p,frac})$ volume of oil after fracturing $(V_{o,frac})$ and the volume of water after fracturing $(V_{w,frac})$, where V_i is the original volume $(V_b, V_p, V_o \ or \ V_w)$ before fracturing

$$V_{i,frac} = V_i - (V_i * W_{decr}) \qquad (5.12)$$

Although there can be slight errors due to rounding, it is assumed that $\emptyset, S_{wi}, k_a, k_o,$ and $k_{r,o}$ remain unchanged after fracturing.
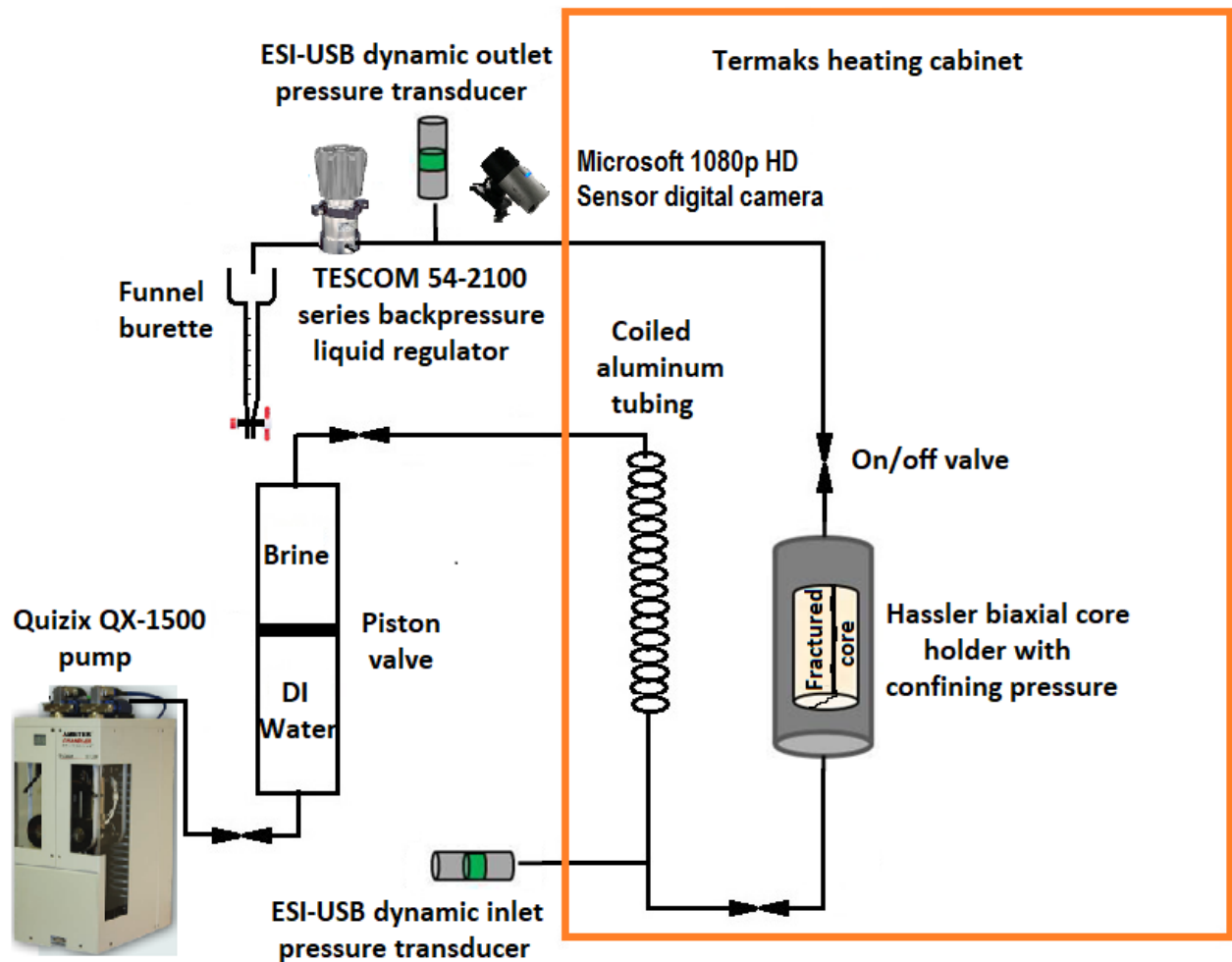
Figure 27 Modified spontaneous/forced imbibition (mod S/FI) test cell.

K. Modified spontaneous imbibition (mod SI) of brine

All cores used in the study were tested using a modified spontaneous imbibition (mod SI) process using FW, PDI or PDI pH~9 brine. The purpose of the mod SI setup (described below) was to facilitate SI at elevated pressures and temperatures and using a variety of fluids (including crude oil). The WW cores B, G and 29 were tested for 24 hours in the mod SI cell. The test on core C was stopped prematurely after three hours as it appeared that SI had stopped. The aged cores were tested for ten days.

The following is a general description of the mod SI test equipment and flow through the test cell with comments regarding equipment selection. The mod SI/FI test cell consisted of a Quizix QX-1500 pump, piston valve, ESI-USB Dynamic inlet pressure transducers, Termaks heating

cabinet, Hassler core holder, Microsoft 1080p HD Sensor digital camera, TESCOM 54-2100 series backpressure liquid regulator (BPR) and a funnel burette to collect effluent and record recovered oil volumes (Figure 27). Due to temperature operating restrictions the pump, piston valve, pressure transducers, camera, BPR and burette were mounted outside the heating cabinet. For the water wet cores (WW) the temperature inside the heating cabinet was 30 °C (lowest temperature setting for the heating cabinet) and 90 °C for the aged cores. The selected brine was transferred from the piston cell, past an inlet pressure transducer, and into the heating cabinet. Inside the heating cabinet the brine traveled through coiled aluminum tubing to ensure it reached the operating temperature inside the test cell prior to entering the bottom of the vertically aligned core holder.

Prior to inserting a core into the core holder, the inlet lines were primed with brine to remove air. For the aged cores, a brine sample was taken from the core holder inlet and tested using the pH meter. The intent was to see if the pH changed during transport through the inlet lines. Measurements were recorded at 10 seconds and then 1, 2, 5, 15 and 30 minutes. Measurements of the injection brine were also taken from the core holder inlet upon completion of each core test. The fractured core halves were weighed and then held apart by two 0.5 mm thick aluminum strips (Figure 28) that were cut 0.3 mm wide and approximately 2 mm shorter than the length of the core. This was to reduce the possibility of the strip extending past the core and preventing the core holder end pieces from properly seating. The aluminum strips provided a volume between the separated core halves (V_{frac}). The separation allowed the brine to contact the three open faces of each core half and prevented the development of a pressure differential across the core matrix that could force fluid into the core. This was verified in pre-tests using inlet and outlet pressure transduces. Brine was injected at rates up to 60 ml/hr with no pressure differential across the fractured core. To reduce the chance of breaking the core, P_{conf} was set using equation 5.4 and five bar instead of ten. Since inlet and outlet pressures were nearly identical an outlet pressure transducer was not used during mod SI tests to reduce dead volumes in the setup.

An outlet line from the core holder transferred effluent outside the heating cabinet where a digital camera took pictures of the transparent fluid line every 10 seconds (Figure 29). This was a necessary control of oil production because the injection rate was low (<1.5 ml/hr) for the aged

cores and some of the produced oil was trapped in the 4.5 ml dead volume of the BPR. Some but not all of the oil trapped in the BPR was recovered upon completion of the tests. This resulted in failure of the first aged core tested since the volume of oil recovered could not be measured with the necessary certainty. The BPR was used to prevent boiling of the lighter components in the crude oil, so for the WW cores the BPR was not used and effluent was transferred directly from the core holder outlet end fitting to the burette.

Figure 28 For mod SI tests spacers were placed between the two fractured halves allowing brine to contact the three open faces of each core half. The use of spacers also prevented the buildup of a pressure differential across the core that could force brine into the core.

For the WW cores a flow rate of 30 ml/hr was used throughout the test. This was necessary because the rate of brine imbibition is much higher for WW cores than it is for aged cores. This flow rate appeared to be sufficient to transport the n-decane at the rate it was being displaced without creating a pressure differential across the core. Various flow rates were used with the aged cores to find an optimal flow regime. If flow occurred too rapidly then brine may not have sufficient time to react with the surface and the test would have to be stopped periodically to fill the piston valve with new brine. If flow was too low, then produced oil may remain trapped in the core holder. For cores J and A an initial flow rate of 60 ml/hr was used to fill the outlet lines and to set the BPR to approximately two bar before reducing the flow rate to 6 ml/hr for core J and 1.5 ml/hr for core A. For core 28 the BPR was heated to 60 °C by wrapping it in a temperature-controlled heating cable around it and flow rate was set to 1.5 from the onset of the

test. This configuration appeared to work the best. The pressure gradually increased to approximately three bar and remained there throughout the ten-day test period. Oil was recovered both initially and near the end of the test for core 28.

The total dead volume in the outlet line system (V_{dead}) was calculated using equation 5.13. It was possible to measure the volume of the BPR (V_{BPR}), the core holder outlet end fitting (V_{EF}) and each segment of tubing in the outlet line system $\left(V_{tubing,i}\right)$ by first draining all fluid from the segment using compressed air, and then injecting DI water into one end using a calibrated syringe. V_{frac} was estimated at two different points. The first by subtracting V_{EF} from the cumulative volume (V_{cum}) taken from the Quizix readings at the time when effluent first appeared out of the core holder outlet end fitting. The second by substituting V_{cum} for V_{dead} in equation 5.13 at the time when effluent reached the burette and then solve for V_{frac}.

$$V_{dead} = V_{BPR} + V_{EF} + V_{frac} + \sum_{i=1}^{n} V_{tubing,i} \tag{5.13}$$

For the WW cores, the volume of oil (V_o) collected in the burette was recorded against elapsed time. The elapsed time for the measurements began when effluent reached the end of the outlet line. For the aged cores volumetric measurements were made by taking a picture of the outlet line every 10 seconds (Figure 29). The volume of the crude oil segment $\left(V_{o,seg}\right)$ was determined by multiplying the length of the crude oil segment $\left(l_{o,seg}\right)$ by the ratio of tubing volume $\left(V_{tubing}\right)$ to tubing length $\left(l_{tubing}\right)$

$$V_{o,segment} = l_{o,seg} \frac{V_{tubing}}{l_{tubing}} \tag{5.14}$$

The volume of volume of oil displaced is equal to the volume of water spontaneously imbibed (V_{wsi}), which was calculated by summing each $V_{o,segment}$. The V_{wsi} was set into equation 3.81 to compute *IAH*. The oil recovery after mod SI (OR_{modSI}) was calculated by dividing V_{wsi} by the initial volume of oil in the fractured core halves $\left(V_{oi,frac}\right)$.

$$OR_{modSI} = \frac{V_{wsi}}{V_{oi,frac}} \tag{5.15}$$

Figure 29 Volumetric measurements of oil were made by multiplying the length of an oil segment by the ratio of the inside tubing volume to its length. This was necessary because oil became trapped in the dead volume of the BPR during mod SI experiments of aged cores.

During the first mod SI of the aged core J there were three phases present in the outlet line: brine, crude oil and air. This was due to a bad valve just prior to the core holder inlet. The valve was replaced upon completion of the test on core J. The presence of air may be a factor in the core J having the highest recovery of the three aged cores tested, which will be discussed in chapter six. The air in the line caused a concave meniscus into the oil segment where the oil and air met. Because of this effect, all oil segments shorter than 0.5 mm were not included in measurements on core J. In addition, the length of each oil segment was reduced by 0.5 mm to account for the meniscus.

Effluent samples were taken from the burette periodically for the WW cores and daily for the aged cores. Due to drift in pH measurements over time while testing the WW cores, a set regime of recording the pH values at 10 seconds and then 1, 2, 5, 15 and 30 minutes was initiated for the aged cores.

L. Modified forced imbibition (mod FI) of brine

A modified forced imbibition (mod FI) procedure was conducted on the fractured cores. A 0.9 mm thick patch of butyl rubber was placed between the two fractured core halves to prevent fluid flowing through the fracture during dynamic flooding (Figure 30). The same brine used during the mod SI procedure was dynamically injected using the procedures outlined in paragraph 6.d. except brine was injected instead of oil. The equipment set up shown in Figure 25 was used for the WW cores and the mod S/FI cabinet shown in Figure 27 was used for the aged cores. The volume of oil recovered was equal to the volume of water forcibly imbibed (V_{wfi}) used in equation 3.85 toward computing *IAH*. It was possible to generate the desired pressure differential (equation 5.6) on all cores except core J (1/2 desired pressure) and core A (no pressure differential). It is assumed there was leakage around the rubber insert for these two cores.
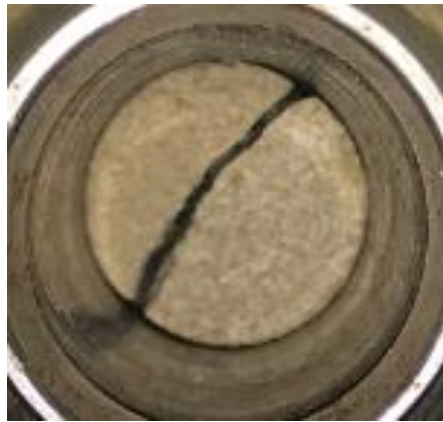
Figure 30 A butyl rubber patch was placed between the fractured halves during modified FI tests to prevent fluid from flowing through the fracture.

The oil recovery after mod FI (OR_{modFI}) was calculated by dividing V_{wfi} by the initial volume of oil in the fractured core halves $(V_{oi,frac})$. Total oil recovery OR_{Total} after mod SI and mod FI is the sum of OR_{modSI} and OR_{modFI}.

$$OR_{modFI} = \frac{V_{wfi}}{V_{oi,frac}} \qquad (5.16)$$

Residual oil saturation after mod SI/FI with brine was computed by subtracting V_{wsi} and V_{wfi} from $V_{oi,frac}$ and dividing the sum from the pore volume of the fractured core halves $(V_{p,frac})$.

$$S_{or} = \frac{V_{oi,frac} - V_{wsi} - V_{wfi}}{V_{p,frac}} \qquad (5.17)$$

70

M. End point relative permeability of water

Upon completion of the mod FI procedure, the endpoint effective permeability of water (k_w) was calculated as described in paragraph 6.b with the following exceptions: WW cores were tested using the equipment shown in Figure 25, aged cores were tested using the mod SI/FI cabinet shown in Figure 27, flow occurred in only one direction and flow began at P_{inj} and was stepped down

$$k_w = \alpha \cdot \frac{\mu_{brine} \cdot q}{A_{core}} \cdot \frac{l_{core}}{\Delta p} \qquad (5.18)$$

The endpoint relative permeability of water $(k_{r,w})$ was then determined by dividing k_w by k_a

$$k_{r,w} = \frac{K_w}{K_a} \qquad (5.19)$$

Due to possible leakage through the fracture, the values obtained for k_w may be artificially high.

N. Modified spontaneous imbibition (mod SI) of oil

Upon completion of $k_{r,w}$ measurements the cores were placed in Amott cells (Figure 15) containing their respective oil (n-decane for WW cores and crude oil for aged cores). The tops of the SI cells were sealed with a rubber stop. The WW cores were left to stand at 25°C while the aged cores were placed in the heating cabinet at 90°C to prevent loss of the lighter oil components. The volume of water displaced was recorded against time. The total volume of water displaced was used to represent the volume of oil spontaneously imbibed (V_{osi}) in equation 3.85 toward computing *IAH*.

O. Modified forced imbibition (mod FI) of oil

The final phase consisted of forcibly imbibing oil into the fractured cores using the procedures outlined in paragraphs 6.k and 6.d. using the respective oil instead of brine. The volume of water recovered was used to represent volume of oil forcibly imbibed (V_{ofi}) in equation 3.85 toward computing *IAH*.

P. End point relative permeability of oil

A final check of $k_{r,o}$ was made using the procedures outlined in paragraph 6.e for the WW cores and paragraph 6.h for the aged cores.

The residual oil saturation (S_{wir}) was calculated using the following formula

$$S_{wir} = 1 - \left(S_{or} + \frac{V_{osi} + V_{ofi}}{V_{p,frac}} \right) \tag{5.20}$$

6. Results and Discussion
A. pH brine study
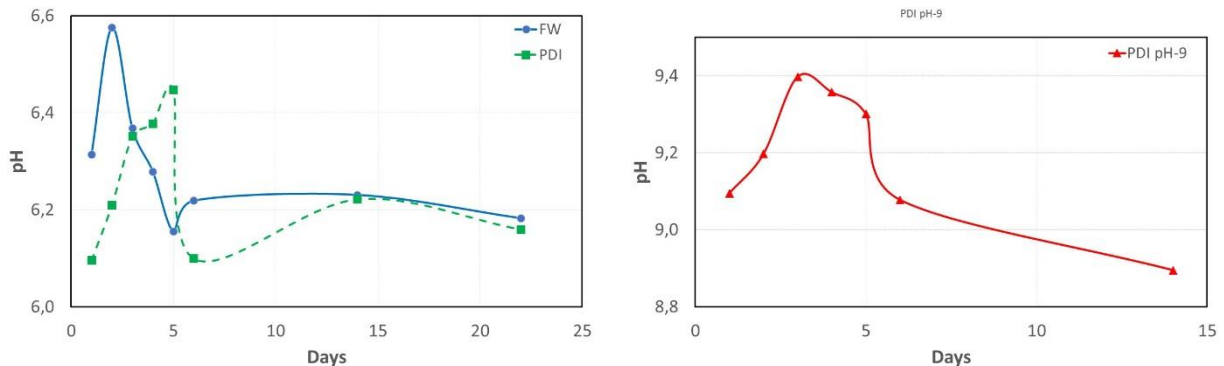
Figure 31 pH curves for the three brines used in the study (FW and PDI left, PDI pH~9 right). Daily pH measurements were recorded for each brine at 10 seconds, 1, 2, 5, 15 and 30 minutes. The plotted pH values are the average of the daily measurements. The general trend for all three brines is a rapid pH rise and fall in the first five days followed by stabilization.

A pH study was conducted to see how brine pH values would change over time due to complexation of minerals in the brine and reaction with CO_2 in the atmosphere. The brines were mixed and stored in sealed glass containers at 25°C. A 10 to 20 ml sample was taken daily, and pH was recorded at 10 seconds, 1, 2, 5, 10, 15 and 30 minutes. These values were averaged and plotted in Figure 31. The general trend for all three brines is a rapid 0.3 increase in pH followed by a rapid 0.4 decrease. There is a slight increase in the FW and PDI brines followed by stabilization. The PDI~9 brine continues a gradual decrease as the hydroxide is slowly neutralized. Although the containers were sealed, the brine was routinely opened for sampling thereby exposing it to the outside air. As discussed in the carbonic acid system in paragraph 3.M.iii, CO_2 from the atmosphere will react with water to form carbonic acid. The carbonic acid deprotonates stepwise to form bicarbonate and eventually hydronium. The produced hydronium is a strong acid that combines with the hydroxide to form water. For this reason, it was necessary to raise the pH level to account for drift.

B. Water-wet cores

All cores drained with n-decane were cylindrical Edwards limestone with similar dimensions and properties of porosity (Ø), initial water saturation (S_{wi}) and absolute permeability (k_a) (Table 9). All four cores were initially saturated with FW brine and drained with n-decane. The

experiments on the water-wet (WW) cores were conducted at 25°C. The color coding used for the cores is FW (blue), PDI (green or purple) and PDI pH~9 (red).

Due to differences in core size, permeability, porosity and fractured face surface area combined with differences in fluid viscosities, it is necessary to scale time to compare recovery data from SI (Shouxiang, Morrow et al. 1997). Dimensionless time (t_D) is determined using equation 6.1 where time (t) is in minutes, permeability (k) is in cm², porosity $(\emptyset)$ is a fraction, interfacial tension (σ) is dyne/cm, viscosities of oil (μ_o) and water (μ_w) are given in Pa·s and the characteristic length (l_C) is determined using equation 6.2.

$$t_D = t\sqrt{\frac{k}{\emptyset}\frac{\sigma}{\sqrt{\mu_o\,\mu_w}}\frac{1}{l_C^2}} \tag{6.1}$$

The characteristic length is the term in equation 6.2 that compensates for the differences in size, shape, boundary conditions and exposed surface area of the core. Where V_b is the bulk volume of the core multiplied by the percent decrease due to fracturing in cm³, n is the number of faces open to imbibition, A_i is the surface area open to imbibition in the ith direction in cm² and l_{A_i} is the distance that the imbibition front travels from the imbibition face to the no-flow boundary in cm.

$$l_C = \sqrt{\frac{V_b}{\sum_{i=1}^{n}\frac{A_i}{l_{A_i}}}} \tag{6.2}$$

Due to the complexity of computing the cross-sectional area of the fractured core faces $(A_3\ to\ A_6)$ in Figure 32 and the average distance that the imbibition front travels from the imbibition face to the no-flow boundary (l_{A_1}) and (l_{A_2}) the following assumptions were used to compute (L_C):

- $A_1 = l_1 \cdot d_1$ $A_2 = l_2 \cdot d_2$ $A_3 = A_4 = A_5 = A_6 = \frac{1}{2}A_0,\ (*)$
- $l_{A_1} = l_{A_2} = \frac{1}{3}D_0,\ (**)$ $l_{A_3} = l_{A_4} = \frac{1}{2}l_1$ $l_{A_5} = l_{A_6} = \frac{1}{2}l_2$

*It is assumed that the original cross-sectional area (A_0) of the unfractured core is equal to the sum of $A_3 + A_5$ (Figure 32**Feil! Fant ikke referansekilden.**) and to the sum of $A_4 + A_6$, therefore $A_3 = A_4 = A_5 = A_6 = \frac{1}{2}A_0$.

**If the core were split exactly in the middle then l_{A_1} would be zero at the edges and one half of the original diameter $\left(\frac{1}{2}d_0\right)$ in the middle. Calculating the average value for l_{A_1} across d_0 gives a value of approximately two thirds the original radius or $\frac{1}{3}d_0$.
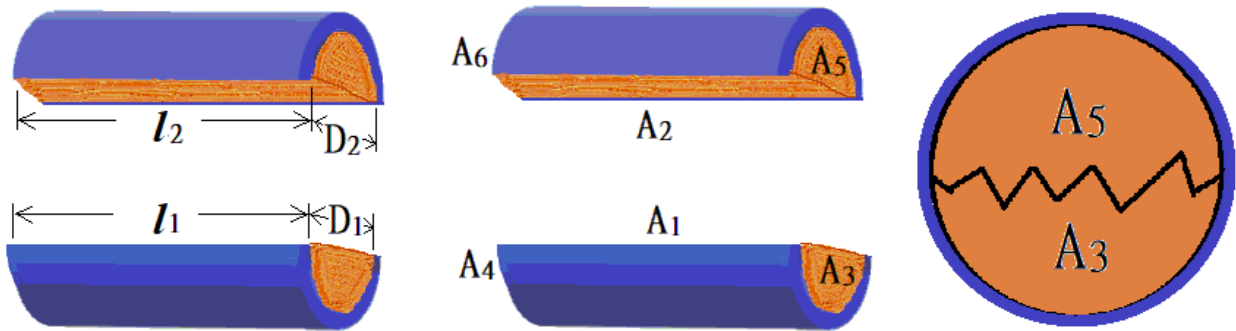
Figure 32 Boundary conditions three faces open (TFO). In the two left-hand drawings core half one is depicted in the bottom view and core half two in the top. The dark blue area shows the no-flow boundary and the light brown represents the three open faces of each core half. The depiction to the right shows a cross-section view with exaggerated roughness of the fracture.

The recovery using dimensionless time can be fitted using the mass transfer function where R is the recovery by imbibition, R_{max} is the total recovery by imbibition and α is the oil production decline constant, typically around 0.05 (Shouxiang, Morrow et al. 1997). The value for α was set to 0.05 for WW cores and 0.005 for aged cores.

$$\frac{R}{R_{max}} = 1 - e^{-\alpha t_D} \tag{6.3}$$

ii.   Modified spontaneous imbibition (mod SI)

The mod SI experiments on the cores drained with n-decane were conducted as described in paragraph 5.K. The results of the tests are presented below.
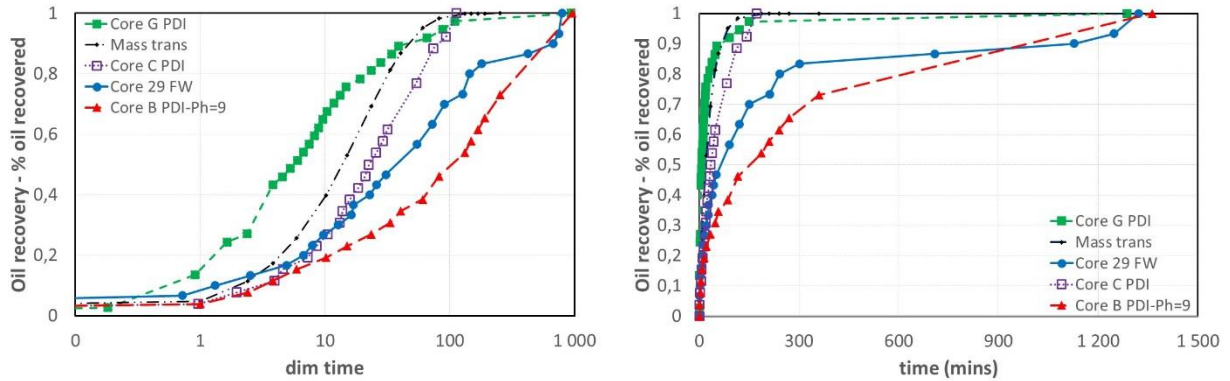
Figure 33 Mod SI of WW cores drained with decane in dimensionless time (left) and in minutes (right) showing the normalized oil recovered for each core versus time. Recovery profiles are adjusted for differences between cores using equation 6.1. The mass transfer profile is plotted using equation 6.3 as a general reference.

Figure 33 shows the normalized oil recovered for each core that was drained using n-decane versus dimensionless time (dim time) (left) and real time (right). Core G (PDI) produced most of its total oil earlier than the cores using FW or PDI pH~9 brines. Core B (PDI pH~9) has delayed production of the non-polar n-decane (Figure 33).
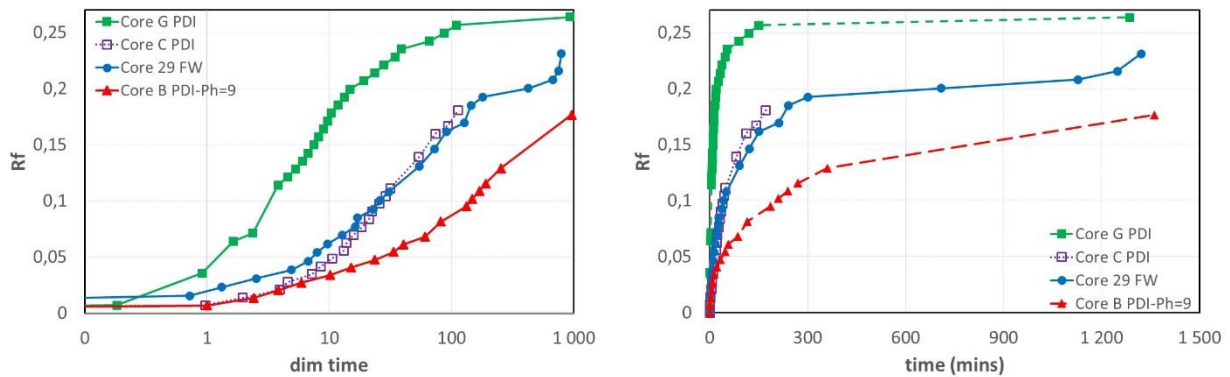
Figure 34 Mod SI of WW cores in dimensionless time (left) and in minutes (right) showing recovery factor (Rf) versus time. Core G (PDI) had the fastest rate and the highest Rf.

Figure 35 shows the WW cores imbibed using PDI brine have the same or better Rf than core 29 (FW) or B (PDI pH~9). Core G (PDI) has the highest Rf (26%) and a faster rate than the other cores, while core B (PDI~9) has the slowest and lowest Rf (18%).
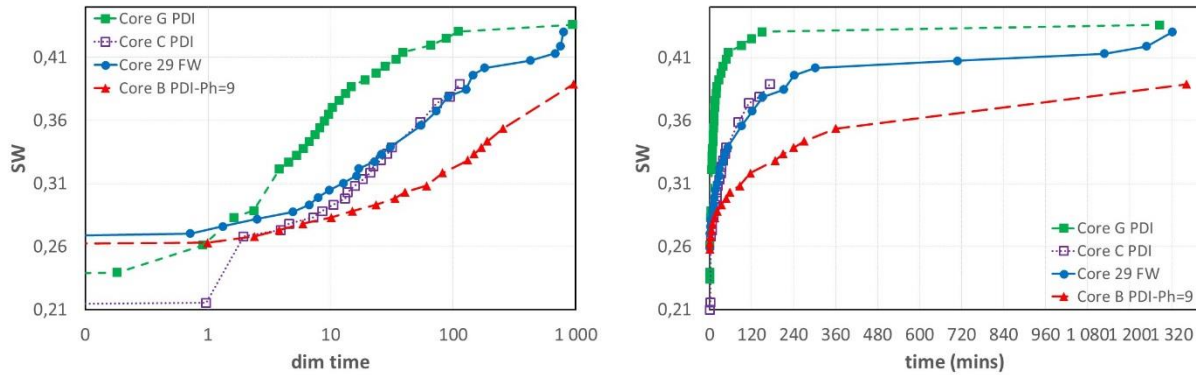
Figure 35 Mod SI of WW cores in dimensionless time (left) and in minutes (right) showing water saturation (S_w) versus time. Core G (PDI) had the highest increase in S_w and the fastest rate of increase in S_w of all the decane cores.

In the WW cores S_w nearly doubles in core G (PDI) going from an S_{wi} of 23% to 43% in the first two hours with a final S_w of 44%. At the start of the mod SI test the S_{wi} of core C (PDI) is nearly 5% less than core 29 (FW) but quickly rises to the same level. The trend of the S_w curve for core C (PDI) indicates that if it had been tested for 22 vice 3 hours it may have had a the higher final S_w than core 29 (FW). Core B (PDI pH~9) exhibited the lowest level and rate of increase in S_w of the WW cores, increasing from $Sw = 29\%$ to 36%. It appears that PDI brine phase is increasing the capillary pressure (P_c) which has an overall positive influence on SI in WW cores.

The graphs depicting the imbibition rates for the cores are not included as there is a lot of scatter and the graphs provide little insight. The general trend for the decane cores is a relatively high initial imbibition rate that decreases exponentially with time.

iii.　　Parametric data

Table 9 contains the parametric data for the WW cores that were drained using n-decane. The first three columns list the measured parameter, units and the average uncertainty ($Avg\Delta$) for the four listed decane cores. (See appendix A for method used to calculate uncertainties). Columns four through seven list the four cores and the brine that was used during the mod SI/FI experiments. The first section (white) details the volumetric data used to calculate the porosity. The next section (light green) lists the absolute and end point permeabilities from each phase of the study. The gold section contains the initial water saturation (S_{wi}) measured after drainage, and the residual oil saturation (S_{or}) and irreducible water saturation (S_{wir}) measured at the end

77

of the mod SI and mod FI tests. The final section (light grey) shows the initial volume of oil (V_{oi}) contained in fractured core along with the volumes of oil recovered by mod SI (V_{wsi}), oil recovered by FI (V_{wfi}), brine recovered by SI (V_{osi}) and brine recovered by FI (V_{ofi}) that were used to calculate the Amott-Harvey displacement-by-water ratio (δ_w), displacement-by-oil-ratio (δ_o) and displacement index (IAH).

Table 9 Parametric data for WW cores and associated mod SI/FI brine used.

	Units	Avg Δ	Decane Cores			
Core ID			**29**	**C**	**G**	**B**
Brine			**FW**	**PDI**	**PDI**	**PDI pH = 9**
Length	cm	0,008	6,930	7,315	7,320	7,563
Diameter	cm	0,003	3,800	3,785	3,788	3,787
Area	cm^2	0,02	11,34	11,25	11,26	11,26
V$_b$	ml	0,1	78,6	82,3	82,4	85,2
V$_p$	ml	0,02	17,54	18,23	18,41	19,89
Ø	%	0,04	22,31	22,15	22,34	23,36
k$_a$	mD	0,3	14,1	16,2	18,1	14,5
k$_o$ (drainage)	mD	0,2	6,6	7,9	9,7	9,7
k$_w$ (mod FI)	mD	0,08	3,07	2,74	7,00	4,16
k$_o$ (mod FI)	mD	0,3	8,6	11,4	12,1	10,9
k$_{ro}$ (drainage)	mD	0,02	0,47	0,49	0,54	0,67
k$_{rw}$ (mod FI)	mD	0,008	0,22	0,17	0,39	0,29
k$_{ro}$ (mod FI)	mD	0,02	0,61	0,70	0,67	0,75
S$_{wi}$ (drainage)	fraction	0,001	0,259	0,210	0,234	0,258
S$_{or}$ (brine mod SI/FI)	fraction	0,009	0,530	0,576	0,526	0,450
S$_{wir}$ (oil SI/mod FI)	fraction	0,009	0,219	0,160	0,207	0,289
V$_{oi}$ (fractured)	ml	0,05	12,98	14,38	14,03	14,72
V$_{wsi}$	ml	0,06	3,00	2,60	3,70	2,60
V$_{wfi}$	ml	0,06	0,70	1,30	0,70	3,20
OR (mod SI)	fraction	0,004	0,231	0,181	0,264	0,177
OR (mod FI)	fraction	0,004	0,054	0,090	0,050	0,217
OR (Total mod SI/FI)	fraction	0,006	0,285	0,271	0,314	0,394
V$_{osi}$	fraction	0	0	0	0	0
V$_{ofi}$	fraction	0,06	4,400	4,800	4,900	5,200
δw	fraction	0,0005	0,8108	0,6667	0,8409	0,4483
δo	fraction	0	0	0	0	0
IAH	fraction	0,0005	0,8108	0,6667	0,8409	0,4483
Fractured weight decr	fraction	0,0001	0,0018	0,0018	0,0047	0,0017

A comparison of drainage relative oil permeability (k_{ro}) in unfractured cores to the mod FI k_{ro} of fractured cores shows an increase in k_{ro} for all cores. The range of increase is small enough to indicate that the mod FI tests were successful in preventing significant fluid flow through the fracture which would result in much higher k_{ro} values. The increase is nearly equal for core 29 (FW) and core G (PDI), 0.14 and 0.13 mD respectively. Core C (PDI) had the highest increase of 0.21 mD, however this improvement would be lower if core C were allowed a longer mod SI time thereby increasing S_w and decreasing k_{ro}. Core B (PDI pH~9) had the lowest increase in k_{ro} of 0.8 mD. This could be an indication of precipitation resulting from a combination of increased multivalent cations and elevated pH levels. It is possible that the hydroxide in the elevated pH brine began to associate with Mg^{2+} to form magnesium hydroxide $(Mg(OH)_2)$ which has a low solubility in water $(K_{SP} = 5.61 \cdot 10^{-12})$. Time permitting, the cores should be cleaned with solvent and a new absolute permeability (k_a) measured to see if there was a decrease in permeability.

The calculated IAH for the WW cores was 0.4483 for B (PDI pH~9), 0.6667 for C (PDI), 0.8108 for 29 (FW) and 0.8409 G (PDI). The V_{wsi} is similar for all cores starting at 2.60 ml for C (PDI) and B (PDI pH~9), 3.0 ml for 29 (FW) and 3.7 ml for G (PDI). The variations for IAH result mainly from the differences in V_{wfi}. This may be due to heterogeneities in the cores or flow through the fracture (even though the desired pressure differential across the core was obtained). Cores B (PDI pH~9) and G (PDI) have the highest total oil recovery (OR_{total}). Despite the overall higher recovery from core B (PDI pH~9) it had the lowest IAH of all the cores, which is attributed to the successful displacement of oil during the viscous flood. Core C (PDI) also had a lower δ_w and IAH.

The results indicate that elevated levels of PDI do not alter wettability of water-wet carbonate core plugs containing n-decane. This was expected as the theory of Smart Water is based on the exchange of divalent cations with polar oil components attached to the surface of the rock and n-decane is a saturated hydrocarbon with no polar components to bind to the rock surface. On the other hand, the test indicates that elevated pH levels of 9 reduce water wetness in carbonate cores containing n-decane. This is a condition that needs to be investigated further.

C. Aged cores

The aged cores were cylindrical Edwards limestone with similar dimensions and properties of porosity ($\emptyset$), initial water saturation (S_{wi}) and absolute permeability (k_a) (Table 10**Feil! Fant ikke referansekilden.**). The three cores were initially saturated with FW brine and then aged and drained with crude oil to intermediate-wet conditions. In a study by Sandnes (2020) using the same limestone, crude oil and dynamic aging process the cores tested intermediate-wet and imbibed oil but no water. The mod SI/FI test procedures on the aged cores in this study were conducted at 90°C to reduce precipitation of wax in the crude oil. The color coding used for the cores is FW (blue), PDI (green) and PDI pH~9 (red).

i. pH study on aged cores

Table 10 pH values for cores 28 (PDI) and J (PDI pH~9) comparing the PHREEQC estimate with values from samples taken from the bottle, core holder (CH) inlet and effluent on the first and last day of the mod SI test.

	PHREEQC	Bottle	CH inlet day 1	CH inlet day 10	Effluent day 1	Effluent day 10
Core 28 (PDI)	5.81	6.85	6.17	7.39	6.44	8.36
Core J (PDI pH~9)	5.84	8.77	7.11	8.31	5.33	6.93

The data in Table 10 lists the predicted PHREEQC pH values and the measured pH values taken from the bottle, core holder inlet and effluent on day one and ten of each mod SI test. The measured values were read 10 seconds after the pH sensor was placed in the brine. Over the ten-day period the pH of both injection brines increases by 1.2, but the increase in effluent pH is greater, 1.9 for core 28 (PDI) and 1.6 for core J (PDI pH~9). This may be an indication of reactions occurring in the COBR system.
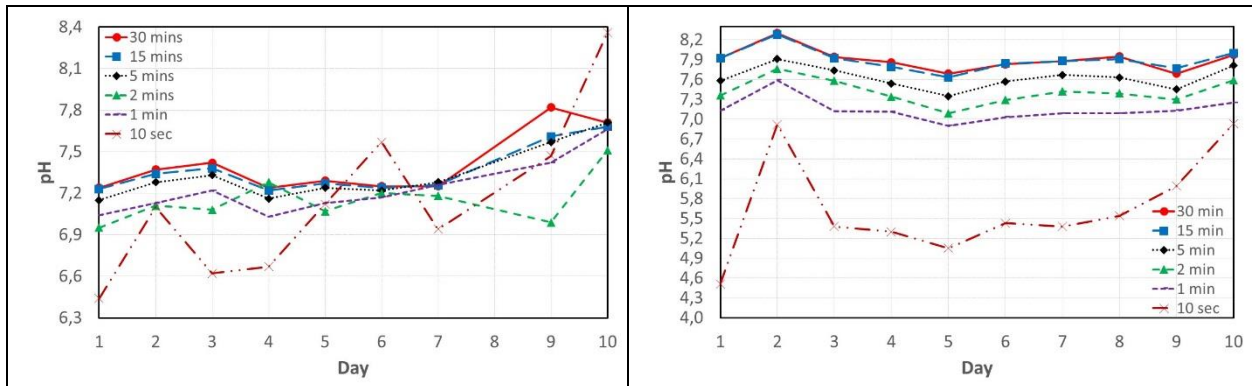
Figure 36 pH curves for core 28 (PDI) (left) and core J (PDI pH~9) (right). The pH measurements were taken daily from the effluent during mod SI tests. The pH was recorded at 10 seconds, 1, 2, 5, 15 and 30 minutes.

The effluent pH was measured daily during the mod SI tests of the aged cores by taking 10-20 ml samples from the burette (Figure 36). The values were recorded at the time intervals stated previously. To reduce the pH drift due to complexation of minerals and reaction of CO_2 from the air an inline pH meter placed close to the core holder outlet is preferred. An attempt was made to do this, but the pH sensor was broken in the process. The meter was under repair during the test of core A (FW) so no pH data is available for this core.

Some insight can be gathered from the curves in Figure 36. For both cores (on a specific day) the pH values rise with each recording from 1 to 30 minutes. The curves begin to stabilize after one minute, and the interval between curves decreases with time, i.e. the 15- and 30-minute curves are nearly identical. Although the 10-second curve for core 28 (FW) fluctuates up and down, the overall trend is increasing with a significant rise over the last four days. A similar trend appears in the ten second curve for core J where pH begins to rise after day 6. It is difficult to say if there is a correlation, but the rise in pH for core 28 (PDI) occurs almost the same time as oil begins to flow (Figure 38). Oil production for core J (PDI pH~9) begins on day three when pH stabilizes and then accelerates on day six and nine, both following an increase in pH the day prior.
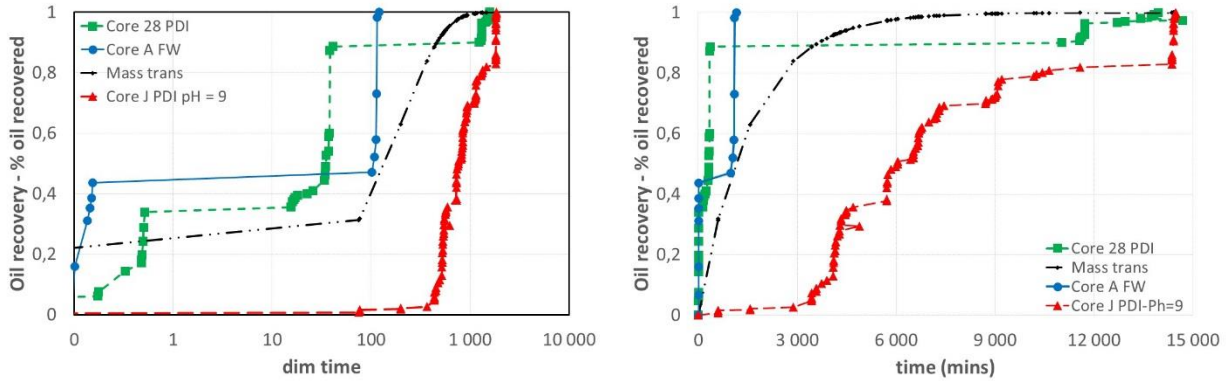
Figure 37 Mod SI of aged cores in dimensionless time (left) and in minutes (right) showing the normalized oil recovered for each core versus time. Recovery profiles are adjusted for differences between cores using equation 6.1. The mass transfer profile is plotted using equation 6.3 as a general reference.

Figure 37 shows the normalized oil recovered for each core versus dimensionless time (dim time) (left) and real time (right). Some interpretation should be applied for the aged cores. Ravari (2011) mentioned in his report the initial production of oil during SI tests at elevated temperatures may be due to thermal expansion of the oil. For core 28 (PDI) and core A (FW) approximately 40% of the oil is produced in the first 15 minutes of the experiment. If this initial oil production is disregarded, then the curves would begin to rise just after dim time 10 and 100 respectively. The explanation for why core J (PDI~9) did not produce initially due to thermal expansion is that it was in the heating cabinet for a longer duration than cores A (FW) and 28 (PDI) which were stored in a different location. The time to transport and weigh the cores allowed them to cool more than core J. The density of the points on the curves in the figure can also provide some insight. Core A (FW) produces very little oil after dim time 100. Core 28 (PDI) is the first to produce at dim time 15 followed by a pause and then production begins again around dim 1000. Core J (PDI~9) is delayed in producing but has a very dense point population showing greater oil production once started. It was noted in chapter five that there was an air leak due to a bad valve during the testing of core J. This may be the reason for the increased oil production in core J rather than the elevated pH level so the test results for core J are inconclusive.
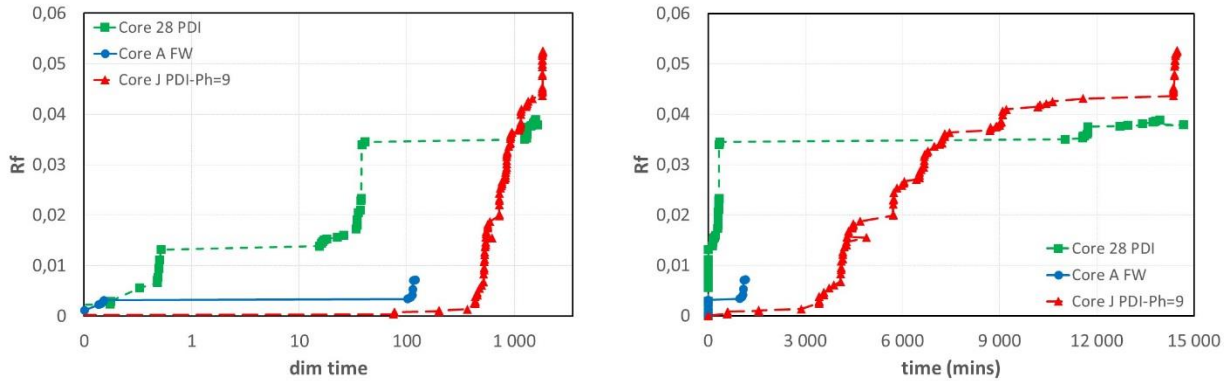
Figure 38 Mod SI aged cores in dimensionless time (left) and in minutes (right) showing the recovery factor (Rf) versus time. For the aged cores although delayed, the Rf was highest for the with elevated pH (core J PDI pH~9).

For the aged cores, oil recovery by spontaneous imbibition of water was low, at 0.06 or less. Figure 38 does show that both cores 28 (PDI) and J (PDI pH~9) begin to produce near the end of the test indicating that Rf values may have increased given more time while production stops in core A (FW) after 20 hours at an Rf of 0.007. This supports the claim that multivalent cations in the brine alter wettability of the rock toward WW by exchanging with polar components on the surface.
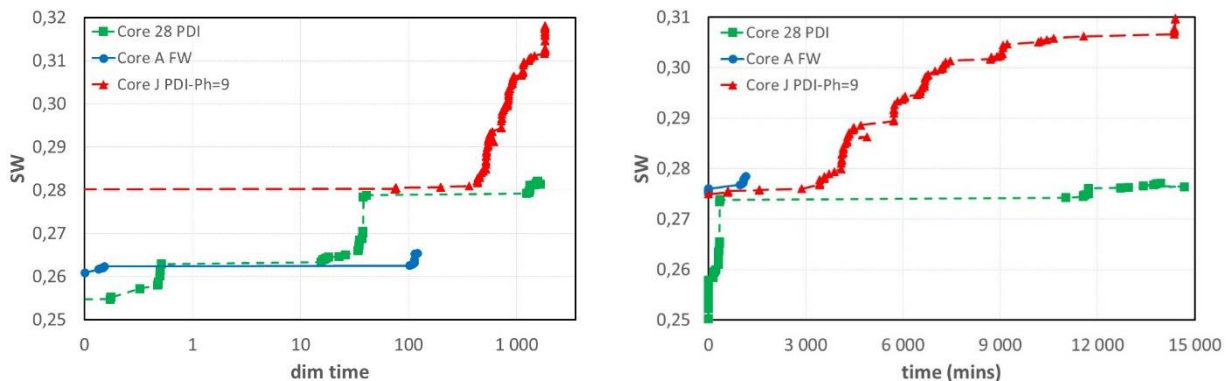
Figure 39 Mod SI of aged cores in dimensionless time (left) and in minutes (right) showing water saturation (S_w) versus time. For the aged cores, although delayed the S_w was higher for core J (PDI pH~9).

The S_w increased approximately 3% higher than S_{wi} for aged cores 28 (PDI) and J (PDI pH~9), while the S_w in core A (FW) remained relatively unchanged ($< 0.5\%$). As discussed earlier, the

increase in S_w occurred earlier for core 28 (PDI) than it did in core J (PDI pH~9) but some of this was due to thermal expansion of oil in core 28.

The graphs depicting the imbibition rates for the cores are not included as there is a lot of scatter and the graphs provide little insight. Except for the aged core J (PDI~9) the general trend for both WW and aged cores is a relatively high initial imbibition rate that decreases exponentially with time. This is most likely a result of initial oil production resulting from thermal expansion. For core J (PDI~9) imbibition is delayed but once initiated continues at a consistently low but steady rate, and core 28 (PDI) also begins a slow but steady production rate following a dormant period. This is consistent with the expectation that a shift toward WW would slowly increase the rate of water SI.

iii. Parametric data

Table 11 contains the parametric data for the cores aged with crude oil. The layout is the same as described for table 9. It is important to note that a good seal was not obtained during the mod FI procedure of core A (FW) due to non-uniform fractured faces. As a result, it was not possible to obtain a pressure differential across the core. Four unsuccessful attempts were made to rectify the problem, but only 2.0 ml of oil was recovered on core A (FW) during the mod FI test and it was not possible to measure k_o. Therefore only V_{oi} and V_{wsi} provide any useful information about this core in the recovery section of table 10.

The IAH indicates slightly oil wet for cores 28 (PDI) and J (PDI~9). With no reliable IAH for core A it is not possible to determine if wettability has shifted toward WW. An important difference during the mod SI tests was that core J (PDI pH~9) began to produce oil after two days and had a $V_{wsi} = 0.70$ ml. Similarly core 28 (PDI) began to produce oil after seven days with a $V_{wsi} = 0.54$, where core A (FW) only produced oil in the first 24 hours with a $V_{wsi} = 0.11$. As mentioned in paragraph 6.C.ii, the initial oil production may be attributed to thermal expansion. Although the recovered volumes are small, there is an indication that the PDI brines began to replace the polar components of the oil that were attached to the surface. Due to time constraints the cores were only tested for 10 days in the mod SI test cell. Ideally the mod SI

experiments should be 20 to 30 days each to allow for reaction time with the surface and diffusion of the brine into the core. The IAH for cores tested using PDI and PDI pH~9 are less than 0.2 of each other indicating that raising pH did not affect wettability alteration when using an oil with polar components.

Table 11 Parametric data for the aged cores. The average uncertainty (Avg Δ) was calculated from the individual aged cores. Permeabilities are from end point tests.

	Units	Avg Δ	Crude Oil Aged Cores		
Core ID			A	28	J
Brine			FW	PDI	PDI pH = 9
Length	cm	0,006	7,535	6,870	7,423
Diameter	cm	0,004	3,786	3,800	3,791
Area (crossectional)	cm^2	0,02	11,25	11,34	11,28
V_b	ml	0,1	84,8	77,9	83,7
V_p	ml	0,05	20,81	18,62	18,90
Ø	%	0,07	24,55	23,90	22,58
k_a	mD	0,4	23,2	21,1	23,7
k_o (drainage)	mD	0,1	12,5	14,0	16,0
k_w (mod FI)	mD	0,4	*	20,5	16,0
k_o (mod FI)	mD	0,06	*	5,06	4,80
k_{ro} (drainage)	mD	0,01	0,54	0,66	0,68
k_{rw} (mod FI)	mD	0,02	*	0,97	0,68
k_{ro} (mod FI)	mD	0,004	*	0,240	0,203
S_{wi} (drainage)	fraction	0,002	0,255	0,248	0,275
S_{or} (mod FI/SI)	fraction	0,005	0,642	0,264	0,269
S_{wir} (mod SI/FI)	fraction	0,005	0,236	0,566	0,660
V_{oi} (fractured)	ml	0,07	15,24	13,90	13,36
V_{wsi}	ml	0,008	0,110	0,540	0,700
V_{wfi}	ml	0,06	2,00	8,40	7,80
OR (mod SI)	fraction	0,0008	0,0072	0,0389	0,0524
OR (mod FI)	fraction	0,006	0,131	0,604	0,584
OR (Total mod SI/FI)	fraction	0,006	0,138	0,643	0,636
V_{osi}	fraction	0,05	0,50	2,00	0,70
V_{ofi}	fraction	0,05	*	1,10	0,70
δw	fraction	0,001	0,052	0,061	0,082
δo	fraction	0,006	1,000	0,650	0,500
IAH	fraction	0,003	-0,948	-0,590	-0,418
Fractured weight decr	fraction	0,0005	0,0167	0,0040	0,0247

7. Conclusions

This study focused on the wettability alteration potential of PDI brines, using Edwards outcrop limestone cores with similar size and properties. Spontaneous imbibition experiments were conducted to assess wettability and wettability change, and Amott-Harvey displacement indicies (IAH), production data and end point relative permeabilites (k_r) were compared.

All cores were initially saturated with a synthetic formation water (FW) and absolute permeability (k_a) was measured. The cores were divided into two groups and either remained water-wet (mineral oil phase used for drainage: decane) or dynamically aged to intermediate/ weakly oil-wet conditions (drained and aged with crude oil). The cores were fractured longitudinally and placed in a modified spontaneous imbibition cell to facilitate high temperature and pressure conditions. The cores were exposed to one of three brines and spontaneous imbibition was measured over time: 1) the synthetic formation water; i.e. the brine composition was equal to the irreducible water saturation in place in the pore volume, 2) a brine with concentrations of potential determining ions (PDI) (Ca^{2+}, Mg^{2+} and SO_4^{2-}) 1.5 times higher than that found in seawater, or 3) PDI brine with the same concentration as 2) but with elevated pH to PDI pH~9.

Question 1

Will increasing the concentration of potential determining ions (PDI) such as calcium (Ca^{2+}), magnesium (Mg^{2+}) and sulfate (SO_4^{2-}) to concentrations 1.5 times the concentrations found in sea water improve the wettability characteristics of Edwards outcrop limestone cores by shifting the wettability of the core from intermediate oil wet to slightly water wet?

For strongly water-wet cores the production levels and rates were equal or better in the cores tested with PDI brine than in the cores tested with FW or PDI brine with elevated pH (PDI pH~9). The Amott-Harvey index was, however, not influenced, suggesting that increased concentrations of PDI do not alter wettability of water-wet carbonate core plugs containing non-polar decane. This was expected as the theory of Smart Water is based on the exchange of divalent cations with polar oil components attached to the surface of the rock, and n-decane is a saturated hydrocarbon with no polar components to bind to the rock surface.

In aged cores exposed to FW in the modified SI cell, oil was produced for 24 hours. Most of this can be attributed to thermal expansion of the oil and hence not attributed to spontaneous imbibition of brine. For the core exposed to PDI brine a small amount of oil was also produced initially due to thermal expansion, however; at day 8 of PDI brine exposure, oil production resumed and continued until the end of the test (10 days). This is in conjunction with a continual rise in effluent pH that began on day seven. The oil production following a dormant period in junction with a rise in pH is a possible indication that sulfate in the brine began to exchange with the polar oil components attached to the surface, causing brine to imbibe into the core to displace oil. It is possible that the increase in pH occurred as the freed carboxylate groups $(RCOO^-)$ associated with hydronium. Amott-Harvey indicies (IAH) for cores tested with PDI and PDI pH~9 brines were similar, at -0.590 and -0.418 respectively, corresponding to oil-wet conditions.

Question 2

Will increasing the pH level of the brine containing PDI to PDI pH~9 have any effect on the wettability alteration of the core samples?

In water-wet cores, spontaneous imbibition and IAH were low in the core tested using PDI pH~9 brine. Hence; brines with high concentrations of multi-valent ions and elevated pH appear to reduce the spontaneous imbibition of water, and influence the water wetness of carbonate cores drained with non-polar decane.

For oil-wet cores, PDI and PDI pH~9 brines produced similar IAH. The core tested using PDI pH~9 brine began to produce oil two days after the other cores, after which the production rate and level were higher. It was mentioned in chapter five that there was an air leak during the testing of the PDI pH~9 core. This could have contributed to the higher performance of the core, however; air exposure should cause pH to fall as the CO_2 reacts with the water to form hydronium, but an increase in pH was recorded when oil production started. The results therefore rather suggest that elevated pH in brines containing higher concentrations of multi-valent cations may increase water wetness of aged carbonate cores.

Does adjusting the temperature from 130°C to 90°C improve the outcome of wettability tests.

In the report by Ravari (2011) the Edwards outcrop limestone core is aged with crude oil and tested using SI and FI. The core is initially tested using SI by FW and immediately produces 5% of OOIP that he attributes to thermal expansion. No additional oil is produced using SI and FW. On day four the test switches to SSW and oil production increases very slowly followed by a jump from 5 to 10% of OOIP between day 11 and 16. Comparatively the cores tested at 130°C have much higher initial production than those tested at 90°C due to thermal expansion (5% vice 3.5% OOIP). The production rates between day 4 and 10 appear to be similar. The core testing at 90°C stopped at day ten, but based on the trends it appears that there is no improvement using 90°C vice 130°C. In future studies, the test period for modified SI should be a minimum of 20 days.

Question 5

Can the program PHREEQ-C be used to predict precipitation of minerals and predict final wettability using surface complexation modeling (SCM)?

The wettability prediction using PHREEQC and surface complexation modeling (SCM) for an open system at 90°C for carbonate cores aged in crude oil was a bond product sum (BPS) of 1.01 for all three brines. The BPS for a closed system was FW (1.03), PDI (0.94) and PDI pH~9 (1.02). A BPS in the vicinity of 1 indicates oil wet. The IAH for the cores was approximately -0.5 using PDI and PDI pH~9. This can be considered an open system initially that moves toward a closed system in time as the CO_2 that enters the brine during mixing and filling reaches equilibrium once it is sealed in the piston valve. This could be a reason for the delay in production by the PDI brines. The association surface complexation reactions and log K values used in this study are only representative of calcite. A more detailed list of the rock minerology such as dolomite and anhydrite with representative log Ks should be used for limestone.

Appendices

A. Uncertainties

Calculation of uncertainties in measurements was conducted using the methods described in the Department of Physics & Astronomy, Undergraduate Lab Manual and Measurement (Department of Physics & Astronomy, Astronomy n.d.) and Instrumentation: Theory and Application (Morris and Langari 2015).

There are three types of limitations to measurements: instrumental, systematic and random. Instrumental reflect the accuracy and limits of the equipment used to make the measurement. Systematic errors are caused by mistakes that do not change during the measurement and therefore effect the accuracy of the readings. Measurements will consistently lie on one side of the true value and will not be apparent. They are either identified and eliminated or they shift the measurement from the true value. Examples of systematic errors include disturbance during the measurement, environmental changes, worn, damaged or uncalibrated equipment.

Random or precision errors occur from unnoticed variations in measuring techniques. Random errors fluctuate around the true value and tend to average out as the number of measurements increases. Examples of random errors include interpolation between scale points of analog equipment,

The mean value (x_{mean}) represents the average value of repeated measurements (x_i) where (n) is the number of measurements taken

$$x_{mean} = \frac{1}{n}\sum_{i}^{n} x_i \tag{A.1}$$

For repeated measurements the standard deviation (σ_s) was calculated using the Bessel correction factor

$$\sigma_s = \sqrt{\frac{\sum_{i=1}^{n}(x_i - x_{mean})^2}{n-1}} \tag{A.2}$$

Equation A.2 reflects the precision of the measurements, but not the accuracy. Therefore the total uncertainty (σ_T) combines the instrument error of the equipment (σ_{instr}) listed in table 9 with either Δx_{avg} or σ_s

$$\sigma_T = \sqrt{\Delta x_{avg}^2 + \sigma_{instr}^2} \tag{A.3}$$

$$\sigma_T = \sqrt{\sigma_s^2 + \sigma_{instr}^2} \tag{A.4}$$

Measured values (x_m) are listed using the mean value and the total uncertainty

$$x_m = x_{mean} \pm \sigma_T \tag{A.5}$$

Table 12 Instrument error of equipment used in the study	
Equipment	Instrument error (σ_{instr})
Caliper	0.002 cm
AND GF-3000 digital scale	0.01 g
ESI pressure transducer	0.25 % of full scale
Gas permeameter flow/pressure (q/P)	0.2 % of q/P
Quizix-QX 1500 pump flow rate (q)	0.1 % of q
Quizix-QX 1500 pump pressure (P)	1 % of P

Propagation of uncertainties

Table 10 lists the formulas used to calculate the uncertainty (Δz) when multiple measurements $(x, \ y, \dots)$, each of which contain uncertainty $(\Delta x, \ \Delta y, \dots)$ are combined.

Table 13 Formulas used to calculate the propagation of errors when combining measurements with uncertainties (Department of Physics & Astronomy n.d.)		
Operation	Equation of the operation	Uncertainty equation
Addition or subtraction	$z = x \pm y$	$\Delta z = \sqrt{(\Delta x)^2 + (\Delta y)^2}$
Multiplication	$z = xy$	$\Delta z = \|xy\| \sqrt{\left(\dfrac{\Delta x}{x}\right)^2 + \left(\dfrac{\Delta y}{y}\right)^2}$
Division	$z = \dfrac{x}{y}$	$\Delta z = \left\|\dfrac{x}{y}\right\| \sqrt{\left(\dfrac{\Delta x}{x}\right)^2 + \left(\dfrac{\Delta y}{y}\right)^2}$
Power	$z = x^n$	$\Delta z = \|n\| x^{n-1} \Delta x$
Multiplication by a constant	$z = cx$	$\Delta z = \|c\| \, \Delta x$
Function	$z = f(x, y)$	$\Delta z = \sqrt{\left(\dfrac{\delta f}{\delta x}\right)^2 (\Delta x)^2 + \left(\dfrac{\delta f}{\delta y}\right)^2 (\Delta y)^2}$

In PHREEQC the user creates an input file consisting of blocks of similar data type that begin with a keyword. The program allows the user to choose one of several pre-existing databases. The selected data base is read at the beginning of a run. Keywords and their associated data are used to amend or augment the database. Keywords are not case sensitive but they must be spelled exactly. The order of the keyword data blocks in a simulation are optional, however the elements on a single line must follow a specified order as listed in the PHREEQC manual. Any data written after the hash mark (#) is not read and normally used for comments. The following is a brief description of the keywords and their elements used in this study.

```
####################################################################
SURFACE_MASTER_SPECIES
        Oil_a           Oil_aCOOH   # Carboxylic acid groups (AN) on the oil surface
        Oil_b           Oil_bNH+    # Amine groups (BN) on the oil surface
        Surf_c          Surf_cCaOH  # Hydrated calcium cation sites on the calcite surface
        Surf_d          Surf_dCO3H  # Hydrated carbonate anion sites on the calcite surface
```

The keyword "SURFACE_MASTER_SPECIES" defines the oil and mineral surface sites and their corresponding surface master species. The first column lists the surface binding-site name (Oil_a, Surf_cCaOH, etc.) followed by the surface master species formula (Oil_aCOOH, Surf_cCaOH, etc.) in column two. The underscore (_) is used when a surface name has more than one binding site.

```
####################################################################
SURFACE_SPECIES
        Surf_dCO3H = Surf_dCO3H # Initial condition for the hydrated carbonate anion site
                log_k           0.0     # on the calcite surface

        Surf_dCO3H = Surf_dCO3- + H+    # Disassociation reaction of the hyd carb site
                log_k           -4.9            # 25°C log K for this surface reaction
                delta_h         -5.0            # default is KJ/mol
        Surf_dCO3H + Ca+2 = Surf_dCO3Ca+
                log_k           -2.8
                delta_h         25.7
        Surf_dCO3H + Mg+2 = Surf_dCO3Mg+
                log_k           -2.2
                delta_h         4.5
```

The SURFACE_SPECIES keyword is used to define the association surface complexation reactions using the 25°C log_k for each surface species. The initial condition for the surface master species is listed first with a log_k = 0 followed by all of the surface reactions and their log_k for that particular surface species. The log_k values can be adjusted for temperature by

including enthalpy of reaction (delta_h) and PHREEQC will adjust using the Van't Hoff equation. Note that valance is written +2 for Ca^{2+} and Mg^{2+}. The same process is repeated for each of the surface master species on the mineral and oil surfaces.

```
###############################################################################
SURFACE 1
        -sites_units density
        #name,        site density, specific area/gram, mass
        Oil_aCOOH   22.0              0.2                  2.6  #Oil surface
        Oil_bNH+    75
        Surf_cCaOH  4.9               0.2                  0.2  #Calcite surface
        Surf_dCO3H  4.9
```

The SURFACE keyword is used to define the amount and composition of each surface. The identifier "-sites_units density" specifies that surface site density is given in sites per square nanometer of surface area. Data for the surface binding sites is then entered starting with the name, site density $\left(\frac{sites}{nm^2}\right)$, specific area per gram $\left(\frac{m^2}{g}\right)$, and mass of the surface area in grams. The site density for oil is computed using the following formula

$$Oil\ site\ density\ \left(\frac{site}{nm^2}\right) = 602 \cdot \frac{TAN\ or\ TBN\ \left(\frac{mg\ KOH}{g\ oil}\right)}{MW\ KOH\ \left(\frac{g}{mol}\right) \cdot Surface\ area\ \left(\frac{m^2}{g}\right)}$$

Where MW is the molecular weight of KOH $\left(56.1\frac{g}{mol}\right)$, and 602 represents Avogadro's constant is $6.0221 \cdot 10^{23}\ mol^{-1}$ times a conversion factor of 10^{-21} to change surface area to $\frac{sites}{nm^2}$ and mg to g for TAN/TBN.

```
###############################################################################
SOLUTION 3                          #PDI pH = 9 brine
        units           mmol/kgw
        density         1.04
        temp            25.0
        pH              9.06
        Na              450
        Mg              90
        Ca              20
        Cl              610
        S(6)            0.89
        water           0.1
```

The SOLUTION keyword defines the temperature and chemical composition of the brine. The identifier "units" is used to set the default concentrations units, here molality (mmol/kgw). The

default for brine density is g/cm^3. Brine temperature (temp) is given in °C. The initial pH of the brine solution is entered if it is not equal to 7.0. The value entered here is from a sample taken at the core holder inlet. The individual elements are listed along with their respective concentrations in mmol/kgw. Sulphur (S(6)) is listed with its valence state in parenthesis to distinguish it from other sulphur redox elements. The valence number is for identification and does not affect calculations. The idendifier water is used to enter the weight of the water used in the test.

###
USE solution 3   #PDI pH9
USE surface 1   #Crude oil and carbonate surfaces

The USE keyword tells PHREEQC which solution and surface to use in batch reaction calculations for the specific simulation. It is possible to run multiple simulations in a single input file.

###
REACTION_TEMPERATURE 1
        90.0

The REACTION_TEMPERATURE keyword defines the temperature in °C that will be applied during the batch reactions.

###
SELECTED_OUTPUT
        -file 4c.PDIpH9.SCM.sel
        -reset false
        -simulation
        -solution
        -pH
        -temp
        -molalities   Surf_dCO3Ca+ Surf_dCO3Mg+ Surf_cCaOH2+   #Carb pos sites
                Oil_aCOO-   #Oil neg sites
                Surf_cCaO- Surf_cCaSO4- Surf_cCaCO3- Surf_dCO3-   #Carb neg sites
                Oil_aCOOCa+ Oil_aCOOMg+ Oil_bNH+   #Oil pos sites
        -saturation_indices Anhydrite Aragonite Calcite Dolomite Gypsum Halite Sulfur

The SELECTED_OUTPUT keyword is used to select output data to be transferred to a file that can be opened into a spreadsheet such as excel. The identifier "-file" is used to name the data file which is refered to as print in PHREEQC. The print file will be saved in the same folder as the PHREEQC input and output files. By entering "-reset false" only those identifiers listed in the subsequent lines will be sent to the print file. The identifiers "-simulation", "-solution", "pH" and

"-temp" send the simulation number, solution number, pH and temperature from the output file to the print file. The identifier "-molalities" will send the concentrations of the listed species to the print file. It is important to note that the mole fraction on the surface is required to compute BPS, not the molality. Currently it is not possible to print the mole fraction or the surface charge. Similarly, "-saturation_indices will send the SI for the minerals listed to the print file.

##

An output file is produced a running the input file. Desired data such as mole fractions and surface charges must be retrieved manually from the output file. The other data that was printed using SELECTED_OUTPUT can be opened using excel. It is necessary to select "All Files (*.*)" in excel when looking for the print file.

The bond product sum (BPS) is calculated using the procedures outlined in paragraph 3.Q.i (Surface Complexation Modelling).

C. PHREEQC Code used to predict BPS and precipitation of minerals

```
TITLE Ginn--SCM    #STO, Calcite, and Brines: FW, SSW, PDI, PDI pH=9 with CO2
      # references
      # Brady et al. (2012) SCM for IOR
      # Erzuah et al. (2017) Wettability Estimation by Sfc Compl Sims
      # Bonto et al. (2019) An overview of the oil-brine interfacial behavior
            #and a new SCM
      # Song et al. (2017) SCM of calcite zeta potential meas in brines
            #with mixed PDI (Ca,CO3,Mg,SO4) for characterizing carbonate
            #wettability
      # Eftekhari et. al. (2017) Thermodynamic Analysis of Chalk-Brine-Oil
            #Interactions
      # Wolthers et. al. (2008) The surface chemistry of divalent metal
            #carboate mineral;/a critical assessment of surface charge and
            #potential data using the charge/distribution multi-site ion
            #complexation model
SURFACE_MASTER_SPECIES
      # Oil
      Oil_a       Oil_aCOOH   # Carboxylic acid group
      Oil_b       Oil_bNH+    # Amin base group
      # Calcite
      Surf_c      Surf_cCaOH  #Hydrated Calcium cation surface site
      Surf_d      Surf_dCO3H  #Hydrated Carbonate anion surface site

SURFACE_SPECIES
      #Oil
      Oil_aCOOH = Oil_aCOOH              #AN Carboxylic acid
            log_k   0
      Oil_bNH+ = Oil_bNH+                #BN Amines
            log_k   0

      Oil_aCOOH = Oil_aCOO- + H+
            log_k   -5.0
            delta_h     0
      Oil_aCOOH + Ca+2 = Oil_aCOOCa+ + H+
            log_k   -3.8
            delta_h     1.2
      Oil_aCOOH + Mg+2 = Oil_aCOOMg+ + H+
            log_k   -4.0
            delta_h     1.2
      Oil_bNH+ = Oil_bN + H+  #log_k & delta_h from Erzuah et al. (2017)
            log_k   -6.0
            delta_h     34                #KJ/mol

      # Carbonate & Calcite
      Surf_cCaOH = Surf_cCaOH
            log_k   0
      Surf_dCO3H = Surf_dCO3H
            log_k   0

      Surf_cCaOH + H+ = Surf_cCaOH2+
            log_k   12.2
            delta_h     -77.5
      Surf_cCaOH = Surf_cCaO- + H+
            log_k   -17.0
```

```
          delta_h      116.4
     Surf_cCaOH + 2H+ + CO3-2 = Surf_cCaHCO3 + H2O
          log_k  24.2
          delta_h      -90.7
     Surf_cCaOH + H+ + CO3-2 = Surf_cCaCO3- + H2O #(NB Surf_cCaCO3 in ref)
          log_k  15.5
          delta_h      -61.6
     Surf_cCaOH + H+ + SO4-2 = Surf_cCaSO4- + H2O #(NB Surf_cCaSO4 in ref)
          log_k  13.9
          delta_h      -72.0

     Surf_dCO3H = Surf_dCO3- + H+
          log_k  -4.9
          delta_h      -5.0
     Surf_dCO3H + Ca+2 = Surf_dCO3Ca+ + H+
          log_k  -2.8
          delta_h      25.7
     Surf_dCO3H + Mg+2 = Surf_dCO3Mg+ + H+
          log_k  -2.2
          delta_h      4.5

SURFACE 1    #STO
     -sites_units      density
     Oil_aCOOH   22.0  0.2   2.59  # sites, area/gram, mass
     Oil_bNH     75.1                # Use formula to compute site of
Surf_aCOOH & Surf_bNH
          #Carbonates
     Surf_cCaOH  4.9   0.2   0.2
     Surf_dCO3H  4.9
#    -diffuse_layer

SOLUTION 1        # FW
     -units      mmol/kgw #mass of solids = 79.04 g/kg water
     pH          7.15
     density     1.0387     #meas using 100 ml brine at 25C
     temp        25
     Na          684
     Mg          25
     Ca          231
     Cl          1196  #charge
     S(6)        0           #SO4-2
     water       .0095966    # kg of water in 10 ml brine

SOLUTION 2        # SSW
     -units      mmol/kgw    #mass of solids = 33.38 g/kg water
     pH          7.00
     density     1.00273     #estimate
     temp        25
     Na          450
     K           10
     Mg          45
     Ca          13
     Cl          525    #charge
     S(6)        24          #SO4-2
     water       .0099392    # kg of water in 10 ml brine

SOLUTION 3        # PDI
```

```
    -units      mmol/kgw
    pH          6.85
    density     1.00226     #meas using 100 ml brine at 25C
    temp        25
    Na          450
    Mg          90
    Ca          20
    Cl          610   #charge
    S(6)        30          #SO4-2
    water       .009673         # kg of water in 10 ml brine

SOLUTION 4          # PDI pH9
    -units      mmol/kgw    #mass of solids = 60.00 g/kg water
    pH          8.77
    density     1.00226             #meas using 100 ml brine at 25C
    temp        25
    Na          450
    Mg          90
    Ca          20
    Cl          610   #charge
    S(6)        30          #SO4-2
    water       .009673         # kg of water in 10 ml brine


GAS_PHASE 1
    CO2(g)    0.000316


REACTION_TEMPERATURE 1
    25.0


REACTION_TEMPERATURE 2
    90.0


USE solution 1     #FW1
USE surface 1      #STO1
USE GAS_PHASE 1
USE reaction_temperature 1


SELECTED_OUTPUT
    -file SCM.Gas.sel
    -reset false
    -Simulation
    -Solution
    -pH
    -temp
    -molalities Surf_dCO3Ca+ Surf_dCO3Mg+ Surf_cCaOH2+    #Carb pos sites
        Oil_aCOO-                                         #Oil neg sites
        Surf_cCaO- Surf_cCaSO4- Surf_cCaCO3- Surf_dCO3- #Carb neg sites
        Oil_aCOOCa+ Oil_aCOOMg+ Oil_bNH+                 #Oil pos sites

    -saturation_indices     Anhydrite  Aragonite  Calcite     Dolomite
    Gypsum      Halite      Sulfur
END

USE solution 2     #SSW
USE surface 1      #STO1
USE GAS_PHASE 1
USE reaction_temperature 1
```

```
END

USE solution 3      #PDI
USE surface 1       #STO1
USE GAS_PHASE 1
USE reaction_temperature 1
END

USE solution 4      #PDI pH 9
USE surface 1       #STO1
USE GAS_PHASE 1
USE reaction_temperature 1
END

USE solution 1      #FW1
USE surface 1       #STO1
USE GAS_PHASE 1
USE reaction_temperature 2
END

USE solution 2      #SSW
USE surface 1       #STO1
USE GAS_PHASE 1
USE reaction_temperature 2
END

USE solution 3      #PDI
USE surface 1       #STO1
USE GAS_PHASE 1
USE reaction_temperature 2
END

USE solution 4      #PDI pH 9
USE surface 1       #STO1
USE GAS_PHASE 1
USE reaction_temperature 2
END

###############################################################
```

Bibliography

Allaby, M. (2019). A Dictionary of Earth Sciences, Oxford University Press.

Anderson, W. (1986). "Wettability Literature Survey- Part 2: Wettability Measurement." Journal of Petroleum Technology **38**(11): 1246-1262.

Anderson, W. G. (1986). "Wettability Literature Survey- Part 1: Rock/Oil/Brine Interactions and the Effects of Core Handling on Wettability." Journal of Petroleum Technology **38**(10): 1125-1144.

Anderson, W. G. (1987). "Wettability Literature Survey- Part 4: Effects of Wettability on Capillary Pressure." Journal of Petroleum Technology **39**(10): 1283-1300.

Appelo, C. A. J. (2005). Geochemistry, groundwater and pollution. Leiden, Balkema.

ASTM (1998 (2003)). ASTM Standard D974, 1998e1, "Standard Test Method for Acid and Base Number by Color-Indicator Titration". West Conshohocken, PA, ASTM International.

Astronomy, D. o. P. (n.d.). Averaging, Errors and Uncertainty. Philadelphia, PA, University of Pennsylvania.

Austad, T. (2013). Water-Based EOR in Carbonates and Sandstones-Chapter 13:New Chemical Understanding of the EOR Potential Using "Smart Water", Elsevier Inc.

Austad, T., S. Strand, M. V. Madland, T. Puntervold and R. I. Korsnes (2008). "Seawater in Chalk: An EOR and Compaction Fluid." SPE Reservoir Evaluation & Engineering **11**(04): 648-654.

Austad, T., S. Strand, T. Puntervold and R. Rostami (2008). "NEW METHOD TO CLEAN CARBONATE RESERVOIR CORES BY SEAWATER."

Bjørlykke, K. and P. Avseth (2010). Petroleum geoscience : from sedimentary environments to rock physics. Heidelberg, Springer.

Boneau, D. F. and R. L. Clampitt (1977). "A Surfactant System for the Oil-Wet Sandstone Of the North Burbank Unit." Journal of Petroleum Technology **29**(05): 501-506.

Bonto, M., A. A. Eftekhari and H. M. Nick (2019). "An overview of the oil-brine interfacial behavior and a new surface complexation model." Scientific Reports **9**(1): 6072.

Boye, N. C., D. Keeping and E. Bakke (2009). Kjemi og miljølære. Oslo, Gyldendal.

Brady, P. V., J. L. Krumhansl and P. E. Mariner (2012). Surface Complexation Modeling for Improved Oil Recovery. SPE Improved Oil Recovery Symposium. Tulsa, Oklahoma, USA, Society of Petroleum Engineers**:** 10.

Brown, T. L., E. H. LeMay, Jr., B. E. Bursten, C. J. Murphy, P. M. Woodward and M. W. Stoltzfus (2017). Chemistry : The Central Science. Upper Saddle River, N.J, Pearson Education.

Buckley, J. S. and T. Fan (2007). "Crude Oil/Brine Interfacial Tensions." Petrophysics **48**(03): 11.

Craig, F. F. (1971). The reservoir engineering aspects of waterflooding. New York, Henry L. Doherty Memorial Fund of AIME.

Fan, T., J. Wang and J. S. Buckley (2002). Evaluating Crude Oils by SARA Analysis. SPE/DOE Improved Oil Recovery Symposium. Tulsa, Oklahoma, Society of Petroleum Engineers.

Fathi, S. J., T. Austad and S. Strand (2010). ""Smart Water" as a Wettability Modifier in Chalk: The Effect of Salinity and Ionic Composition." Energy & Fuels **24**(4): 2514-2519.

Fernø, M. A., M. Torsvik, S. Haugland and A. Graue (2010). "Dynamic Laboratory Wettability Alteration." Energy & Fuels **24**(7): 3950-3958.

Gambill, W. R. (1959). "How to estimate mixtures viscosities." Chem. Eng. **66**: 123.

Green, D. W. (1998). Enhanced oil recovery. Richardson, Tex, Henry L. Doherty Memorial Fund of AIME, Society of Petroleum Engineers.

Grotzinger, J. and T. H. Jordan (2010). Understanding earth. New York, W.H. Freeman.

Indira, L. and G. R. Chatwal (2010). College chemistry. : II. Mumbai India, Himalaya Pub. House. **II**.

Jennings, H. Y. (1967). "The effect of temperature and pressure on the interfacial tension of benzene-water and normal decane-water." Journal of Colloid and Interface Science **24**(3): 323-329.

Lewis, W. and L. Squires (1934). "The structure of liquids and the mechanism of viscosity." Refiner Nat. Gasoline Manuf **13**: 448.

McMurry, J. (2012). Organic chemistry. Belmont, Calif., Brooks Cole.

McPhee, C., J. Reed and I. Zubizarreta (2015). Developments in Petroleum Science, Elsevier Science & Technology.

Merck (2012). Milli-DI. M. Millipore. Darmstardt, Germany, Merck KGaA. **PF1041EN00**.

Morris, A. S. and R. Langari (2015). Measurement and Instrumentation : Theory and Application. Saint Louis, UNITED STATES, Elsevier Science & Technology.

Noller, C. R., R. O. C. Norman, M. C. Usselman and S. S. Zumdahl (2016). Chemical compound. Encyclopædia Britannica Encyclopædia Britannica, inc. .

Parkhurst, D. L. and C. A. J. Appelo (2013). Description of input and examples for PHREEQC version 3: a computer program for speciation, batch-reaction, one-dimensional transport, and inverse geochemical calculations. Techniques and Methods. Reston, VA**:** 519.

Ravari, R. R. (2011). Water-Based EOR in Limestone by Smart Water PhD, University of Stavanger.

Reid, R. C. (1987). The properties of gases and liquids. New York, McGraw-Hill.

Salathiel, R. A. (1973). "Oil Recovery by Surface Film Drainage In Mixed-Wettability Rocks." Journal of Petroleum Technology **25**(10): 1216-1224.

Sandnes, M. F. (2020). Wetting Stability of Aged Limestone in the presence of HPAM polymer, The University of Bergen.

Schlumberger. (2017). "The Oilfield Glossary: Where the Oil Field Meets the Dictionary." from http://www.glossary.oilfield.slb.com/.

Shariatpanahi, S. F., S. Strand, T. Austad and H. Aksulu (2012). "Wettability Restoration of Limestone Cores Using Core Material From the Aqueous Zone." Petroleum Science and Technology **30**(11): 1082-1090.

Sheng, J. (2010). Modern Chemical Enhanced Oil Recovery: Theory and Practice, Elsevier Science.

Shouxiang, M., N. R. Morrow and X. Zhang (1997). "Generalized scaling of spontaneous imbibition data for strongly water-wet systems." Journal of Petroleum Science and Engineering **18**(3): 165-178.

Smith, M. B. (2010). Organic Chemistry : An Acid--Base Approach. Bosa Roca, Bosa Roca: CRC Press LLC.

Song, J., Y. Zeng, L. Wang, X. Duan, M. Puerto, W. G. Chapman, S. L. Biswal and G. J. Hirasaki (2017). "Surface complexation modeling of calcite zeta potential measurements in brines with mixed potential determining ions (Ca^{2+}, CO_3^{2-}, Mg^{2+}, SO_4^{2-}) for characterizing carbonate wettability." Journal of Colloid And Interface Science **506**: 169-179.

Speight, J. G. (2007). The chemistry and technology of petroleum. Boca Raton, Fla, CRC Press.

Strand, S., E. J. Høgnesen and T. Austad (2006a). "Wettability alteration of carbonates—Effects of potential determining ions (Ca^{2+} and SO_4^{2-}) and temperature." Colloids and Surfaces A: Physicochemical and Engineering Aspects **275**(1): 1-10.

Tie, H. and N. R. Morrow (2005). Low-Flood-Rate Residual Saturations in Carbonate Rocks. International Petroleum Technology Conference. Doha, Qatar, International Petroleum Technology Conference**:** 11.

Tipura, L. (2008). Wettability Characterization by NMR T_2 Measuments in Edwards Limestone Master, University of Bergen.

Van Cappellen, P., L. Charlet, W. Stumm and P. Wersin (1993). "A surface complexation model of the carbonate mineral-aqueous solution interface." Geochimica et Cosmochimica Acta **57**(15): 3505-3518.

Wolthers, M., L. Charlet and P. Van Cappellen (2008). "The surface chemistry of divalent metal carbonate minerals: A critical assessment of surface charge and potential data using the charge distribution multi-site ion complexation model." American Journal of Science **308**.

Zhang, P. and T. Austad (2006). "Wettability and oil recovery from carbonates: Effects of temperature and potential determining ions." Colloids and Surfaces A: Physicochemical and Engineering Aspects **279**(1): 179-187.

Zhang, P., M. Tweheyo and T. Austad (2007). "Wettability alteration and improved oil recovery by spontaneous imbibition of seawater into chalk: Impact of the potential determining ions Ca^{2+}, Mg^{2+}, and SO_4^{2-}." Colloids and Surfaces A: Physicochemical and Engineering Aspects **301**: 199-208.